NASA CR-135282
BOEING D180-20746-1

DEVELOPMENT OF A HIGH TEMPERATURE CAPACITIVE PRESSURE TRANSDUCER

by R. L. Egger

BOEING

prepared for

NASA
National Aeronautics and Space Administration

Lewis Research Center

Contract NAS 3-19556

1. Report No.	2. Government Accession No.	3. Recipient's Catalog No.
NASA CR-135282		

4. Title and Subtitle	5. Report Date
DEVELOPMENT OF A HIGH TEMPERATURE PRESSURE TRANSDUCER	October 1977
	6. Performing Organization Code

7. Author(s)	8. Performing Organization Report No.
Richard L. Egger	D180-20746-1
	10. Work Unit No.

9. Performing Organization Name and Address	11. Contract or Grant No.
Boeing Aerospace Company Seattle, Washington	NAS3-19556
	13. Type of Report and Period Covered
12. Sponsoring Agency Name and Address	Contractor Report
National Aeronautics and Space Administration Washington, D.C. 20546	14. Sponsoring Agency Code

15. Supplementary Notes

Project Manager, Herbert L. Minkin, NASA Lewis Research Center, Cleveland, Ohio

16. Abstract

High temperature pressure transducers capable of continuous operation while exposed to 650°C were developed and evaluated over a full-scale differential pressure range of ±69 kPa. The design of the pressure transducers was based on the use of a diaphragm to respond to pressure, variable capacitive elements arranged to operate as a differential capacitor to measure diaphragm response and on the use of fused silica for the diaphragm and its supporting assembly. The uncertainty associated with measuring ±69 kPa pressures between 20°C and 650°C was less than ±6%.

17. Key Words (Suggested by Author(s))	18. Distribution Statement
Pressure transducer Capacitive transducer Transducer High temperature transducer	Unclassified - unlimited

19. Security Classif. (of this report)	20. Security Classif. (of this page)	21. No. of Pages	22. Price*
Unclassified	Unclassified	114	

* For sale by the National Technical Information Service, Springfield, Virginia 22161

TABLE OF CONTENTS

LIST OF FIGURES

LIST OF FIGURES, CONTINUED

LIST OF FIGURES, CONTINUED

LIST OF FIGURES, CONTINUED

1.0 SUMMARY

The objective of this program was to develop a pressure transducer capable of continuous operation at 650°C over a full scale differential pressure range of ± 69 kPa and with a dynamic response to 2000 Hz.

The scope of the effort was limited to developing, evaluating, and improving pressure transducer static pressure response up to temperatures of 650°C. Developmental efforts were associated with fabrication techniques as well as with techniques to improve performance.

The design of the pressure transducers was based on the use of a diaphragm to respond to pressure, variable capacitive elements arranged to operate as a differential capacitor to measure diaphragm response to pressure and on the use of fused silica for the diaphragm and its supporting assembly. Sputter-deposited platinum-tantalum oxide films were used to form capacitive plates on the fused silica components.

Pressure transducer performance was plagued at the beginning of the program by excessive zero shifts with temperature and changes in sensitivity with temperature above 450°C. Fused silica pressure-sensing assemblies were successively fabricated and evaluated, with succeeding units incorporating progressive modifications. The zero shift and change in sensitivity problems were found to be caused by changes in the fused silica electrical properties at elevated temperature; the problems were reduced by incorporating ground planes on the fused silica sensor assembly components and by modifying the signal conditioning used to reduce its sensitivity to the electrical property changes.

The technical discussion in this report emphasizes pressure transducer design, problem areas and developmental modifications made during the program to improve performance.

The final results of the program are represented by the design, fabrication procedures and performance of the final pressure transducers that were built and tested. A deficiency in the final design concerns leakage in the transducer between the measured-pressure medium and the reference-pressure medium. Final fabrication procedures are relatively uncomplicated and have the possibility of being simplified further by substituting the use of a thick film conductor composition for the sputtering process that was used to deposit the conductive films.

Without making temperature corrections, the final transducers were capable of measuring static pressures of ± 69 kPa at temperatures between 20°C and 650°C with an uncertainty of less than ±6%; below 600°C the uncertainty was less than ±3%.

2.0 INTRODUCTION

2.1 PURPOSE

The objective of this program was to develop a pressure transducer capable of continuous operation at 650°C over a full scale differential pressure range of ±69 kPa and with a dynamic response to 2000 Hz. The intended use of the transducer is in the development and testing of aircraft engines where the temperature and dynamic pressure environment exceeds the capabilities of currently available pressure transducers.

2.2 CURRENT STATE-OF-THE-ART

High temperature static pressures can be easily measured by using a duct to transfer the pressure to any of a variety of pressure transducer types located in a moderate temperature environment. For accurate measurement of dynamic pressures, however, it is necessary that the pressure transducer be located at or in the medium being measured. Water-cooled units can be used when an adequate water supply can be made available and when the cooling effects at the transducer can be tolerated. The KP-1910 series pressure transducers marketed by Kaman Sciences Corporation in Colorado Springs, Colorado closely represent the extent of the current state-of-the-art. Their eddy current based pressure transducers purportedly operated between 25°C and 540°C with a ±10% zero shift, a ±10% change in sensitivity and an average frequency response between 0 and 2000 Hz of within about 30%. The KP-1910 series transducers are somewhat sensitive to cable effects and transient temperatures.

The intent of this program was to extend the current state-of-the-art in terms of maximum operating temperature and in terms of performance at high temperature.

2.3 APPROACH

The approach was based on a conceptual design comprising the use of a diaphragm to respond to the pressure, air-dielectric variable capacitive elements arranged to operate as a differential capacitor to measure the diaphragm response, the use of fused silica for the diaphragm and its supporting assembly and deposited metallic films to form the capacitive plate elements. The attraction of the conceptual design was based on the temperature insensitivity of air-dielectric variable differential capacitors and on the unique combination of desirable electrical, mechanical and thermal properties of fused silica. Many of the individual aspects of the conceptual design have been previously used to build transducers; the principal task here was to develop the techniques which would enable the transducers to operate to 650°C.

The approach included, as part of this program, the successful development of techniques to:

1. Bond together fused silica components to form the sensing assembly.

2. Deposit thin conductive films on the fused silica components that would reliably withstand the bonding temperature and repeated cycles to 650°C.

3. Attach transition lead wires to the conductive films.

2.4 DESCRIPTION OF PROGRAM EFFORT

Program efforts were directed toward component design, toward developing the techniques required to fabricate the fused silica pressure-sensing assemblies, toward evaluating experimental sensing assemblies at up to 650°C and toward modifying the design and techniques to improve performance. Prior to the start of the program, some fused silica bonding and film deposition experiments had been made; these experiments were made primarily to support the conceptual design. This program began with a detailed design of the fused silica sensor components, with design considerations for lead wires and with an overall case design to house the sensor. Figure 1 shows the basic physical design of the fused silica sensor assembly components that were chosen and used throughout the program. As shown, the sensor assembly consists of three fused silica components: two identical recessed discs (with holes) and a thin diaphragm. After a search was made, Mindrum Precision Products in Cucamonga, California was selected to manufacture the components using high purity fused silica obtained from Dynasil Corporation of America.

Much of the development was accomplished with trial-and-error evaluations which included temperature cycles to 650°C and higher. Both before and after the fused silica sensor components were received, inexpensive, commercially available fused silica discs (25.4 mm in diameter and 1.6 mm thick) were used to develop and evaluate deposited films, fused silica bonding techniques and techniques for bonding lead wires to the deposited films. Over the duration of the program, attempts were made to fabricate twenty-two fused silica sensor assemblies. The sensors were fabricated successively, usually with variations such as in the distance between the capacitive plates, diaphragm thickness, deposited film pattern, fused silica surface smoothness, bonding procedure, film deposition technique and lead wire attachment technique. Of the twenty-two sensor assemblies, ten were pressure tested at temperatures up to 650°C using a fixture that permitted temporary installation and removal of the sensors. A photograph of the test fixture with a sensor inside is shown in Figure 2. Of the ten sensor assemblies tested, three were installed in stainless steel cases and again pressure tested at temperatures to 650°C.

The first sensor was installed in a case about one-third of the way through the program. Its performance was limited by large zero shifts above 450°C and appreciable changes in sensitivity above 590°C. Subsequently, the signal conditioning was modified and the deposited conducting film patterns were changed to include ground planes to reduce the zero shift and change in sensitivity at elevated temperatures. The second and third sensor assemblies

were installed in cases at the end of the program and their performance represents the final results of the effort.

Section 3.0 lists the target specifications. Although the dynamic response of the pressure transducers was an important design requirement, the developmental efforts emphasized optimizing the static pressure response characteristics to 650°C. No dynamic pressure response evaluations were made as a part of this program.

Section 4.0 discusses the design parameters, material properties, technique developments, signal conditioning and developmental problems and solutions.

Section 5.0 summarizes the sequential steps used to fabricate and assemble the pressure transducers that were built at the end of the program.

Section 6.0 describes performance data with emphasis on the final results.

The conclusions in Section 7.0 include recommendations for improvements that could facilitate fabrication of the transducers and broaden their application.

3.0 TARGET SPECIFICATIONS

3.1 PHYSICAL

3.1.1 Size: 12.7 mm diameter x 19 mm long

3.1.2 Mounting: Flush with mounting adapters

3.1.3 Reference pressure access: Tube from the transducer for connection to a remote pressure source

3.1.4 Electrical sensor: Differential capacitive half-bridge

3.1.5 Electrical leads: At least 0.9 m long extending from case to a room temperature connector

3.2 OPERATIONAL

3.2.1 Pressure range: ± 69 kPa differential

3.2.2 Pressure overrange: 207 kPa

3.2.3 Temperature: Continuous operation ambient to 650°C

3.2.4 Frequency response: Amplitude ratio within 5% of unit for frequencies up to 2000 Hz

3.2.5 Non-linearity: Less than 1% of full scale

3.2.6 Hysteresis: Less than 1% of full scale

3.2.7 Zero shift with temperature: Within 1% of full scale

3.2.8 Sensitivity change with temperature: -.018% (or less) per °C between 21°C and 650°C

3.2.9 Mechanical integrity: Withstand vibration consistent with curve G of MIL-STD-810B which is ± 147 m/sec^2 peak from 90 to 2000 Hz and at reduced levels below 90 Hz at 21°C

3.2.10 System output: ±5 volts full scale

4.0 TECHNICAL DISCUSSION

4.1 CONCEPTUAL DESIGN AND OPERATION

The transducer design was influenced by requirements to operate continuously at 650°C without external or auxiliary cooling, to provide both static and dynamic response over a full-scale pressure range of ± 69 kPa, to operate while fully exposed to the temperature environment, to be as small as practicable and to be insensitive to temperature magnitudes as well as temperature changes and gradients.

In the configuration used in this program, a diaphragm was bonded between two recessed discs to form the pressure-sensing assembly (referred to hereafter as the sensor). Both of the discs contained holes through which gas could pass to reach the diaphragm. Through the holes in the respective discs, one side of the diaphragm is exposed to the reference pressure while the other side is exposed to the pressure to be measured. The diaphragm was designed to deflect in response to the difference in the pressure to be measured and the reference pressure.

The differential capacitive displacement sensor used to sense the diaphragm deflection was formed by depositing conductive films on both sides of the diaphragm and on the recessed disc surfaces facing the diaphragm. The films act as capacitive plate elements to form two capacitors - one on each side of the diaphragm. As the pressure to be measured causes the diaphragm to deflect, one capacitor increases in capacitance while the other decreases. With the plates on opposite sides of the diaphragm electrically common and an ac excitation voltage applied across the plates on the two recessed discs, the two capacitors form an electrical half-bridge. The half-bridge output is nulled when the two capacitances are equal and it remains nulled when they both increase or both decrease equal amounts. When one capacitor increases and the other decreases, an output is created with a polarity that is dependent on which capacitors increased and decreased.

Air-dielectric differential capacitors have advantages for sensing motion at elevated temperatures: the dielectric constant of air changes negligibly with temperature which is desirable because the output is dependent on the dielectric constant of the media between the plates; the differential configuration doubles the output, tends to linearize gap-change non-linearities and inherently cancels unwanted effects that are common to both capacitances. A differential capacitor formed with two capacitors is shown in Figure 3. A differential capacitor is shown in a half-bridge configuration in Figure 4.

Fused silica has a unique combination of desirable properties for use as the diaphragm (and recessed disc) material: the modulus of elasticity is relatively low and changes less with temperature than the modulus of high temperature metal alloys; the volume resistivity is high and (since it is available with extremely high purity) its volume resistivity remains relatively high at temperatures to 650°C; it does not oxidize or undergo phase changes at temperatures below about 1100°C; it is highly elastic at temperatures to over

650°C, which is essential to limiting hysteresis effects; the thermal coefficient of expansion of fused silica is about one-thirtieth that of most high temperature alloys and as a result undesirable thermal expansion and thermal gradient effects are reduced proportionately.

From a use standpoint, a flush diaphragm type transducer is very desirable. The possibility of rearranging the same fused silica components to form a flush diaphragm type differential capacitive transducer with only one active arm was considered but was not developed. The compromise in such a configuration would be reduced output and increased non-linearity.

4.2 SENSOR DESIGN PARAMETERS

Structural response of the diaphragm and the resulting capacitance change were the primary considerations in determining the physical parameters of the sensor. In designing the sensor, the intent was to make the capacitance change as large as possible without introducing non-linearities or exceeding stress levels in the diaphragm that would result in hysteresis or failure. With air as the dielectric, the capacitance is a function of the plate area and the distance between the plates:

$$C = 0.0866\frac{A}{d}$$

where C is the capacitance (neglecting edge effects) in picofarads, A is the common plate area in square centimeters and d is the distance between the plates in centimeters. If the plate area is considered constant, the capacitance change is a function of the distance between the plates and the change in the distance between the plates. Smaller distances and larger changes in distance result in larger changes in capacitance, as shown in the following equation:

$$\Delta C = 0.0866A\frac{d_2 - d_1}{d_1 d_2}$$

where ΔC is the change in capacitance in picofarads, A is the common plate area in square centimeters, d_1 is the initial distance between the plates in centimeters and d_2 is the final distance between the plates in centimeters.

The change in distance is a function of the structural response of the diaphragm:

$$\delta = \frac{3Pr^4(1-\mu^2)}{16Et^3}\left[\left(\frac{x^4}{r^4} + 1\right) - 2\left(\frac{x^2}{r^2}\right)\right]$$

where δ is the deflection of the diaphragm at a particular point, P is the differential pressure, r is the effective diaphragm radius, μ is Poisson's ratio of the diaphragm material, E is Young's modulus of the diaphragm material, t is the diaphragm thickness and x is the radial distance from the center of the diaphragm to the particular point on the diaphragm.

The maximum stress induced in the diaphragm is:

$$\sigma = \frac{3Pr^2}{4t^2}$$

where σ is the maximum stress, P is the differential pressure, r is the effective radius of the diaphragm and t is the diaphragm thickness.

A pressure transducer case outside diameter of 12.7 mm was specified. The recessed discs and diaphragm outside diameters were chosen to be 10.16 mm so that the sensor assembly could be housed within a case. The diameter of the recess in the discs was chosen to be 8.128 mm and the deposited capacitive plate diameter was chosen to be 6.096 mm as shown in Figure 5. These dimensions were consistent (within manufacturing tolerances) throughout the program. The recess diameter represents the effective diaphragm diameter except for a slight chamfer on the corner and variations in the bond-line width. The graph in Figure 6 shows the calculated deflections of diaphragms with three different effective diameters as a function of diaphragm thickness.

With the effective diameter relatively fixed, the variable design parameters are reduced to the diaphragm thickness and the air-gap distance between the plates (which varies with the depth of the disc recess and the bond line thickness). The graphs in Figures 7 and 8 show calculated total capacitance changes resulting from a differential pressure of 69 kPa. Figure 7 shows the capacitance changes for four different initial distances between plates on the diaphragm and disc as a function of diaphragm thickness when the effective diaphragm diameter is 8.128 mm. (Note that the distances between the plates on each side of the diaphragm are assumed to be equal when the differential pressure is zero.) Figure 8 shows the capacitance changes for three effective diaphragm diameters as a function of diaphragm thickness when the distance between the plate on the diaphragm and disc is 101.6 µm.

As noted, the theoretical values for capacitance change in Figures 7 and 8 assume the capacitive plates are perfectly symmetrical. Practical grinding tolerances will result in some degree of asymmetry which in turn will result in a variation in response to positive and negative pressure. For a sensor with a 254 µm thick diaphragm and an effective diameter of 8.128 mm, the response to positive and negative pressure will differ by 0.96% when one plate distance is 96.52 µm and the other is 106.68 µm. For the same sensor, the response will differ by 2.6% when one plate distance is 88.9 µm and the other is 114.3 µm. In practice, it was found that the recess depths could be ground to within tolerances of ± 8 µm and could be matched in pairs to within ± 1.3 µm. Although other factors such as variations in bond line thickness can affect the response to positive and negative pressure, it appears that practical control of tolerances can limit the difference in response to about 0.1%.

The diaphragm thicknesses and plate distances used in Figures 6, 7 and 8 are in the range of those that were purposely varied and used in the sensors built

and tested. The effective diameter was not purposely varied but the range of those used in Figures 6 and 8 is consistent with the variation that could have resulted from component tolerances, bevel variations and bond-line variations. The table in Figure 9 lists sensors built and tested, their diaphragm thicknesses, their plate distances and the measured total capacitance change resulting from applying 69 kPa differential pressure.

Although the design operating pressure was ± 69 kPa, it was desired that the transducer operate without degraded performance after having been exposed to 207 kPa. The diaphragm stress levels associated with the diaphragm thicknesses and effective diameters used in Figure 8 are shown in Figure 10. Breaking stress levels for brittle materials such as fused silica are heavily dependent on surface imperfection, internal flaws and sample size. Modulus of rupture values vary so that the breaking stress for a particular sample cannot be predicted with as great a degree of accuracy as could be with corresponding metal samples. Dynasil Corporation and Corning Glass Works both manufacture fused silica and both list a value of 50.2 MPa for the modulus of rupture (or breaking stress) of abraded fused silica. If 50.2 MPa is used to represent the maximum allowable diaphragm stress, and if the diaphragm effective diameter is assumed to vary up to 8.636 mm, then (using Figure 10) the minimum diaphragm thickness that will withstand a differential pressure of 207 kPa is about 225 μm.

In general, the test data were found to be in reasonable agreement with the calculations (as shown, for example, by comparing the values in Figures 7 and 8 with those in Figure 9). The one sensor assembly that was tested to 207 kPa had a diaphragm thickness of 254 μm. The effect of the 207 kPa pressure was a slight (0.3%) but permanent increase in hysteresis during cycling to ± 69 kPa pressures.

4.3 SUMMARY OF DEVELOPMENTAL PROBLEMS AND SOLUTIONS

The developmental effort included distinct problem areas that required disproportionately more effort. In terms of fabrication, these problems consisted of the bonding of the fused silica components, the application and integrity of conductive films on the fused silica components and the attachment of lead wires to the conductive films. In terms of performance, the initial sensors built were found to have excessive zero shifts and changes in sensitivity at temperatures above 450°C.

The bonding problems were solved by obtaining and learning to use an experimental low expansion devitrifying frit from Corning Glass Works. Acceptable conductive films were obtained by experimenting with various processes, combinations of materials and application techniques. The lead wire attachment problems were solved by applying a boro-silicate glass over the lead-wire-to-film connection to provide strength or by using a thick film conductor composition to make the attachment. Bonding, conductive film and lead wire attachment techniques are discussed further in individual sections that follow.

The zero shift and sensitivity change with temperature problems were caused

by changes in the electrical properties of the fused silica at elevated temperature. The change in properties resulted in excessive out-of-phase, as well as in-phase, unwanted signal components. (Capacitive signal components are considered in-phase and resistive signal components are considered out-of-phase.) The presence of some out-of-phase component was expected; the sensor was designed to nominally cancel out-of-phase components and the signal conditioning was designed to be insensitive to them. The electrical property changes were found to be greater than expected and as a result the degree of cancellation in the sensor and insensitivity of the signal conditioning were not sufficient.

The zero shift and sensitivity change with temperature problems were reduced greatly by modifications to the signal conditioning and by the addition of conductive film ground planes to the sensor.

Fused silica properties, conductive film ground planes and signal conditioning are also discussed further in sections that follow.

4.4 FUSED SILICA BONDING TECHNIQUES

Bonding of fused silica components after conductive films had been formed on their surfaces was inherent in the sensor conceptual design. Bond requirements included:

1. Adequate strength at 650°C to withstand the forces induced by 207 kPa.

2. Creep-free, elastic properties that would not produce hysteretic diaphragm deformation.

3. Consistent bond-line thickness.

4. Electrical insulating properties sufficient to prevent low leakage paths between conductors passing through or under the bond-line.

5. A bonding temperature below that which would cause degradation of the conductive film (about 1000°C).

Initial bonding experiments were made with a boro-silicate transfer tape purchased from Vitta Corporation in Wilton, Connecticut (and designated by Vitta as Type G-1015). The boro-silicate transfer tape bonding temperature was 900°C. It was easy to use, had a very consistent bond-line thickness and had good mechanical properties at room and moderate temperatures. Above about 500°C, however, the boro-silicate softened, creating hysteresis effects in the sensor response to differential pressure.

Alumino-silicate transfer tape made from Dow Corning Type 1720 alumino-silicate glass was special-ordered from Vitta. This material produced acceptable bonds only after being fired at temperatures above 1200°C - resulting in severe degradation of the deposited conductive film. Attempts to directly fuse the fused silica components using bonding pressures on the order of 200 kPa were unsuccessful at temperatures up to 1200°C.

An experimental low expansion devitrifying frit was obtained from Corning Glass Works. The frit, designated "E-Frit Sample No. 1" was evaluated and eventually (after determining proper application techniques) found to be acceptable. The frit was fired to form a bond at 950°C and the resulting bond met the five requirements listed above.

Corning considers the constituents of the frit proprietory. They describe the frit as having glass and crystalline phases after being fired. The crystalline phase is irreversibly formed at 950°C without any further changes occurring on subsequent heating cycles to 950°C. Although the frit has no sales-code release designation and is not sold as a line product, Corning has indicated it can be made available on special order.

The frit was furnished as a fine powder and applied to surfaces to be bonded by mixing with either nitrocellulose and amyl acetate or Emflow 43 and Reagent 16 (obtained from Electro Materials Corp. of America). The slurry formed with the Emflow 43 and Reagent 16 was easier to apply with a screen printer and produced a bond equal to, or slightly better than, the nitrocellulose and amyl acetate slurry.

Frit application experiments included applying the frit (in slurry form) in four different ways:

1. The frit was applied with a screen printer. Two coats were applied to each recessed disc. Each coat was dried at 80°C. The discs and diaphragm were mated dry.

2. The frit was applied with a screen printer. One coat was applied to each disc and diaphragm mating surface. All four coats were dried at 80°C. The discs and diaphragm were mated dry.

3. The frit was applied with a screen printer. One coat was applied to a recessed disc bonding surface and one coat was applied to a diaphragm bonding surface. The disc and diaphragm were mated wet and dried at 80°C. The operation was repeated for mating the other disc to the other side of the diaphragm.

4. The frit was applied manually with a dental pick under a microscope. One coat was applied to a recessed disc bonding surface. The coated disc and the diaphragm were mated wet and dried at 80°C. The operation was repeated for mating the other disc to the other side of the diaphragm.

The screen printer used was a Model PDSA-33-BC-FHY, made by Affilitated Manufacturers, Inc. in Whitehouse, New Jersey.

The temperature cycle generally used for firing the frit consisted of heating at a rate of about 220°C per hour with a one-half hour hold period at 200°C (to drive off binder solvents), a one-half hour hold period at 600°C (to drive off binder residuals) and a one-hour hold period at 970°C (to ensure that the bond line temperature was stabilized above 950°C). A zirconia block was placed

on top of the mated components during firing of the frit to effect a pressure of about 50 kPa on the bond line surface.

With respect to application of the frit and alignment of the components, the first technique was the most desirable; the results obtained, however, were the most inconsistent. The third and fourth application techniques above produced consistently good results, indicating that it is more desirable to mate all the surfaces before the slurry is dried. On a one-at-a-time basis, the fourth technique was more efficient than the third. All of the sensors evaluated had good bonds, but only the last five built used the fourth technique described above.

4.5 CONDUCTIVE FILMS

In the final sensor design, conductive films were used to form the capacitive plates, to provide terminal pads to which small wires were attached, to provide electrically conductive paths from the plates through the bond line to the terminal pads, and to form ground planes. Films were developed that survived bonding temperatures of up to 1000°C. Resistance of the films was not critical to the performance of the sensor as long as it remained relatively low. Resistances across the plates and between the plates and the terminal pads were on the order of five to twenty ohms.

The difficulty in establishing conductive films on fused silica for this application results from the thermal expansion mismatch between fused silica and any kind of electrically-conducting solid material and from the extreme temperature and temperature change (from 20°C to about 900°C). A number of materials and techniques were considered; the following four were evaluated:

1. Hanovia Liquid Bright Platinum No. 6857
2. Ion deposited platinum
3. Sputter deposition
4. DuPont Thick Film Conductor Composition 8553

The Liquid Bright Platinum was obtained from Hanovia Liquid Gold Division of Engelhard Industries. It was found to produce good conductive films that could withstand (at least one cycle to) 650°C. After exposure to 900°C, the film either disappeared or lost its electrical conductivity.

Ion deposited platinum films were applied using a Model CV-8 electron beam gun and Model BJD-1800 vacuum system manufactured by Airco Temescal in Berkley, California. The films were not tenacious. It was difficult to control their thickness and they generally failed upon exposure to temperatures of 650°C.

Sputter deposition techniques were developed and used (with variations) in the attempts to build all twenty-two of the sensors. A considerable amount of effort was devoted to developing acceptable sputtered films. The follow-

ing list summarizes the development and some of the problems:

1. Sputtering system - the sputter deposition was accomplished with a Model 822 system manufactured by Materials Research Corp. in Orangeburg, New York.

2. Film composition - acceptable films were deposited using platinum only and using platinum-tantalum oxide layers. The platinum-tantalum oxide films were better than the platinum-only films with respect to adhesion and degradation at extreme temperatures. The tantalum oxide layers were formed by sputtering tantalum in the presence of oxygen. The platinum and tantalum oxide layers appeared to form a cermet after having been exposed to 950°C. The platinum-only films remain shiny after exposure to elevated temperatures whereas the platinum-tantalum oxide films look tarnished. Small wires could not be thermal compression bonded to platinum-tantalum oxide films after they had been exposed to high temperature but they could be bonded to platinum-only films after exposure to temperature and this was an advantage of the platinum-only films.

   Sputtered gold and gold-platinum layered films were evaluated, but they consistently peeled off when exposed to elevated temperature.

3. Film thickness - the thickness of the applied film is a critical parameter. The thicknesses of both platinum only and platinum-tantalum oxide films are reduced appreciably after a first cycle to 950°C. If the initial film is applied too thick (> 3×10^{-7} μm) it crazes or peels when subjected to high temperatures; if it is applied too thin (< 2×10^{-7} μm) its electrical characteristics are poor or inconsistent after having been exposed to high temperatures. In some instances, additional film layers were applied over films that had been exposed to high temperatures.

4. Fused silica surface smoothness - initial film deposition experiments were made using relatively inexpensive commercially available fused silica discs with optically clear surfaces. When the first purchase of fused silica components for the sensor was made, optically clear surfaces were specified for the diaphragm (for mechanical strength reasons), but rougher surfaces were allowed for the discs (for economic reasons). Films applied to the rougher surfaces either agglomerated, partially diffused in the surface or sublimed when heated to high temperatures. Variations in sputtering technique did not improve the film on rough surfaces, but fire-polishing the fused silica prior to deposition did. Fire polishing, however, was found to cause surface distortions. Subsequently, all sensor component surfaces were polished so that they were optically clear.

5. Sharp edges - film failures occurred on sharp fused silica edges similar to the manner in which they failed on rough surfaces. Recessed disc edges were chamfered and polished to eliminate the problem.

6. Sputtering control parameters - the film thickness was controlled by the power settings on the sputtering system and by the time allowed for each process step. Optimum control settings were determined by trial-and-

error.

7. Effects of masks - masks, such as those shown in Figures 11 and 12, were used to control the pattern of the sputtered film. In using the masks, the thickness of the film varied somewhat with the pattern width so that the film thickness was less where the pattern was narrow. It was also suspected that the optimum control settings were different for sputtering with and without masks.

8. Component orientation - the sputtering deposition rate is somewhat related to the relative orientation of the sputter target to the surfaces being coated but the relationship is apparently dependent on the particular control settings being used and on whether masks are used. Good films could be deposited on surfaces parallel and normal to the target when no masks were used; with the same control settings the films normal to the target were inconsistent when masks were used. Where (masked) films were required on component surfaces at 90^{o} to each other, the component was either rotated so that both surfaces were at 45^{o} to the target or coated in multiple operations with a surface to be coated facing the target in each operation.

Typical steps and control settings used to sputter deposit the platinum-tantalum oxide films are listed below:

1. Sputter tantalum in presence of oxygen with no bias, 5 microns argon pressure, 2 microns oxygen pressure and 300 watts of cathode power for 2.0 minutes.

2. Sputter platinum with 10% bias, 7 microns argon pressure and 300 watts of cathode power for 1.0 minute.

3. Sputter platinum with no bias, 7 microns argon pressure and 300 watts of cathode power for 3.25 minutes.

4. Sputter tantalum in presence of oxygen with no bias, 5 microns argon pressure, 2 microns oxygen pressure and 300 watts of cathode power for 6.0 minutes.

5. Sputter platinum with 10% bias, 7 microns argon pressure and 300 watts of cathode power for 2.0 minutes.

DuPont Thick Film Conductor Composition 8553 was obtained, evaluated and used near the end of the program to attach lead wires to the sputtered films. The material is easy to use and forms a very tenacious bond to fused silica when the thickness is controlled. It contains platinum, gold and "probably" borosilicate glass. It can be applied manually, or by screening, and fires at $930^{o}C$. The electrical properties of films formed with 8553 are completely satisfactory and the film appears to be a good substitute for the sputtered platinum-tantalum oxide films.

4.6 FILM LEAD WIRE ATTACHMENT

Using microelectronic circuit lead bonding techniques, attempts were made to thermal compression bond 25 μm diameter gold wire to sputtered platinum films using a Model 8-150-D3 Thermal Compression Pulse Wire Bonder manufactured by Unitek in Monrovia, California. The resulting bonds were good at room temperature but failed after continued exposure to 650° apparently because the platinum film alloyed with the gold causing a loss of adhesion to the fused silica.

Platinum wire, 25 μm in diameter, could be thermal compression bonded to platinum films when full soft wire was used but the resulting bonds, as well as the wire, were weak. Full soft platinum ribbon 25 μm by 76 μm could also be thermal compression bonded to platinum films but the bonds were also weak. To thermal compression bond to platinum-tantalum oxide films that had been exposed to 950°C, a new layer of platinum had to be deposited over the exposed film.

Acceptable lead wire attachments were made by fusing a short piece of 25 μm diameter full soft platinum wire to a 76 μm diameter platinum wire, thermal compression bonding the short 25 μm wire to the platinum film and then firing borosilicate glass over the bond and 25 μm to 76 μm junction. The borosilicate glass was formed by dissolving Vitta Type G-1015 transfer tape with amyl acetate to form a thin paste. The borosilicate thin paste vitrifies at 900°C and forms a tenacious bond to the conductive film and fused silica.

Although DuPont Thick Film Conductor Composition 8553 wasn't obtained and evaluated until near the end of the program, its use appears to provide the best means of attaching lead wires to the deposited films. Using 8553, 25 μm diameter and even 76 μm diameter platinum wire can be attached directly to platinum-tantalum oxide films after they have been exposed to 950°C. The photograph in Figure 13 shows samples of 8553 applied to a 25.4 mm diameter fused silica disc that had previously been coated with a platinum-tantalum oxide film and heated to 950°C. The disc was also heated to 900°C several times after the 8553 samples were applied. One sample of 8553 is shown attaching a 25 μm diameter platinum wire to the film, another is shown attaching a 76 μm diameter platinum wire and three of the 8553 samples shown are simply strips applied directly over the sputtered film. Two of the three strips have been scratched with a dental pick to evaluate the adhesion characteristics.

Further discussions of lead wire connections are included in Sections 4.8 and 5.0.

4.7 FUSED SILICA PROPERTIES

Both the electrical and mechanical properties of fused silica are critically important to the design and performance of the sensor. In terms of sensor performance, the stabilities of the properties with temperature are as critical as the absolute values at room temperature. Eight of the most important properties are discussed below.

1. Thermal expansion - the low thermal expansion of fused silica results in correspondingly reduced effects from thermal gradients and improved resistance to thermal transients and thermal shock. The thermal expansion of fused silica as a function of temperature is compared to that of Inconel x-750 (a common high temperature structural alloy) in Figure 14.

2. Young's modulus - the diaphragm response to pressure is inversely proportional to Young's modulus; the change in diaphragm response to pressure with temperature is inversely proportional to the change of Young's modulus with temperature. Young's modulus of fused silica and Inconel x-750 is shown as a function of temperature in Figure 15. Note that the modulus of Inconel x-750 changes considerably more with temperature than the modulus of fused silica. The approximately 8.8% increase in the modulus of fused silica between 20°C and 650°C has the effect of proportionately decreasing the sensor sensitivity.

3. Poisson's ratio - Figure 16 shows Poisson's ratio of fused silica and Inconel x-750 versus temperature. The approximately 15% increase in the fused silica Poisson's ratio between 20°C and 650°C has the effect of decreasing the diaphragm sensitivity less than 1%.

(The theoretical net effect of increases with temperature of Young's modulus and Poisson's ratio is to cause the fused silica sensor sensitivity at 550° to be about 9.6% less than at 20°C. Empirical data from sensor evaluations, however, consistently demonstrated that the change in sensitivity between 20°C and 650°C was about 7.5%. No explanation was found for the difference.)

4. Modulus of rupture - the average level to which the diaphragm can be stressed without failure is indicated by the modulus of rupture (or breaking strength). Average modulus of rupture of abraded fused silica versus temperature is shown in Figure 17. Since the values increase with temperature, the diaphragm is stronger at high temperature that at room temperature.

5. Elastic limit - hysteretic performance will result from inelastic properties of the diaphragm. Fused silica is highly elastic and its elastic limit (in terms of stress level) approaches the modulus of rupture.

6. Dielectric constant - undesirable, unbalanced, (but unavoidable) capacitances exist in the fused silica sensor components in parallel with the gas dielectric capacitances between the plates. The fused silica capacitances can be initially balanced out, but changes in the dielectric constant with temperature can cause zero shifts in the sensor output. The dielectric constant versus temperature is shown in Figure 18 to be relatively constant with temperature.

7. Volume resistivity - the fused silica components provide the electrical insulation between the plates and between the deposited film leads. When unbalanced resistances in the fused silica become large with respect to the impedance of the pressure-induced capacitance changes, resistive phase components occur in the signal which saturate the signal conditioning electronics. At ten kilohertz, the pressure-induced capacitance changes are on the order of 200 to 300 megohms. The dc volume resistivity of fused silica versus temperature is shown in Figure 19.

8. Loss tangent - increases in the loss tangent in the fused silica components are suspected of causing problems similar to (and difficult to distinguish from) those caused by decreases in the volume resistivity. Increasing the frequency of the sensor excitation voltage decreases the relative effect of changes in both the volume resistivity and the loss tangent. The loss tangent of fused silica at one kilohertz and at ten kilohertz versus temperature is shown in Figure 20.

The properties of fused silica are heavily dependent on the purity of fused silica - especially the electrical properties at elevated temperature. Fortunately, ultra high purity fused silica, produced synthetically using a chemical vapor deposition process, is available from several sources. Two grades of fused silica were used to make sensor components; both were obtained from Dynasil Corporation of America in Berlin, New Jersey. Dynasil 4000 was used in the attempts to build the first eight sensors and Dynasil 1000 was used in the attempts to build the final fourteen sensors. Dynasil considers the 1000 to be of higher purity than the 4000, however the determination is made by testing for transmittance in the far ultraviolet rather than by quantitative analysis. Figure 21 lists typical (for both the 1000 and 4000 grades) high purity fused silica impurities reported by Dynasil. Differences in performance related to the use of the two grades of silica could not be verified. Contrary to the relationship to purity, one of the sensors made using the Dynasil 4000 performed better than any of the sensors made using the Dynasil 1000. Energy dispersive x-ray analysis of recessed discs made of both grades did not find significant impurity differences.

The decrease in volume resistivity, or increase in loss tangent, or both caused degradation in the performance above about 450°C in the initial sensors. The following modifications were made (with success) to reduce the problem:

1. The distance between the plates and the diaphragm thickness was reduced to increase the sensitivity and thereby reduce the relative magnitude of the out-of-phase components.

2. Ground planes were incorporated to reduce capacitance, loss tangent and resistivity effects.

3. The excitation frequency was increased from 3.39 kHz to 10 kHz to increase the in-phase signal component and relatively reduce

the loss tangent and resistivity effects.

4. Excitation and signal phase relationships in the signal conditioning were optimized to reduce the sensitivity to out-of-phase signal components.

4.8 GROUND PLANES

To improve the performance of the sensor at elevated temperature, ground planes were incorporated using deposited conductive films to isolate or "guard" the signal sensed by the capacitive plates on the diaphragm. The ground planes were electrically connected to the signal conditioning system ground. The effect of the ground planes was to isolate the unwanted resistances and capacitances that were electrically parallel with the "gas-dielectric" capacitors formed by the deposited film plates.

Figures 22 through 24 illustrate the effect of the ground planes. Figure 22 is a simple differential capacitor without ground planes, arranged to resemble the fused silica sensor assembly. Figure 23 is the electrical circuit of the differential capacitor shown in Figure 22. The unwanted parallel resistances and capacitances are shown in Figure 23 inside dashed lines. Figure 24 is similar to Figure 22 except ground planes have been added. In Figure 25 it can be seen that the ground planes decouple the signal output electrode from the excitation electrodes so that changes in the unwanted resistances and capacitances will not produce a signal voltage component.

Physically, ground planes were formed on both sides of the diaphragm where the diaphragm was to be bonded to the recessed discs and also on the back face of one of the discs so that the sensor lead wire connection could be isolated from the excitation plate in the recess on the opposite side of the disc. Prior to incorporating ground planes the diaphragm looked like that shown in Figure 26 and the back face of the disc looked like the one on the sensor in Figure 27. Figure 28 is a sketch showing the orientation of the components, with ground planes, for assembly. Figure 29 is a photograph of one side of the sensor components and Figure 30 is a photograph of the other side.

Forming the ground plane pattern on the diaphragm began as a difficult problem but ended with a simple inexpensive technique. The configuration and space available for separating the ground plane from the capacitive plates prevented the use of simple aluminum masks. Photo-resistive coatings could not be used to selectively etch unwanted film because the film is not easily etched. Depositing an aluminum film over the areas which were to be free of platinum-tantalum oxide film, then depositing platinum-tantalum oxide film over the entire diaphragm surface and then using an etchant that penetrated the platinum-tantalum oxide film and removed it while removing the aluminum film beneath it was found to be successful but complicated and expensive.

A computerized laser trimmer (Electro Scientific Industries Model 25) provided a simple inexpensive means of removing the film. Diaphragms were first coated on both sides and the edges (in two sputtering operations). The laser trimmer

was then used to remove the film (from both sides at the same time) to form the pattern shown in Figures 29 and 30. The pair of electrically isolated "ears" on the diaphragm were formed to prevent shorting of the deposited film paths on the recessed discs to the ground plane on the diaphragm. The laser trimmer did not remove film from the edge of the diaphragm; to isolate the ears and the film forming the capacitive plate on the diaphragm from the ground plane the film on the side was removed with a fine diamond grinding wheel.

The lead wire connecting to the capacitive plate on the diaphragm consisted of 25 μm diameter and 76 μm diameter platinum wires fused together and inserted in a tiny fused silica tube so that the fused junction was inside the tube. The 25 μm end was attached with Thick Film Conductor Composition 8553 to the sides of the discs and edge of the diaphragm to provide continuity to the plates on the diaphragm and symmetry with respect to the plates on the discs. Borosilicate glass was used to hold the wire firmly inside the tube and to bond the tube to the ground plane deposited on the back side of the recessed disc as shown in Figure 31.

The lead wires connecting to the ground planes on the sensors were attached to the shields of the excitation lead wires when the sensor assemblies were installed in the cases.

4.9 SIGNAL CONDITIONING

Physically, each signal conditioning channel consisted of a carrying case, a dc power supply module and a signal conditioning mode card. The mode card fits into the dc power supply module, which in turn, fits into the carrying case - as shown in Figures 32 and 33. The carrying case (Model 2993) was purchased from Endevco in San Juan Capistrano, California and modified only to the extent of installing connectors on the rear panel. The dc power supply (Model 4470) was also purchased from Endevco and used without modification. The mode card was originally designed at Boeing for use with high temperature differential capacitive strain gages. The mode cards are now available from HITEC Corporation in Westford, Massachusetts (they are currently manufactured by Endevco for HITEC).

The following items summarize the features of the signal conditioning:

1. Designed specifically for use with differential type capacitive transducers.

2. Supplies low voltage, low frequency balanced and isolated ac excitation to the transducer.

3. Capacitively coupled input to eliminate dc noise voltage effects.

4. Charge sensitive input to reduce cable length effects.

5. Designed to sense extremely small changes in capacitance.

6. Demodulates the ac signal to produce a bipolar analog output.

7. Provides capacitive and resistive balance controls.

8. Provides calibration signals.

9. Relatively insensitive to out-of-phase (resistive) signal components - up to saturation of the electronics.

10. Attenuates ac noise signals.

A block diagram of the signal conditioning is shown in Figure 34. Electrical connections between the transducer and signal conditioning are shown in Figure 35. The signal input circuit, including the charge amplifier, is shown in Figure 36. Figures 37 through 41 show the excitation, balance, calibration, gain and multiplier demodulator circuits. Figure 42 demonstrates schematically the operation of the multiplier circuit. The multiplier output signal, as shown in Figure 42, is filtered to remove the ac component, leaving a dc analog signal proportional to the diaphragm position.

The phase relationship of the ac excitation voltages (shown in Figure 37) and the phase relationship of the amplifier input signal and excitation at the input to the multiplier (in Figure 41) are critical to the elimination of out-of-phase (resistive) signal component effects. Optimum performance is obtained when the ac excitation voltages are exactly 180^{o} out of phase and when the amplified input signal and excitation at the multiplier inputs are exactly in phase. In the "as received" condition, these mode card phase relationships are dependent on the characteristics and tolerances of the electronic components used (which is adequate for most applications). After the first few sensors were evaluated and it was apparent that out-of-phase resistive components were producing an output, resistances and capacitances on the mode card were adjusted slightly to improve the phase relationships.

The ac excitation frequency of the mode cards obtained from HITEC was 3.39 kHz. At the same time the mode card phase relationships were improved, the ac excitation frequency was increased to 10 kHz. The components on the mode cards furnished by HITEC are shown in the circuit diagram in Figure 43. Changing from 3.39 kHz consisted of the following modifications:

Component	From	To
R21, R22, R23, R24	24.9 kΩ (nom.)	8.0 kΩ (nom.)
R33	47.5 kΩ	24.9 kΩ
R17	11 kΩ	20 kΩ
C7	0.01 μF	0.047 μF
C6	0.047 μF	0.01 μF
R27, R28	20 kΩ	4.99 kΩ

Desirable effects resulting from increasing the frequency were: decreased effects of parallel resistances in the sensor, decreased (sensor) loss tangent change with temperature and increased system dynamic response. At 3.39 kHz, cable length changes (between the transducer and signal conditioning) up to 30 m have less than a 1% effect. Although cable length effects with 10 kHz excitation were not evaluated, they can be expected to increase with frequency. At 10 kHz, cable length changes up to 10 m probably cause less than a 1% effect.

4.10 TRANSDUCER CASE

The design and development of the transducer case for housing the sensor was considered secondary to proving and improving the sensor performance. The function of the case was to:

- Provide protection for the sensor and sensor lead wires.
- Provide means for easily mounting and demounting the unit.
- Provide a transition from the small sensor lead wires to larger high temperature extension cables.
- Provide a means to seal the pressure media being measured from the reference pressure.

The seal for isolating the measure and reference pressures consisted of a 0.254 mm diameter annealed gold wire formed in the shape of an o-ring and positioned between the sensor assembly and a lip in the outer case. A Rene 41 spring was compressed against the reference side of the sensor assembly to keep the sensor assembly pressed against the gold o-ring. After temperature cycling to 650°C the seals leaked (with varying degrees). No attempt was made in the program to improve the seal design. Any further efforts associated with this type of pressure transducer should include improvement of the seal design as a primary effort.

The case design and assembly procedures are described in detail in Section 5.0.

5.0 TRANSDUCER FINAL DESIGN AND ASSEMBLY

The transducer final design is considered here to be the design used for Sensor S/N's 19 and 21 which were fabricated and installed in cases, evaluated, and delivered to NASA Lewis Research Center at the end of the program. Significant developments leading to the final design were discussed in Section 4.0. The items below summarize the final design and assembly in sequential steps:

(SENSOR ASSEMBLY)

1. Dynasil 1000 fused silica diaphragm and recessed discs were obtained from Mindrum Precision. Recess depths of 88.9 μm, recess diameters of 8.128 mm and diaphragm thicknesses of 254 μm were specified. All recessed disc corners were chamfered, recessed disc surfaces were polished optically clear and both diaphragm surfaces were polished optically clear. Figure 44 is a drawing of the sensor components.

2. Platinum-tantalum oxide films were sputtered on the fused silica components. Capacitor plate diameters were 6.096 mm. Components with sputtered and laser-trimmed films are shown in Figures 29 and 30.

3. Fused silica components with sputtered films were heated to 950°C to improve the film adhesion quality and verify that continuity of the films would be retained.

4. Low expansion devitrifying frit was sequentially applied manually with a dental pick to each recessed disc bonding surface, after which the diaphragm was sequentially mated wet to each disc and dried at 80°C. Component mating orientations are shown in Figure 28.

5. Pressure of about 50 k Pa was applied to the mated components during firing. The temperature cycle used for firing the frit consisted of heating at a rate of about 220° per hour with one-half hour hold periods at 200°C and 600°C and a one-hour hold period at the maximum temperature of 970°C.

6. Platinum wires 25 μm and 76 μm in diameter were fused together and inserted through a small fused silica tube (0.9 mm o.d., 0.5 mm i.d. and 3.8 mm long). The wire and tube assembly was positioned on the sensor over the deposited film ground plane and above the deposited film lead from the diaphragm. Boro-silicate glass slurry was applied inside tube and at interface of tube and deposited film ground plane, then dried at 80°C.

7. Thick Film Resistor Composition 8553 was applied to surfaces of sensor assembly to provide electrical continuity (where required) across the bond line and to attach platinum wire transition leads to the deposited films. Sensor assembly was heated to 80°C to dry the 8553 and give it the strength to hold the platinum wires in position.

8. Sensor assembly was heated to 900°C to fire the borosilicate and 8553. Photographs of a completed sensor are shown in Figures 45 and 46.

(FABRICATION OF CASE ASSEMBLY COMPONENTS)

9. Case assembly components shown in the drawings of Figures 47a, 47b, 47c, and 47d were purchased and machined.

10. The -6 alumina washer (Figure 47b) was ground to provide relief for the tiny fused silica tube and for the deposited film terminals.

11. The -12 end cap assembly components shown in Figure 47c were brazed in a vacuum furnace at 1050°C.

12. Adapter fittings, shown in the drawing in Figure 48 and in the photograph (on each side of an outer case) in Figure 49, were machined.

(TRANSDUCER ASSEMBLY)

13. The transducer components shown in Figure 50 were assembled as shown in the -1 assembly drawing of Figure 47d. (The gold o-ring is not shown in Figure 50.) These components were assembled using the fixture shown in Figure 51. The components are shown in the process of being assembled in Figure 52. A magnified photograph of part of the transducer in the assembly fixture is shown in Figure 53.

14. The -2 outer case (Figure 47b) was electron beam welded to the -3 end plate of the -12 end cap assembly (Figure 47c). The completed assembly is shown in Figures 54 and 55.

(HIGH TEMPERATURE EXTENSION CABLES)

15. One-meter long flexible high temperature cables with stainless steel conductors, quartz fiber electrical insulation and braided stainless steel shields were used to connect to the -8 and -9 (Figure 47a) leads of the transducer. The flexible cables are available as Types 030-1/30SS and Q30-2/30SS from Maser Hitemp Wires, Division of Addington Laboratories, in Covina, California.

16. Cable transition couplings shown in Figures 56 and 57 were assembled on transducer leads and cables as shown in Figure 58. Lead wires and coupling components were spot-welded together. A pressure transducer with high temperature lead wires and an adapter fitting is shown in Figure 59. (The transition couplings in Figure 59 are an earlier version of the couplings shown in Figure 58.)

6.0 TRANSDUCER PERFORMANCE

6.1 DEVELOPMENTAL EVALUATIONS

The table in Figure 60 compares the characteristics of sensors and signal conditioning configurations that were evaluated and provides a summary that relates configuration changes to performance.

Referring to Figure 60, Sensor S/N 2 was the first unit evaluated and although it performed well at intermediate temperatures, it exhibited large zero shifts and changes in sensitivity at 650°C. The distance between the plates of Sensor S/N 5 was greater than in Sensor S/N 2, but the results of evaluations of Sensor S/N 5 were similar to those of Sensor S/N 2 and confirmed that the performance was dependent on other factors that were common to both units.

Sensor S/N 7 was evaluated in three different manners: first, mounted in the test fixture with 3.39 kHz excitation; second, mounted in the test fixture with 10 kHz excitation and optimized phasing in the signal conditioning; and third, mounted in a case with 10 kHz excitation and optimized phasing in the signal conditioning. (At the time that the signal conditioner excitation frequency was changed to 10 kHz, the phase relationship between the excitation voltages was adjusted to within a few minutes of 180° and the phase relationship of the sensor and excitation inputs to the multiplier were adjusted to within a few minutes of 0°.) With 3.39 kHz excitation, the zero shift at 650°C of Sensor S/N 7 was comparable to the shifts exhibited by Sensor S/N's 2 and 5. The reduced diaphragm thickness of Sensor S/N 7 increased its sensitivity to pressure, but did not appreciably improve the zero shift or sensitivity change characteristics at 650°C. Changing from 3.39 kHz to 10 kHz excitation and optimizing the signal conditioner phase relationship considerably improved the performance at 650°C. Increasing the frequency decreased the effects of parallel resistances in the sensor - thus decreasing the effects of the resistive (out-of-phase) signal component. Optimizing the phase relationships did not reduce the resistive phase signal component but did reduce its ability to produce a demodulated analog output signal. No explanation was found for the slightly degraded performance of Sensor S/N 7 when it was installed in a case.

Sensor S/N 8 was the first unit to incorporate ground planes and the resulting improved performance at 650°C is evident in Figure 60. The results of the evaluations of Sensor S/N 8 confirmed that the zero shift with temperature was being caused by stray parallel resistances and capacitances in the sensor assembly, that stray resistances were producing out-of-phase (resistive) signal components which were saturating the signal conditioning electronics at 650°C and that the large changes in sensitivity at 650°C were being caused by the saturation. Sensor S/N 8 also demonstrated that greatly reducing the distance between plates increased the sensitivity to pressure without causing detrimental effects.

Sensor S/N's 19 and 20 were both evaluated at two different signal conditioner gain levels - one which produced five volts output at 69 kPa and one which produced two volts. The values in Figure 60 indicate that out-of-phase (resistive) components were still affecting the sensor performance at 650°C and that the effects are greatly reduced at reduced gains.

The thinnest diaphragm used in any of the sensors evaluated was 203 μm thick. In Figure 61, the deviation (from a linear output) of Sensor S/N 7 (with a 203 μm diaphragm) shows no evidence of non-linearity resulting from the relatively greater diaphragm displacement. (Reducing the distance between plates - with a slightly thicker diaphragm - also showed no evidence of non-linearity as can be seen in the data from Sensor S/N's 19 and 21 which is discussed below in Section 6.2.)

The choice of the optimum diaphragm thickness was also influenced by the effect of overpressures. Figure 62 lists the response of Sensor S/N 8 (with a 254 μm thick diaphragm) to differential pressures as high as 207 kPa. The hysteresis prior to being subjected to overpressure was established as ±0.1% f.s.; after being exposed to +207 kPa and -95 kPa at 20°C, and +138 kPa at 650°C, the hysteresis at 20°C increased to 0.3% f.s. Considering the increased stress levels that would occur in a 203 μm thick diaphragm and the surface imperfection sensitivity of fused silica, a nominal diaphragm thickness of 245 μm was used in all sensors after Sensor S/N 8.

6.2 FINAL RESULTS

The performance of Sensor S/N's 19 and 21 represents the final results of the program. The sensitivity change with temperature of Sensor S/N 19 with the signal conditioner gain adjusted for five volts output at 69 kPa and 20°C is shown in Figure 63. At 650°C the signal conditioning electronics are saturated and the sensitivity is reduced as explained in the preceding section. At 604°C however, the sensor is performing properly. All the data which are shown in Figures 64 through 80 and discussed below were obtained with the signal conditioner gain adjusted for two volts output at 69 kPa and 20°C.

Figures 64 and 65 show the sensitivity change with temperature, after being corrected for zero shift, of Sensor S/N's 19 and 21 respectively. Sensitivities of both units are affected at 650°C, although not in the same manner. It is apparent that the signal conditioning electronics approached saturation between 619°C and 650°C (in Figure 64) causing a disparity in the positive pressure sensitivity at 650°C. It is probable that the reduced change in negative pressure sensitivity of Sensor S/N 21 at 650°C, as shown in Figure 65, was also caused by saturation in the signal conditioning.

Figures 66 and 67 depict all the data recorded from Sensor S/N's 19 and 21 in a series of pressure cycles at stabilized temperatures to 650°C. Sensor outputs were recorded at 13.8 kPa increments at each temperature during two positive pressure cycles to 69 kPa followed by two negative pressure cycles and a final positive pressure cycle. Although zero shifts can be adjusted at the signal conditioner, no adjustments were made. Considerably more than

one-half of the error band can be attributed to data that were recorded above 600°C. It should be noted in Figures 66 and 67 that some of the errors resulting from the change in sensitivity with temperature (as shown in Figures 64 and 65) are reduced when the data include zero shifts.

Figures 68 and 69 show the zero shift with temperature of Sensor S/N's 19 and 21. The fact that Sensor S/N 19 has a positive shift while Sensor S/N 21 has a negative shift might indicate that the zero shift is caused by small differences in dimensional tolerances rather than by the general design. Although tests were not made to determine the response to transient temperatures, the Sensor S/N 21 zero shift increased to 5.6% while it was cooling from 650°C as shown in Figure 69.

Figures 70 through 76 represent a sequential series of temperature tests; they show the deviation of the output of Sensor S/N 19 from a straight line through zero as a function of pressure at temperatures to 650°C. The graphs reflect neither the zero shift with temperature nor the change in sensitivity with temperature - simply the response to two positive, two negative and one positive pressure cycles. The initial zero shift with temperature at the start of each series of pressure cycles was subtracted from each measurement. In addition, a single (but different) full-scale (69 kPa) output voltage was used to establish the linearity base at each temperature. Figures 77 through 80 show the same kind of data from a sequential series of temperature tests of Sensor S/N 21.

Up to 538°C, the maximum deviation shown for the outputs of either Sensor S/N 19 or Sensor S/N 21 is ±0.7% f.s. In Figure 70, the maximum deviation shown for Sensor S/N 19 at 619°C is ±0.9% f.s. At 650°C the maximum deviations for Sensor S/N's 19 and 20 are ±4.5% f.s. and 2.3% f.s. respectively. At 20°C after the pressure and temperature cycles, the deviations of the sensors were no greater than ±0.7% f.s.

7.0 CONCLUSIONS

- These pressure transducers were designed and built for dynamic pressure measurement applications. The dynamic pressure response should be evaluated.

- Without making temperature corrections the pressure transducers, as built and evaluated in this program, can be used to measure static pressures up to 69 kPa at temperatures between 20°C and 650°C with an uncertainty of less than ±6%; below 600°C the uncertainty is less than ±3%.

- Some limited improvement in the response at 650°C could be made by modifying the signal conditioning electronics to further reduce the effects of the out-of-phase resistive components.

- There is a possibility of contamination through the holes in the recessed disc that could affect the sensor response. A flush mounted design that would eliminate the possibility of contamination and offer improved dynamic response should be built and evaluated.

- Thick film conductor compositions should be considered as a substitute for the sputtered conductive films.

- The manner in which the sensor assembly is held and sealed within the stainless steel case should be improved. A "positive" seal would be most desirable.

- Larger-diameter pressure transducers would be easier to build and could be expected to have better performance than smaller-diameter units Attempts to build smaller-diameter pressure transducers should not be attempted until the items listed above have been resolved.

- The techniques developed and used in this program could be used to build high temperature accelerometers.

BIBLIOGRAPHY

1. Ettre, Kitty. "Sealing Quartz Parts with Glass Transfer Tape", Fusion, November 1970.

2. Shand, E. B. Glass Engineering Handbook, Second Edition, New York, McGraw-Hill Book Company, 1958, 484 pp.

3. Fused Silica Catalog No. 702, Dynasil Corporation of America, Berlin, New Jersey.

4. High Temperature Optical Glasses, Low Expansion Materials, Fused Silica No. 7940 Catalog, Corning Glass Works, Corning, New York.

5. Bruckner, R. "Properties and Structure of Vitrious Silica I and II", Journal of Non-Crystalline Solids, Vol. 5, Part I: pp 123-175, North-Holland Publishing Company.

6. Owen, A. E. and R. W. Douglas. "Electrical Properties of Vitreous Silica", Journal Society of Glass Technology, Vol. 43, 1959.

7. Coble, D. L. and L. B. Weckesser. "Electrical, Mechanical and Thermal Properties of Alumina, Fused Silica and Pyroceram 9606". Engineering Memo, Applied Physics Laboratory, John Hopkins University, Silver Spring, Md., Dec. 7, 1964.

8. Nieberding, W. C. and D. R. Englund, Jr., Modularized Instrument System for Turbojet Engine Test Facilities, NASA TMX-68123, Sept. 1972.

9. Hopper, R. T. "How to Apply Noble Metals to Ceramics", Ceramic Industry Magazine, June 1963, p. 65.

10. Kubaschewski, O. "Practical Aspects of Metallurgical Thermodynamics - Applications to the Platinum Metals", Platinum Metals Review, Vol. 15, No. 4, October 1971, p. 134.

11. U. S. Patent No. 3,852,672, "Four-Quadrant Multiplier-Notch Filter Demodulator", E. J. Nelson, 1973.

12. Capacitive Strain Measuring System, Operation Manual Written at Boeing Aerospace Company, January 1973. Available from HITEC Corp., Westford, Ma.

13. Cheney, R. and N. E. Samek. "Sputtered Thin Films for Pressure Transducers", Research/Development, Vol. 28, No. 4, p. 53, April 1977.

14. Coon, G. W. A Capacitive Accelerometer Suitable for Telemetry, NASA Technical Memorandum, NASA-TM-X-2644, NASA Ames Research Lab, Sept. 1972.

BIBLIOGRAPHY, CONTINUED

15. Coon, G. W. and D. R. Harrison, "Miniature Capacitive Accelerometer", Instrumentation Technology, Vol. 14, No. 3, p. 52, Mar. 1967.

16. U. S. Patent No. 3,027,769, Diaphragm Type Capacitance Transducer, G. W. Coon, 1962.

17. U. S. Patent No. 2,581,359, Electromagnetic Pressure Sensitive Device, J. Clark, 1947.

18. U. S. Patent No. 2,952,000, Pressure Measuring Apparatus, C. Wolfe, 1960.

19. U. S. Patent No. 3,238,479, Transducer, P. K. Church, 1963.

20. U. S. Patent No. 2,907,320, Pressure Capacitance Transducer, C. R. DeWese, et al, 1959.

21. U. S. Patent No. 3,405,559, Pressure Transducer, E. F. Moffatt, 1968.

22. U. S. Patent No. 3,645,137, Quartz Pressure Sensor, E. J. Hazen, 1972.

23. U. S. Patent No. 3,793,885, Diaphragm Construction for Differential Pressure Transducer, R. L. Frick, 1974.

24. U. S. Patent No. 3,618,390, Differential Pressure Transducer, R. L. Frick, 1974.

25. U. S. Patent No. 3,800,413, Differential Pressure Transducer, R. L. Frick, 1974.

26. U. S. Patent No. 3,697,835, Capacitive Pressure Transducer, G. Satori, 1972.

27. U. S. Patent No. 3,703,828, Capacitance Variometer, E. R. Bullard Jr., 1972.

28. U. S. Patent No. 3,750,476, Pressure Transducer, N. L. Brown, 1973.

29. Vick, G. L., et al, High Temperature Solid State Pressure Transducers for Military Jet Engine Environments, Air Force Flight Dynamics Lab. Report No. AFFDL-TR-73-145, Oct. 1973.

30. Timoshenko, S. Theory of Plates and Shells, McGraw-Hill Book Company, New York, 1940, pp 492.

31. Pastan, H. L. Principles of Dynamic Pressure Measurement, Feb. 1963, pp 12.

32. Nyland, T. W., D. R. Englund and R. C. Anderson, On the Dynamics of Short Pressure Probes: Some Design Factors Affecting Frequency Response, NASA TND-6151, Feb. 1971.

33. Ladwig, J. E. A Precision Capacitive Pressure Transducer Suitable for Airborne Applications, Instrument Society of America Preprint No. 16.11-2-66, Oct. 1966.

34. Lawford, V. N. Pressure Measurements in Sodium Systems, Instrument Society of America Paper No. 71-627, Oct. 1971.

35. Jones, R. V. and J. C. S. Richards. "The Design and Some Applications of Sensitive Capacitance Micrometers", Journal of Physics E: Scientific Instruments, Vol. 6, 1973.

36. Schofield, J. W., "A Linear Capacitance Micrometer", Journal of Physics E: Scientific Instruments, Vol. 5, 1972.

37. Rule, E., F. J. Suellentrop and T. A. Perls, "Capacitive Accelerometers with Optimum Frequency-Response Characteristics", The Journal of the Acoustical Society of America, Vol. 33, No. 1, Jan. 1961.

38. Cook, G. W. "Measuring Minute Capacitance Changes", Electronics, Jan. 1953.

39. Levine, R. J. Capacitance Transducer Theory Design Formulae and Associated Circuitry, Instrument Society of America Preprint No. 13.1-2-65, Oct. 1965.

40. "Capacitive Pressure Sensors", Instruments and Control Systems, Vol. 35, May 1962.

41. Norris, E. B. and Yeakley, Development of System for Monitoring In-Service Strains in Power Plant Piping, Prepared by Southwest Research Institute for Electric Power Research Institute, EPRI NP-186, Jan. 1976.

42. 2000°F Accelerometer Development, Interim Technical Report, Contract F33615-75-C-3027, submitted by Kaman Sciences Corp. to Air Force Flight Dynamics Laboratory, May 1975.

43. Schneider, J. C. and Richard K. Duke. Phase II Development of 1093°C (2000°F) Prototype Microphone Transducer, Air Force Flight Dynamics Laboratory Technical Report AFFDL-TR-74-136, Dec. 1974.

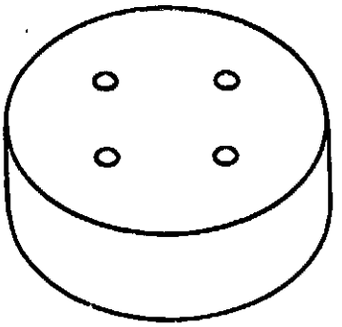

RECESSED DISC

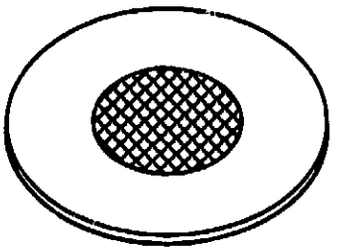

DIAPHRAGM

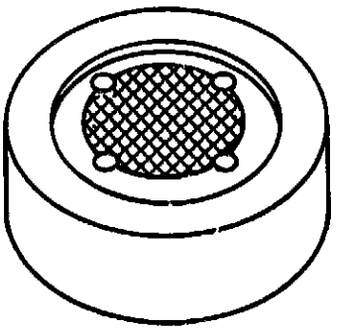

RECESSED DISC

Figure 1. Fused Silica Sensor Assembly Components

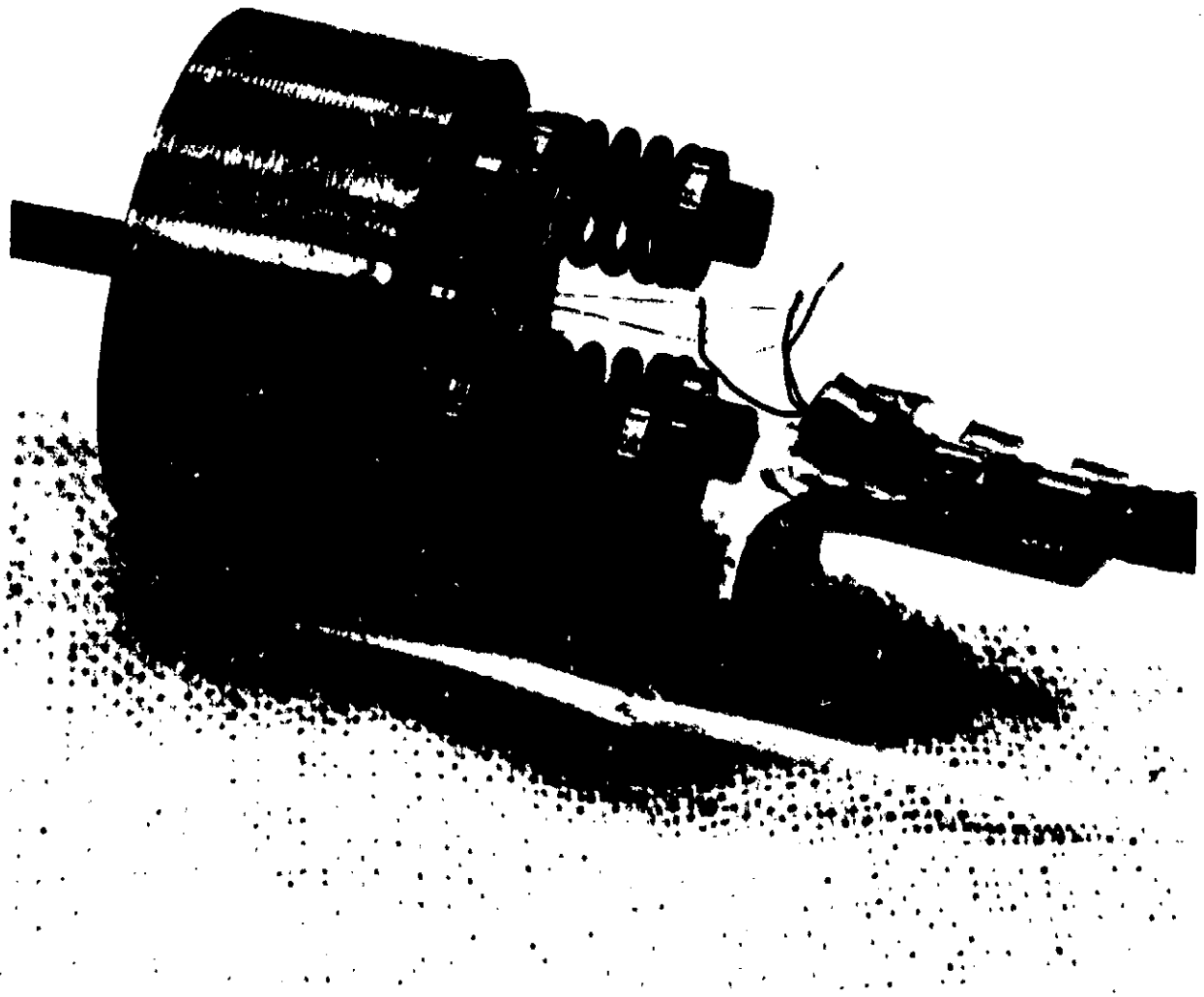

Figure 2. Sensor Assembly Test Fixture

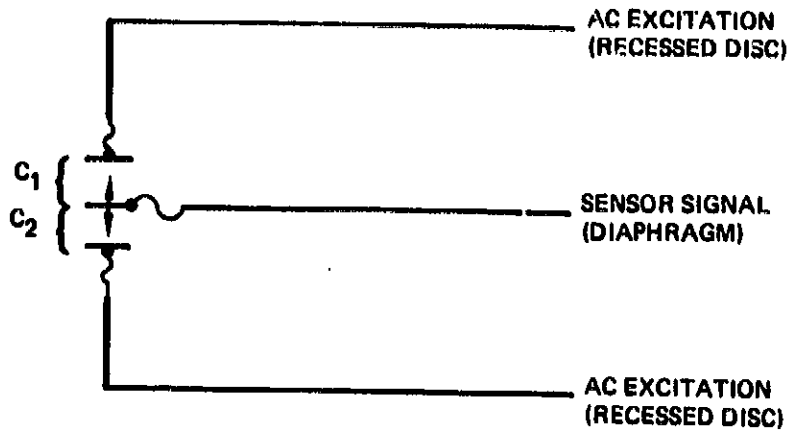

Figure 3. Differential Capacitor Formed With Two Capacitors

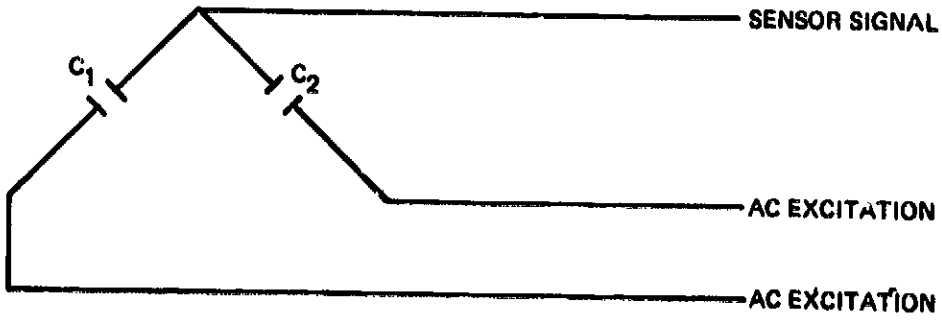

Figure 4. Differential Capacitor in Half-Bridge Configuration

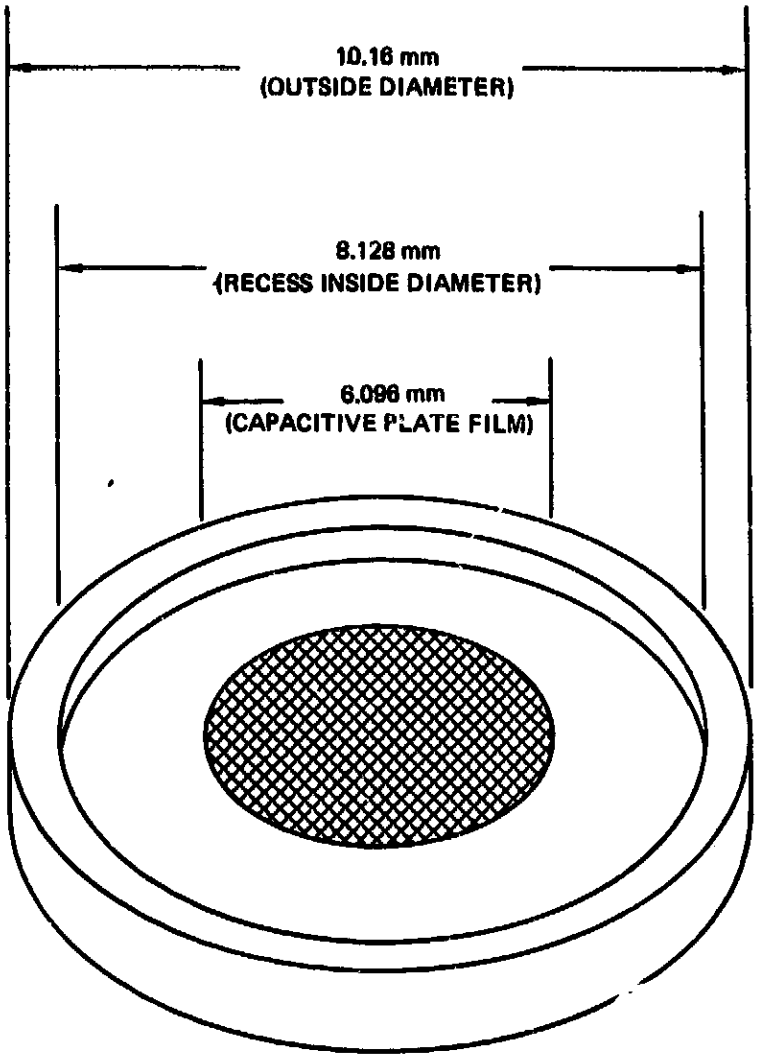

Figure 5. Recessed Disc Design Diameters

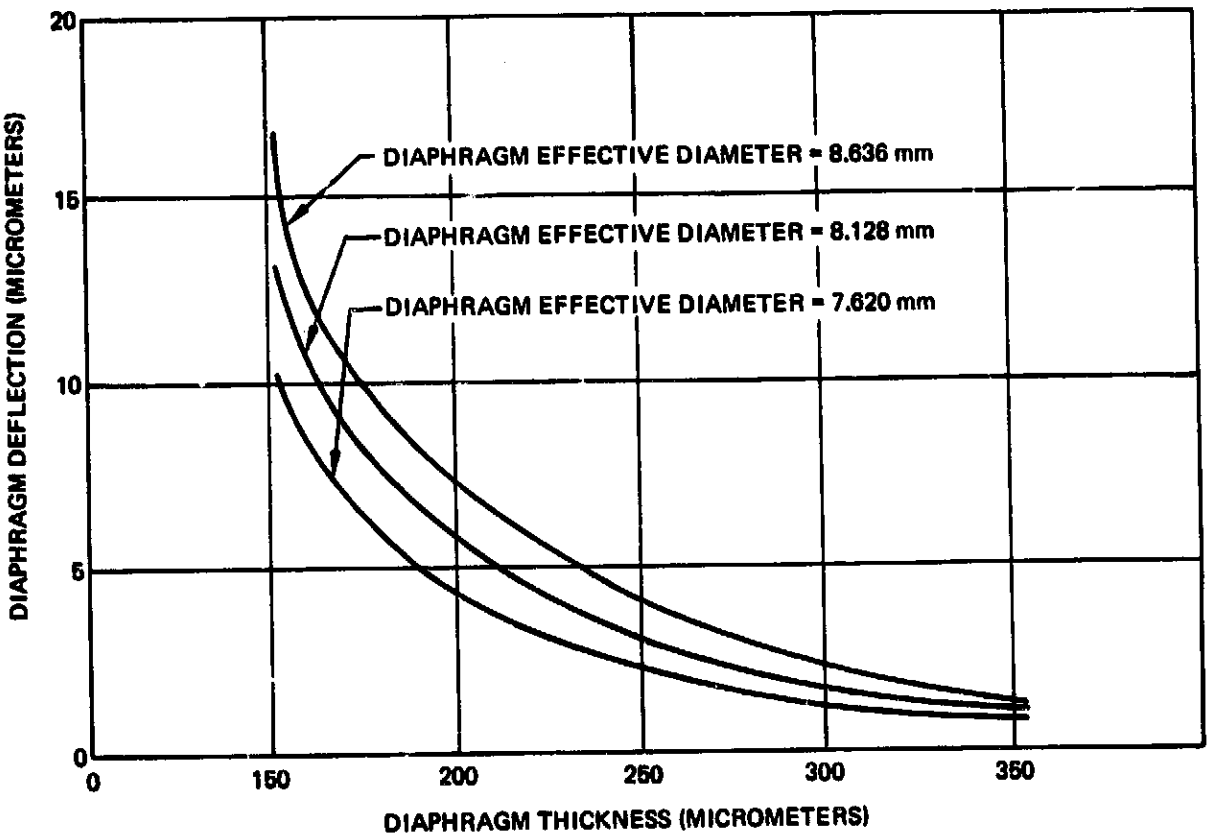

Note: The curves above are calculated values for the deflection of the center of the diaphragm in response to a differential pressure of 69 kPa.

Figure 6. Diaphragm Deflections as a Function of Thickness and Effective Diameter

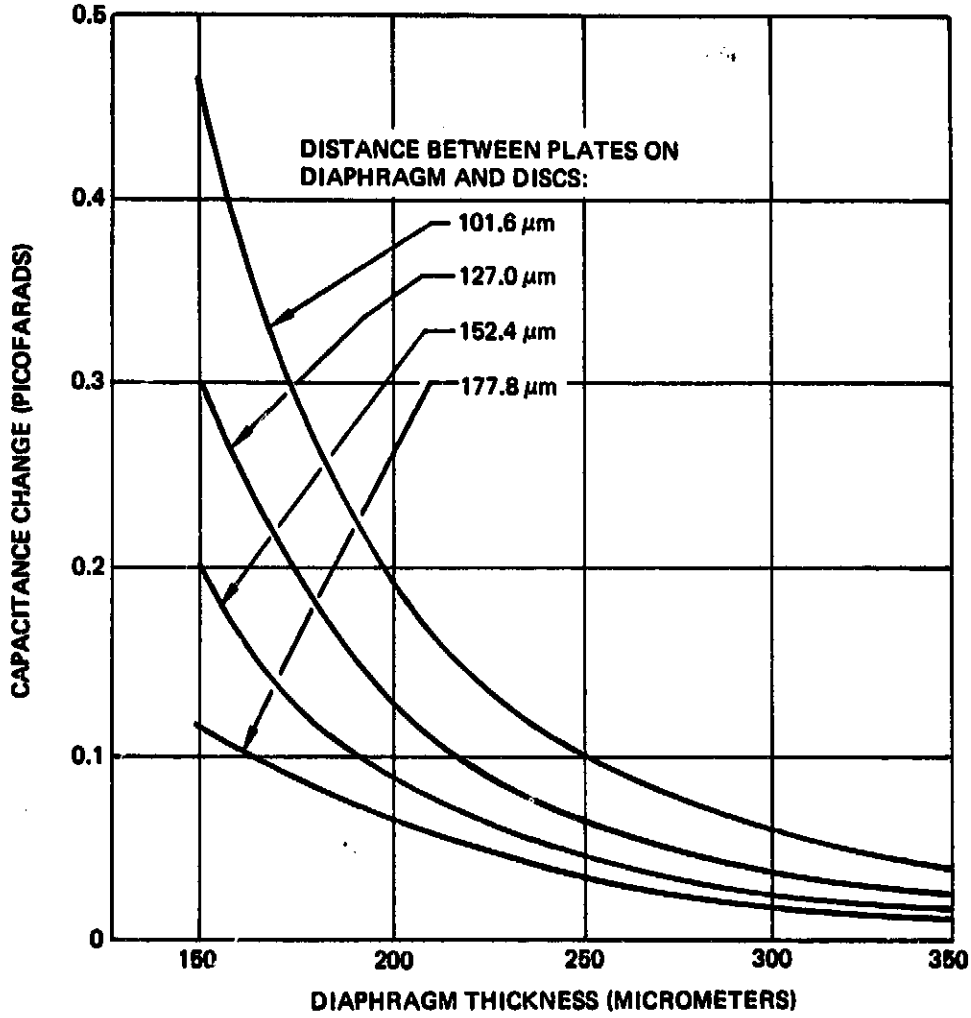

Note: The calculated capacitance changes above represent the sum of both differential capacitive elements with an effective diaphragm diameter of 8.128 mm in response to a differential pressure of 69 kPa.

Figure 7. Capacitance Change as a Function of Diaphragm Thickness and Plate Distance

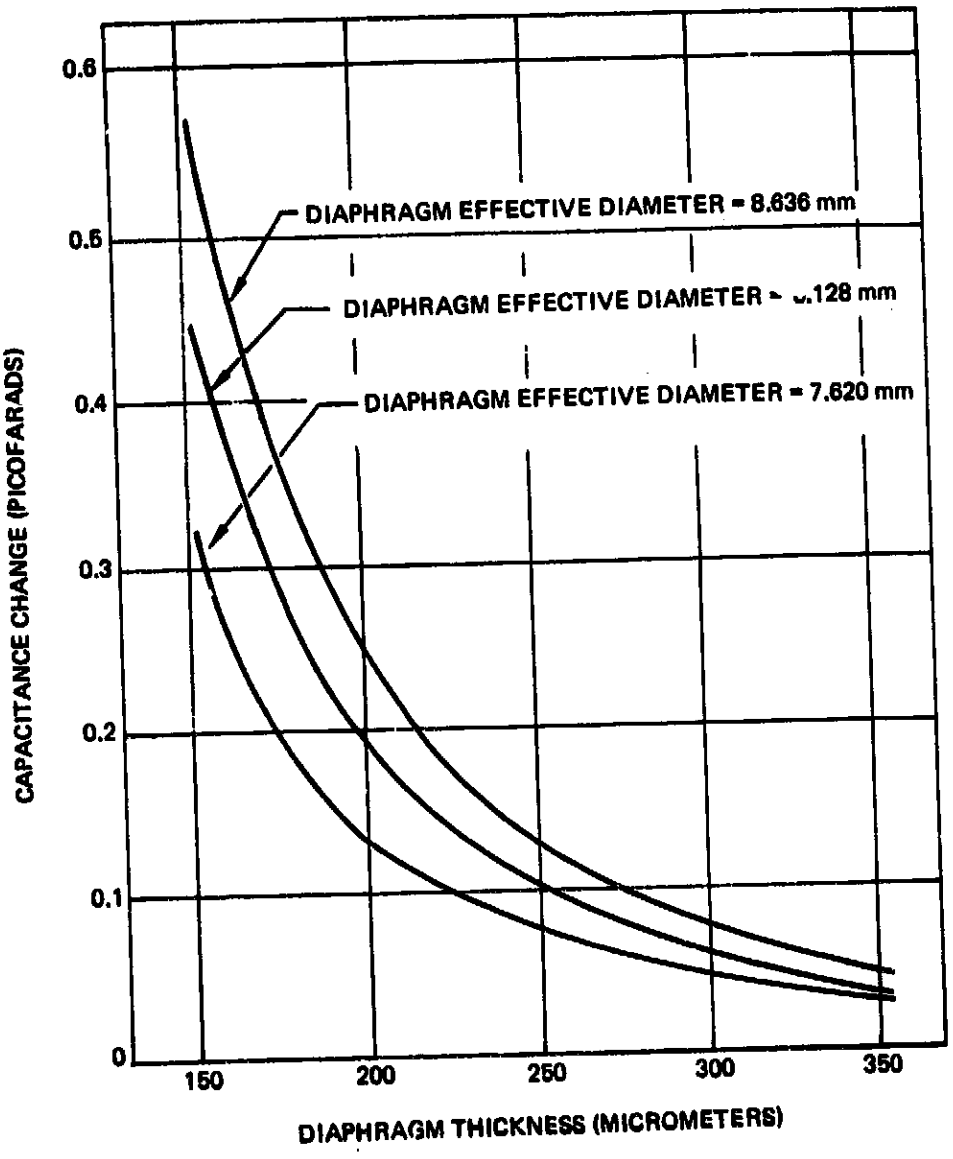

Note: The curves above represent the sum of both differential capacitive elements with a distance of 101.6 μm between plates on the diaphragm and discs in response to a differential pressure of 69 kPa.

Figure 8. Capacitance Change as a Function of Diaphragm Thickness and Effective Diameter

Sensor number	Diaphragm thickness (μm)	Distance between plates (μm)	Total capacitance change (pF)
2	305	150	0.0315
5	305	180	0.0287
6	305	180	0.0243
7	203	180	0.072
8	254	100	0.111
16	248*	110*	0.081
19	248*	110*	0.072
20	248*	110*	0.075
21	243*	130*	0.0688
22	243*	110*	0.106

*Asterisked values are considered more accurate.

Figure 9. Measured Total Capacitance Changes

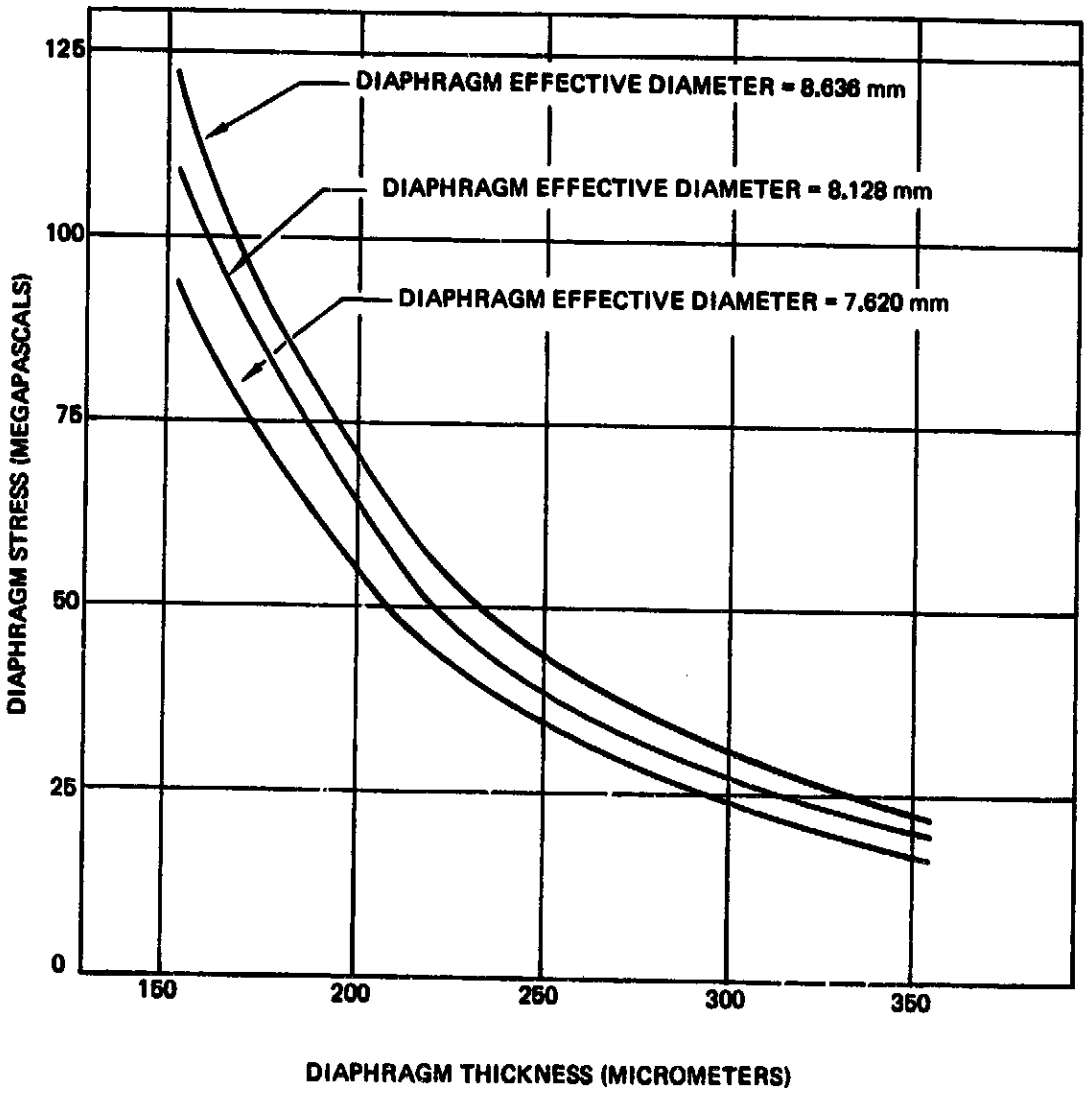

Note: The curves above are calculated maximum diaphragm stresses in megapascals resulting from an applied differential pressure of 207 kPa.

Figure 10. Maximum Diaphragm Stresses

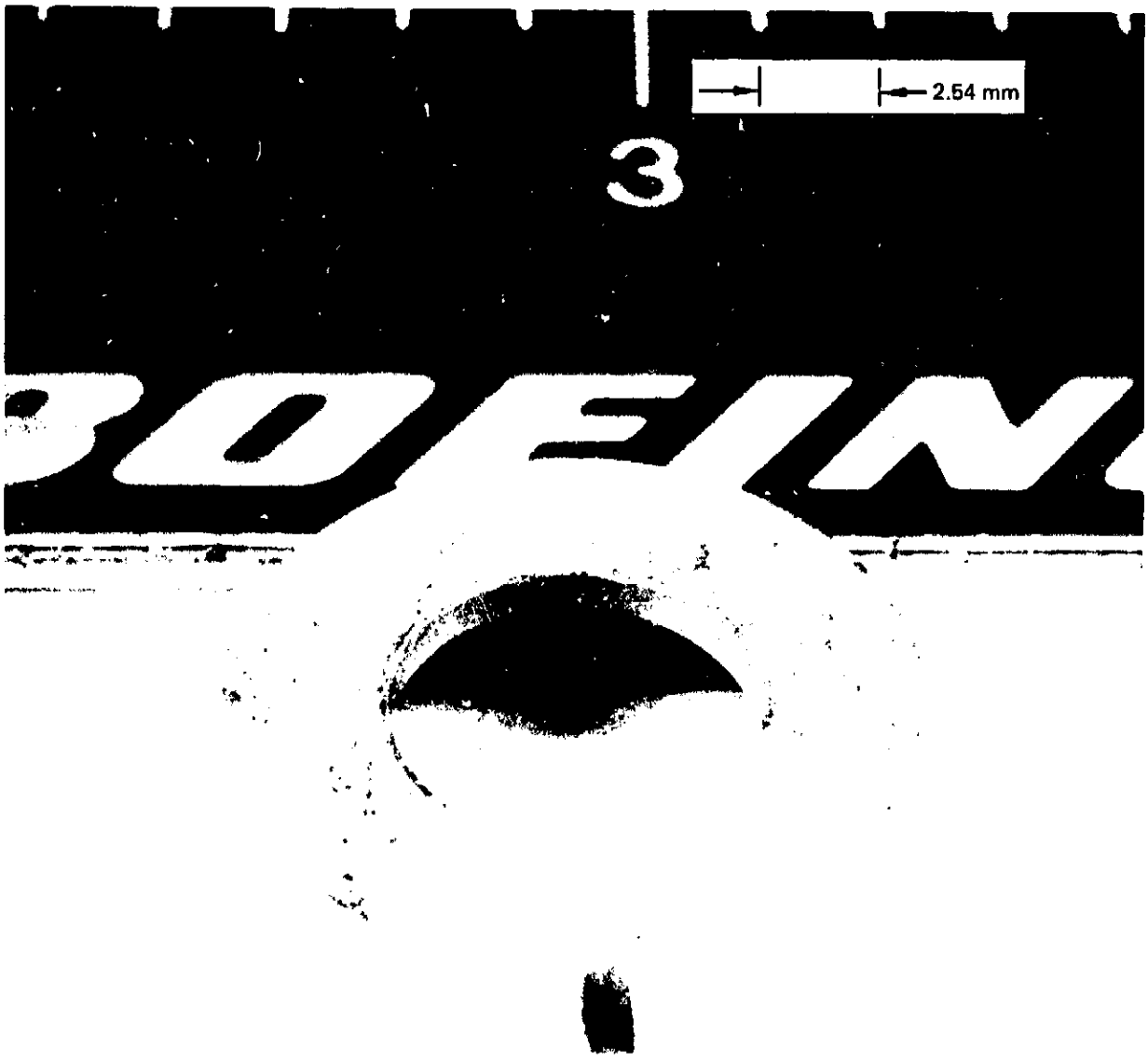

Figure 11. Sputtering Mask for Recessed Disc Capacitor Plate

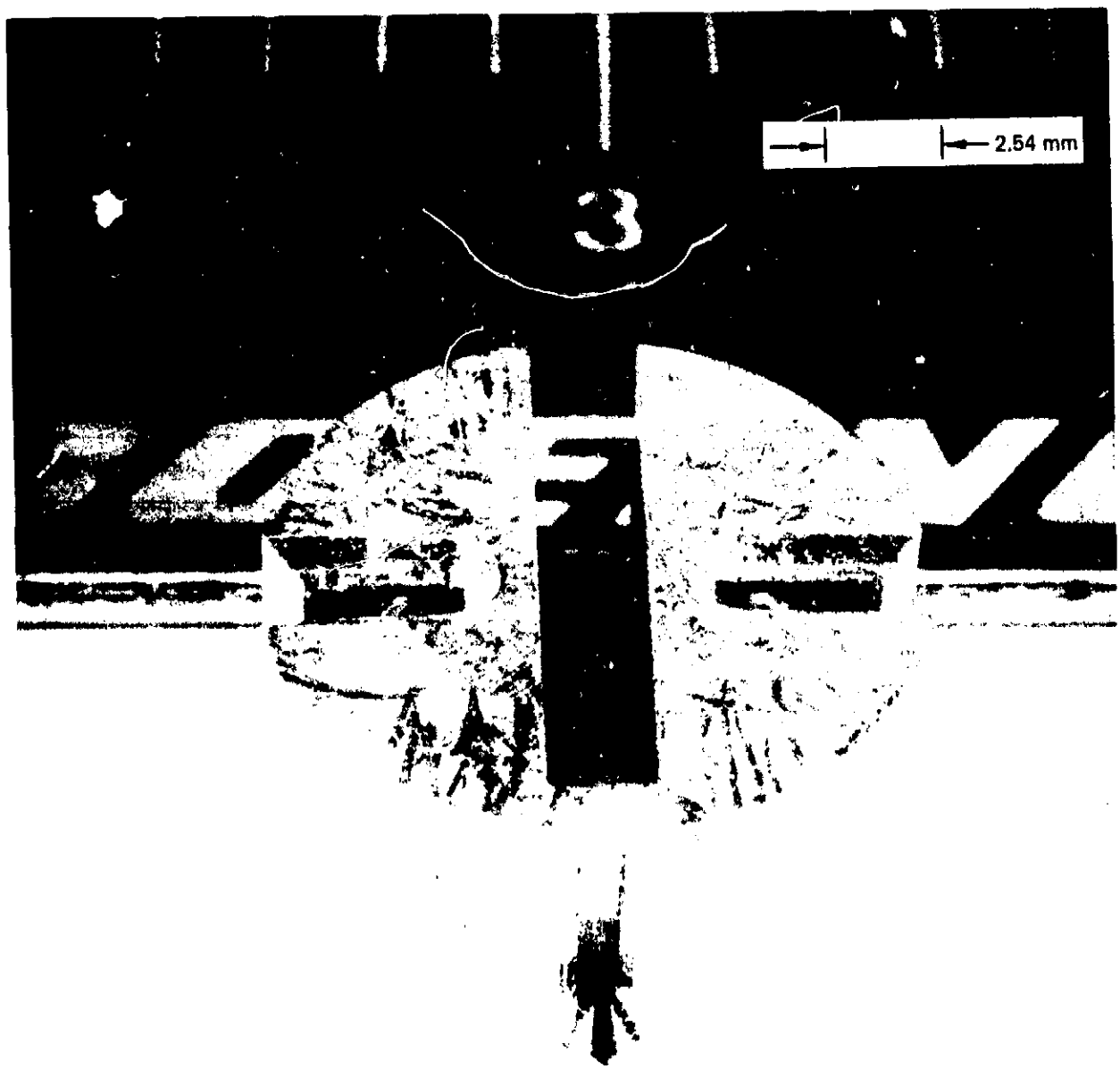

Figure 12. Sputtering Mask for Terminals on Back of Disc

Figure 13. Thick Film Conductor Composition of Platinum-Tantalum Oxide Film

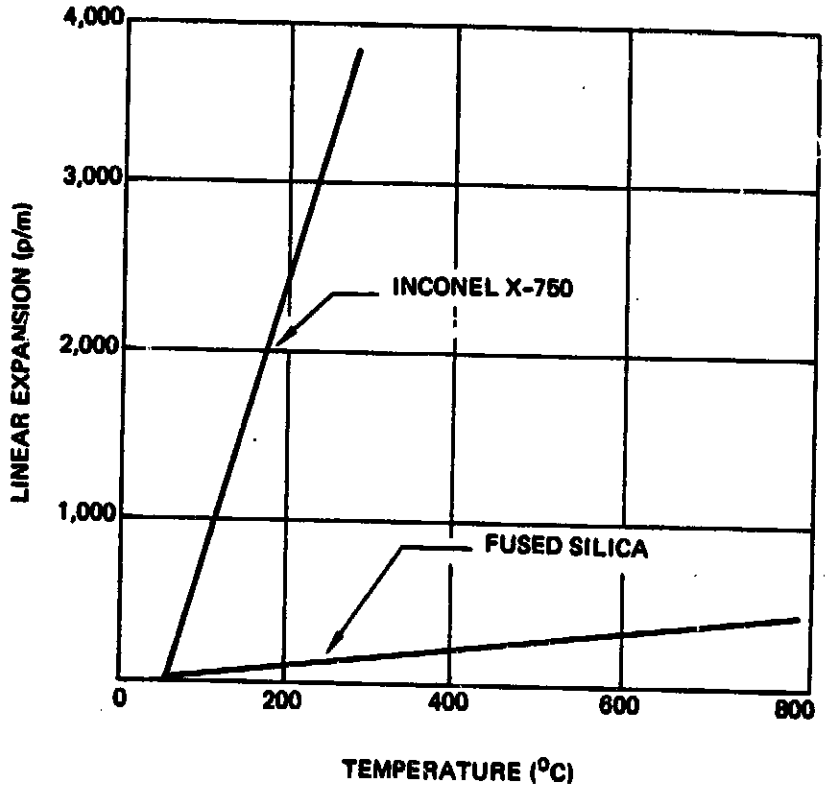

Figure 14. Thermal Expansion of Fused Silica and Inconel X-750 as a Function of Temperature

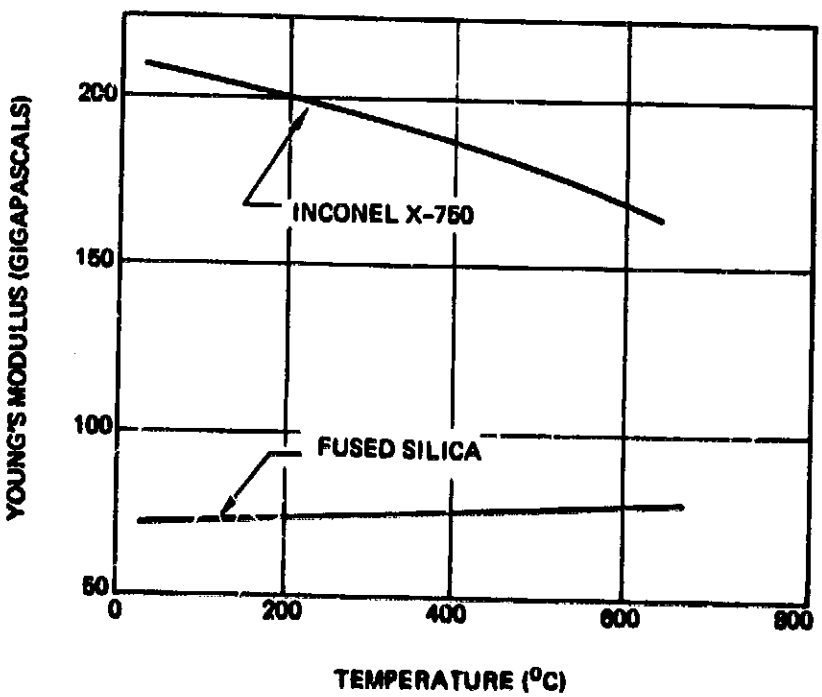

Figure 15. Young's Modulus of Fused Silica and Inconel X-750 as a Function of Temperature

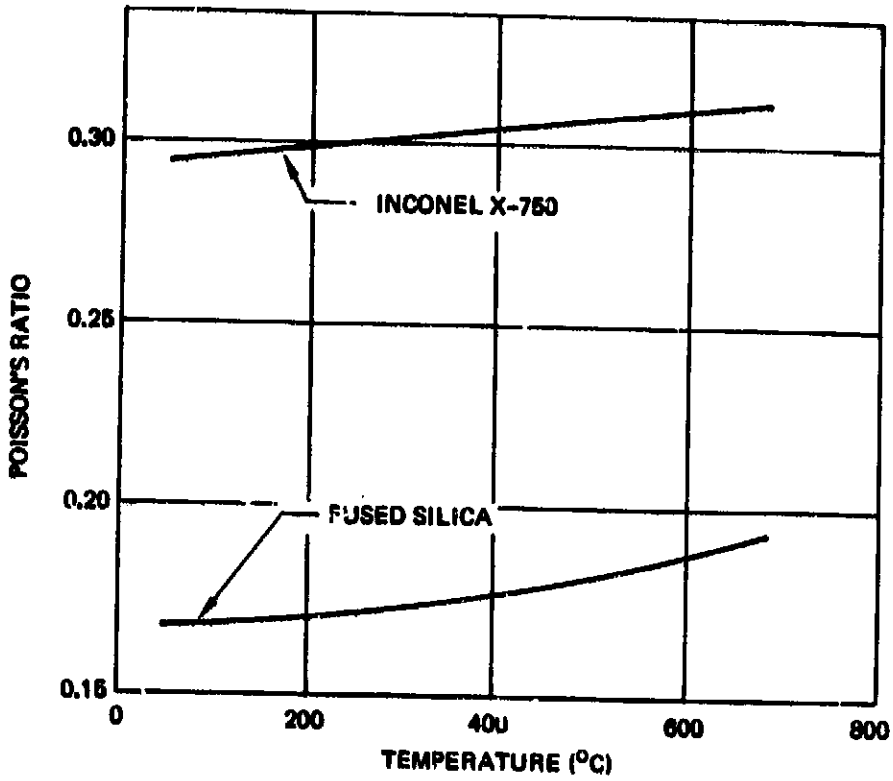

Figure 16. Poisson's Ratio of Fused Silica and Inconel X-750 as a Function of Temperature

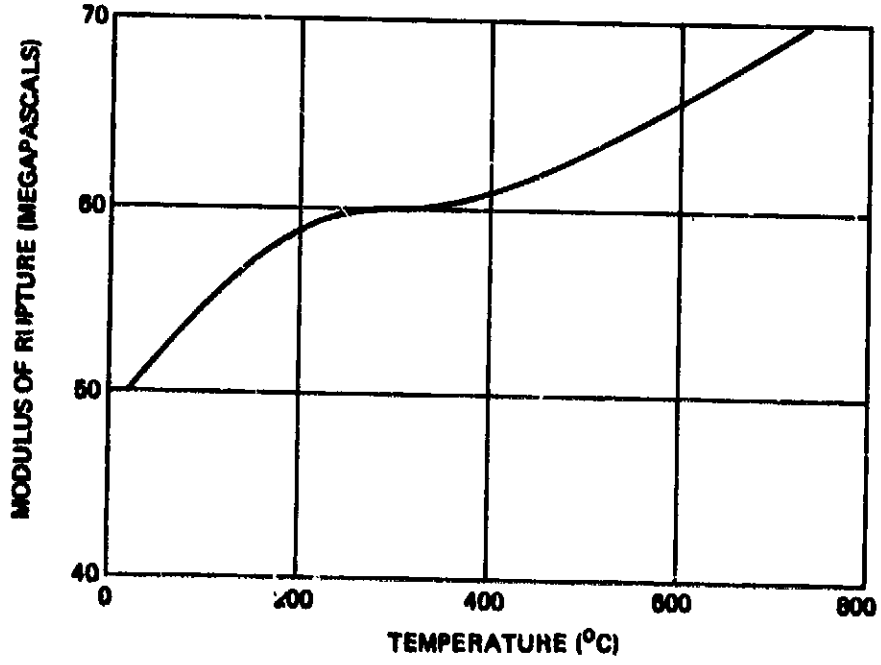

Figure 17. Modulus of Rupture of Fused Silica Versus Temperature

Temperature (°C)	Dielectric constant	
	1 kHz	10 kHz
25	3.826	3.826
100	3.834	3.834
200	3.843	3.843
300	3.858	3.856
400	3.898	3.870
500	3.992	3.886

Figure 18. Dielectric Constant of Fused Silica Versus Temperature

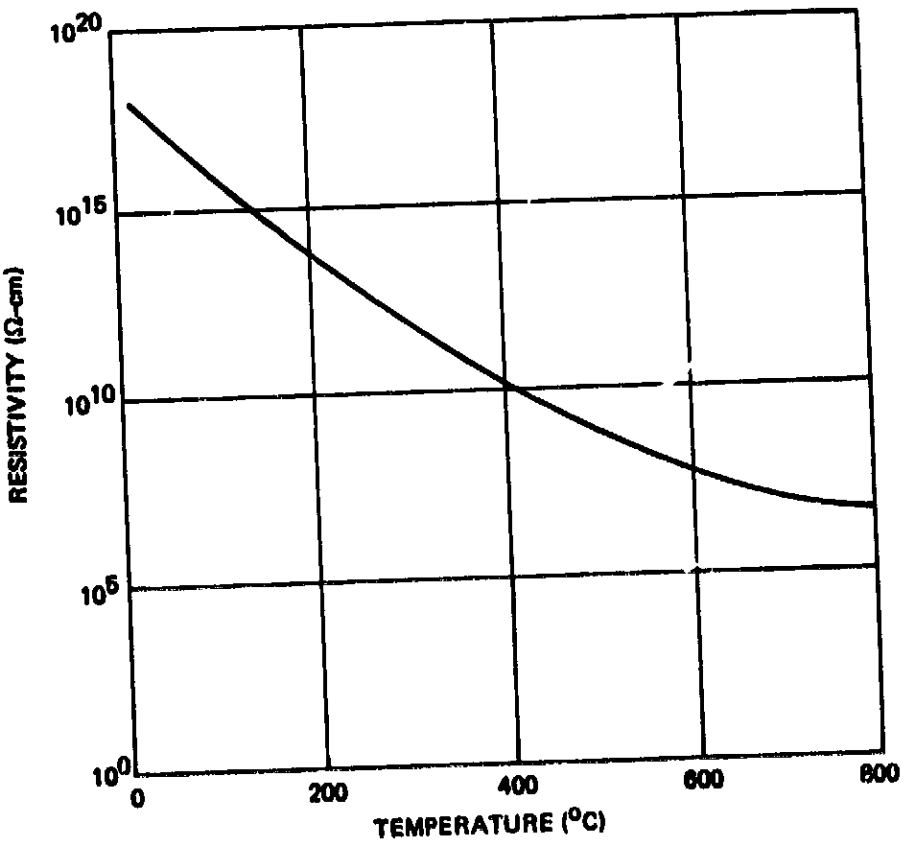

Figure 19. Volume Resistivity of Fused Silica Versus Temperature

Temperature (°C)	Loss tangent	
	1 kHz	10 kHz
25	< 0.000002	< 0.000005
100	< 0.000002	< 0.00002
200	0.00016	0.00003
300	0.00930	0.00093
400	0.207	0.0207
500	1.356	0.140

Figure 20. Loss Tangent of Fused Silica Versus Temperature

Element		Impurities (p/m)
Aluminum	(Al)	< 0.02
Antimony	(Sb)	0.0004
Arsenic	(As)	ND*
Beryllium	(Be)	< 0.03
Bismuth	(Bi)	< 0.04
Boron	(B)	< 1.0
Bromine	(Br)	0.0025
Cadmium	(Cd)	< 0.08
Cesium	(Cs)	ND
Chlorine	(Cl)	88.5
Chromium	(Cr)	0.006
Cobalt	(Co)	0.001
Copper	(Cu)	ND
Gallium	(Ga)	< 0.02
Germanium	(Ge)	< 0.06
Gold	(Au)	0.001
Iron	(Fe)	0.20
Lithium	(Li)	0.20
Manganese	(Mn)	ND
Rubidium	(Rb)	ND
Silver	(Ag)	ND
Sodium	(Na)	0.02
Thallium	(Tl)	< 0.05
Titanium	(Ti)	ND
Vanadium	(V)	ND
Zinc	(Zn)	ND

Note: The water content is approximately 600 to 1,000 p/m.
*ND = not detectable

Figure 21. Dynasil Fused Silica Impurities

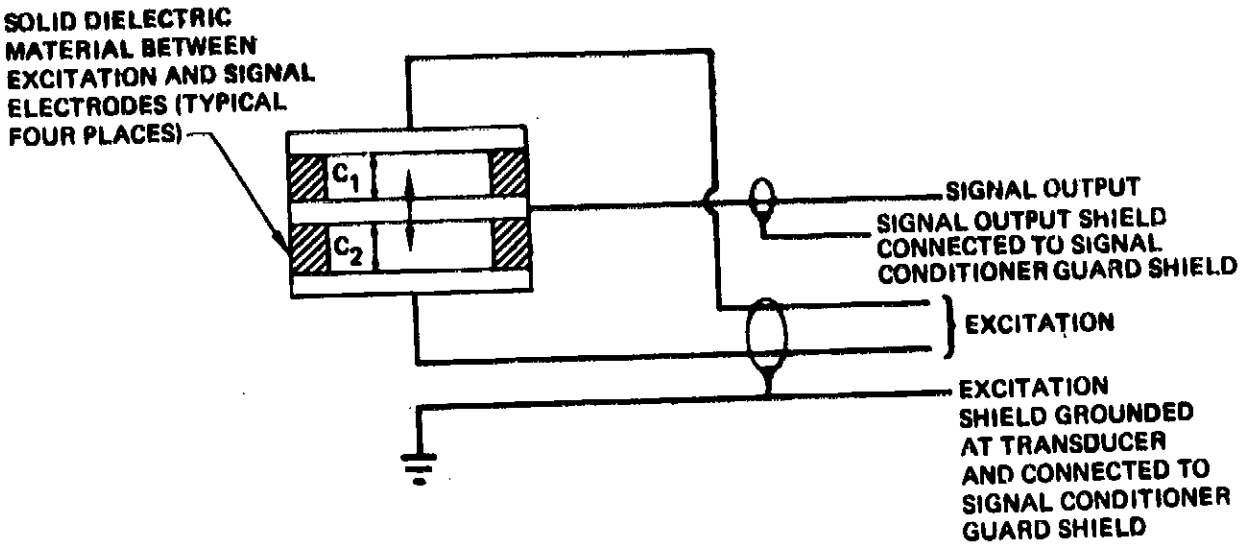

Figure 22. Differential Capacitor Without Ground Planes

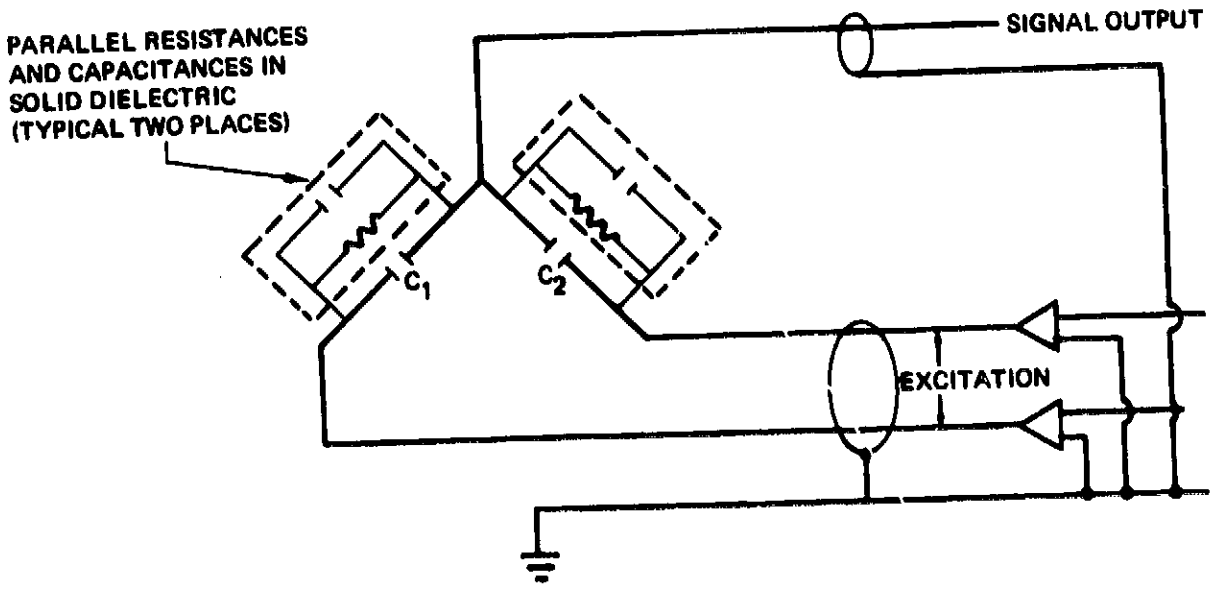

Figure 23. Differential Capacitor Circuit Without Ground Planes

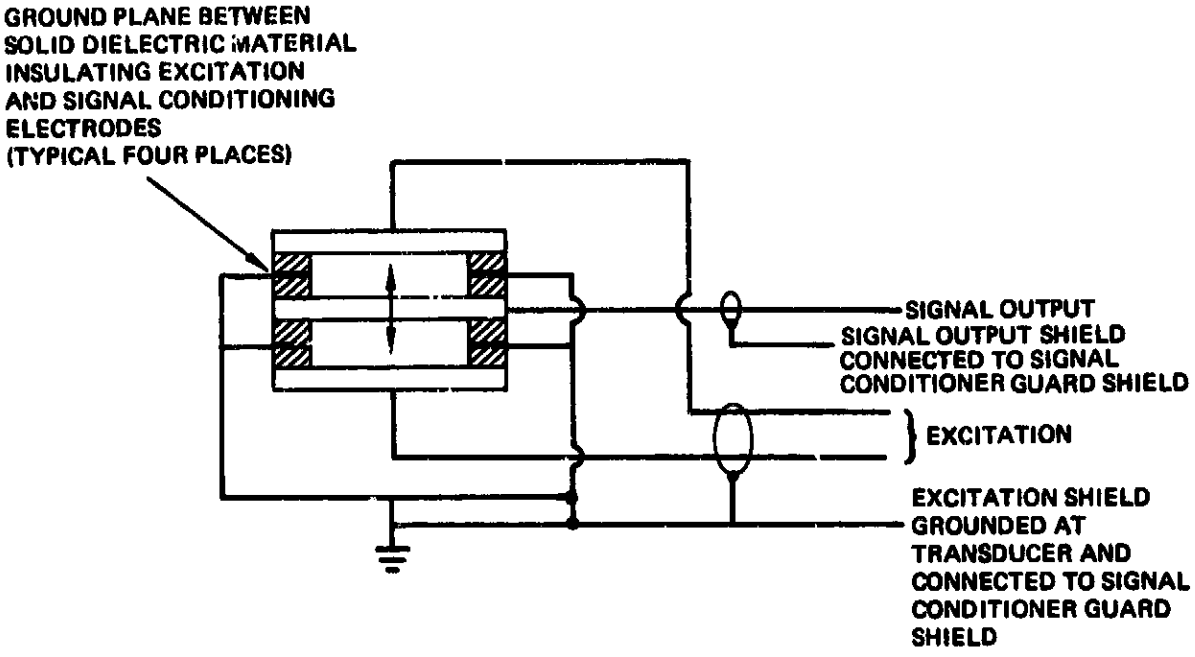

Figure 24. Differential Capacitor With Ground Planes

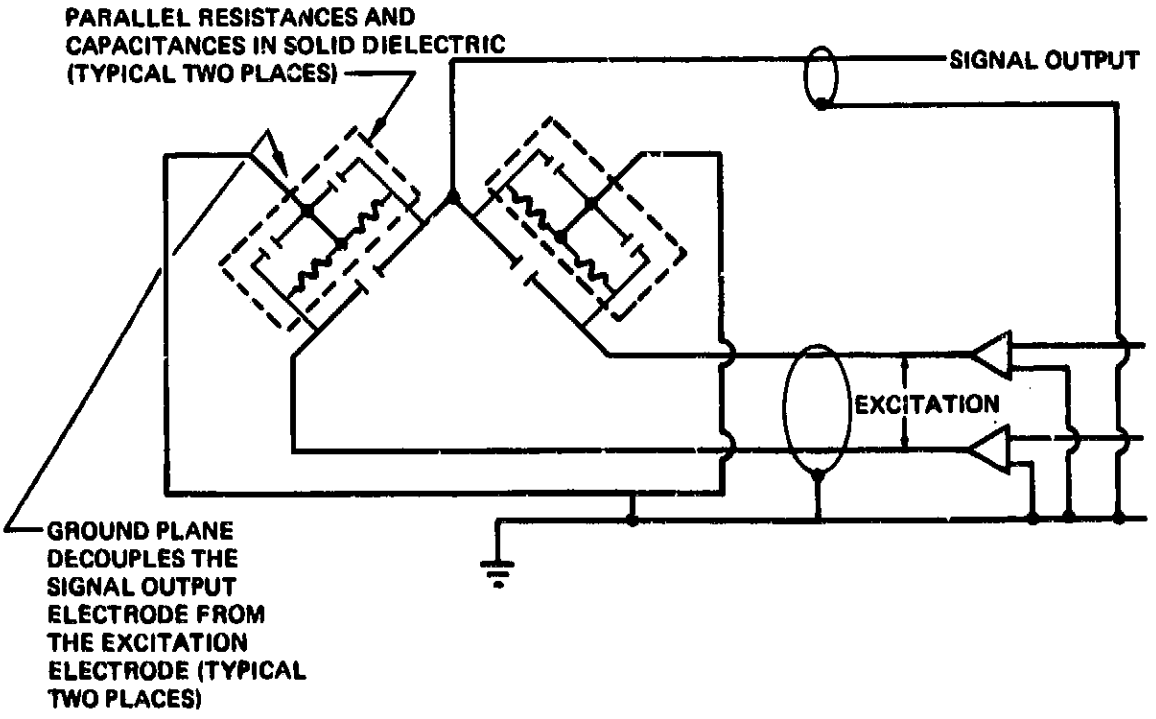

Figure 25. Differential Capacitor Circuit With Ground Planes

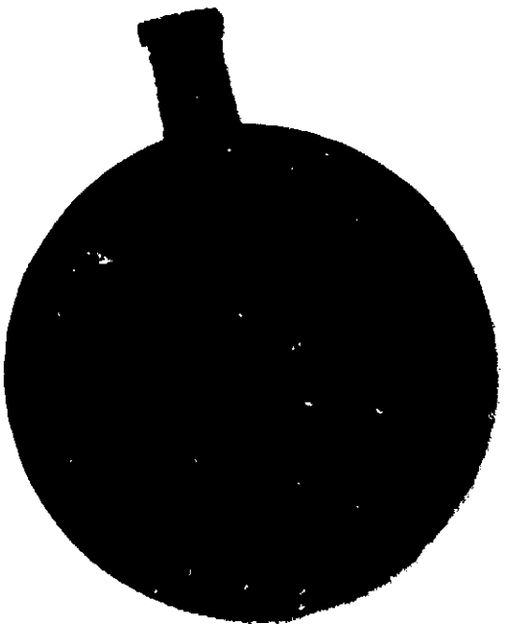

Figure 26. Diaphragm and Conductive Film Without Ground Planes

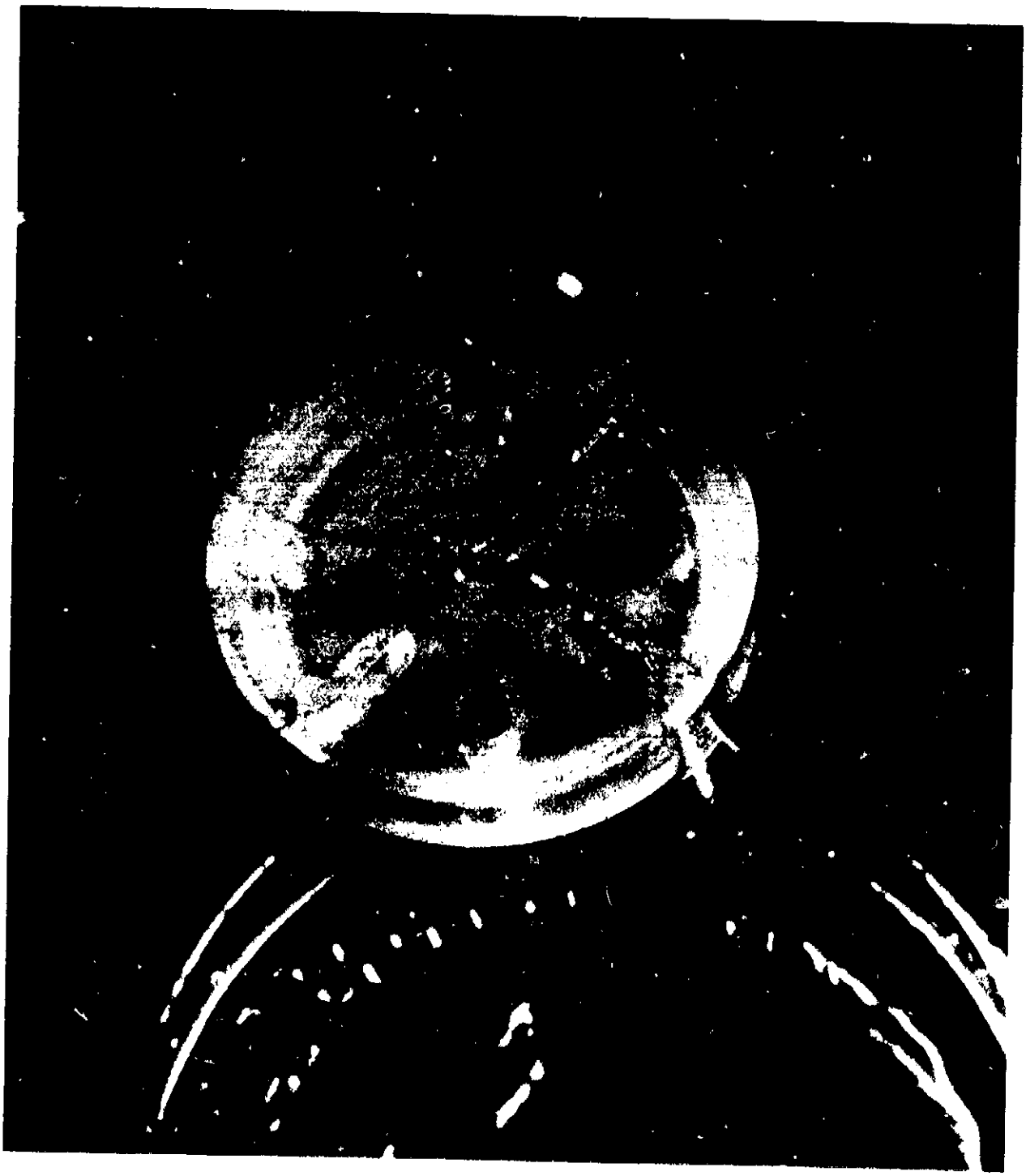

Figure 27. Sensor Assembly Without Ground Planes

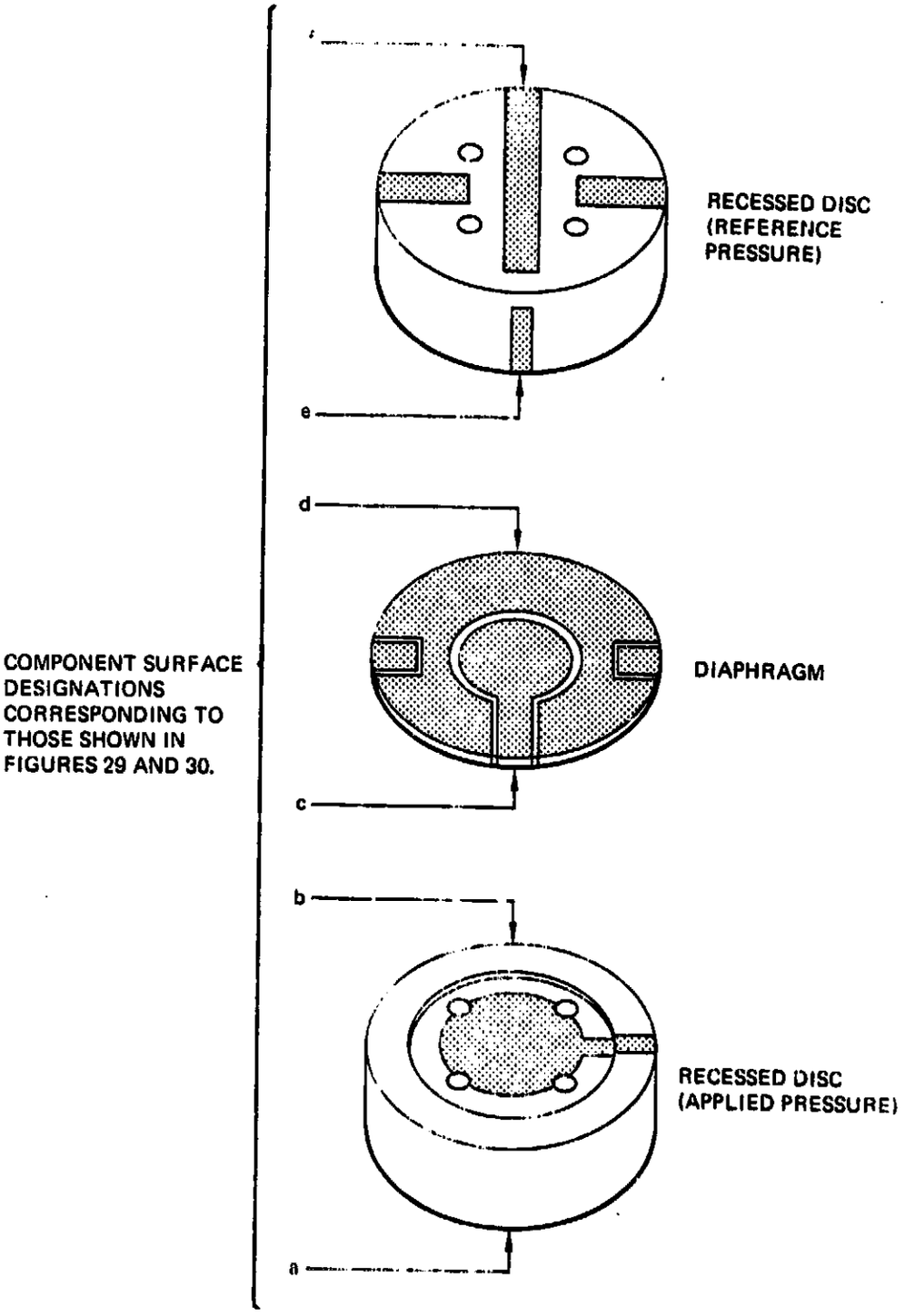

Figure 28. Stacking Orientation of Sensor Components

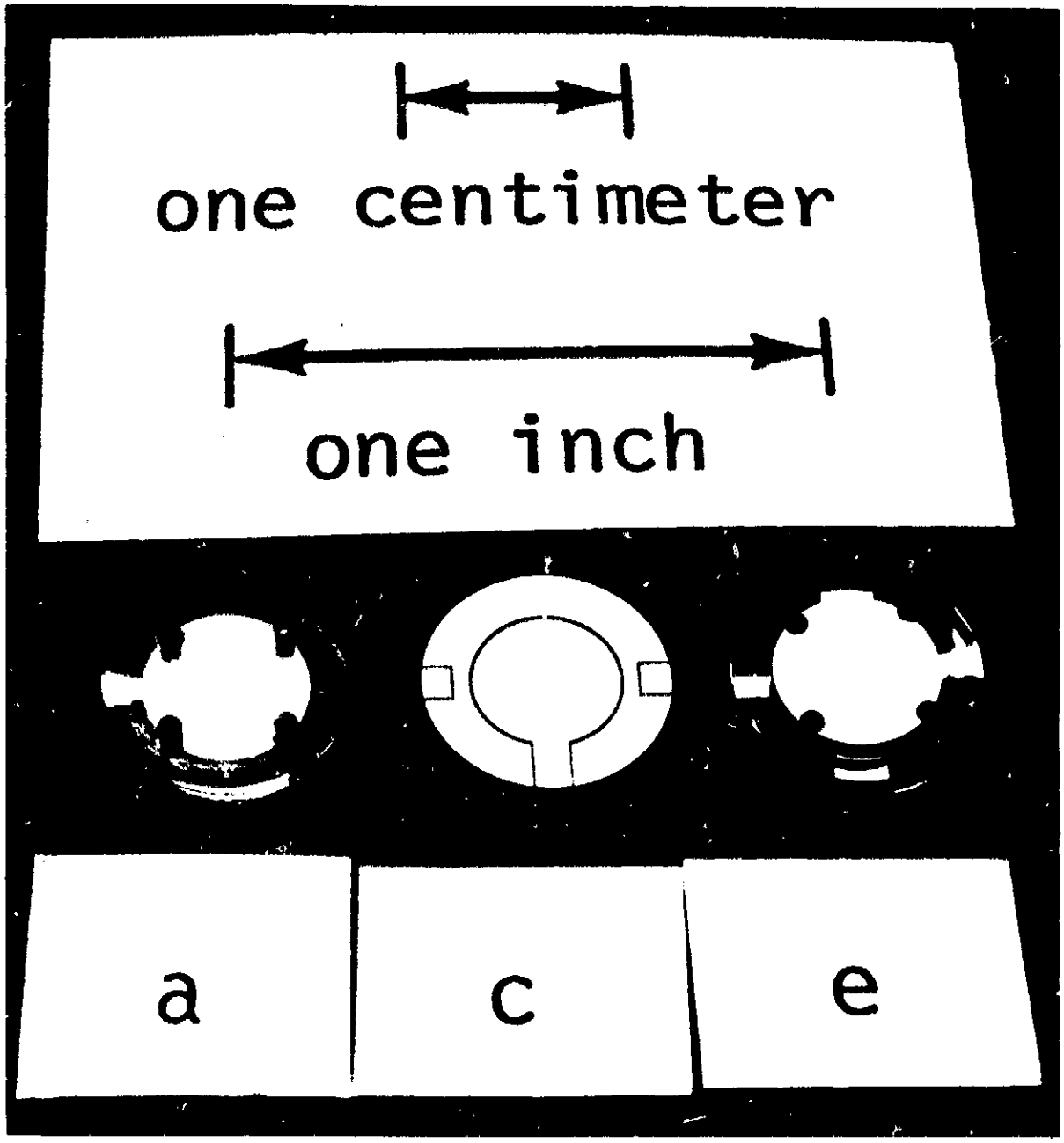

Figure 29. Sensor Components With Ground Planes

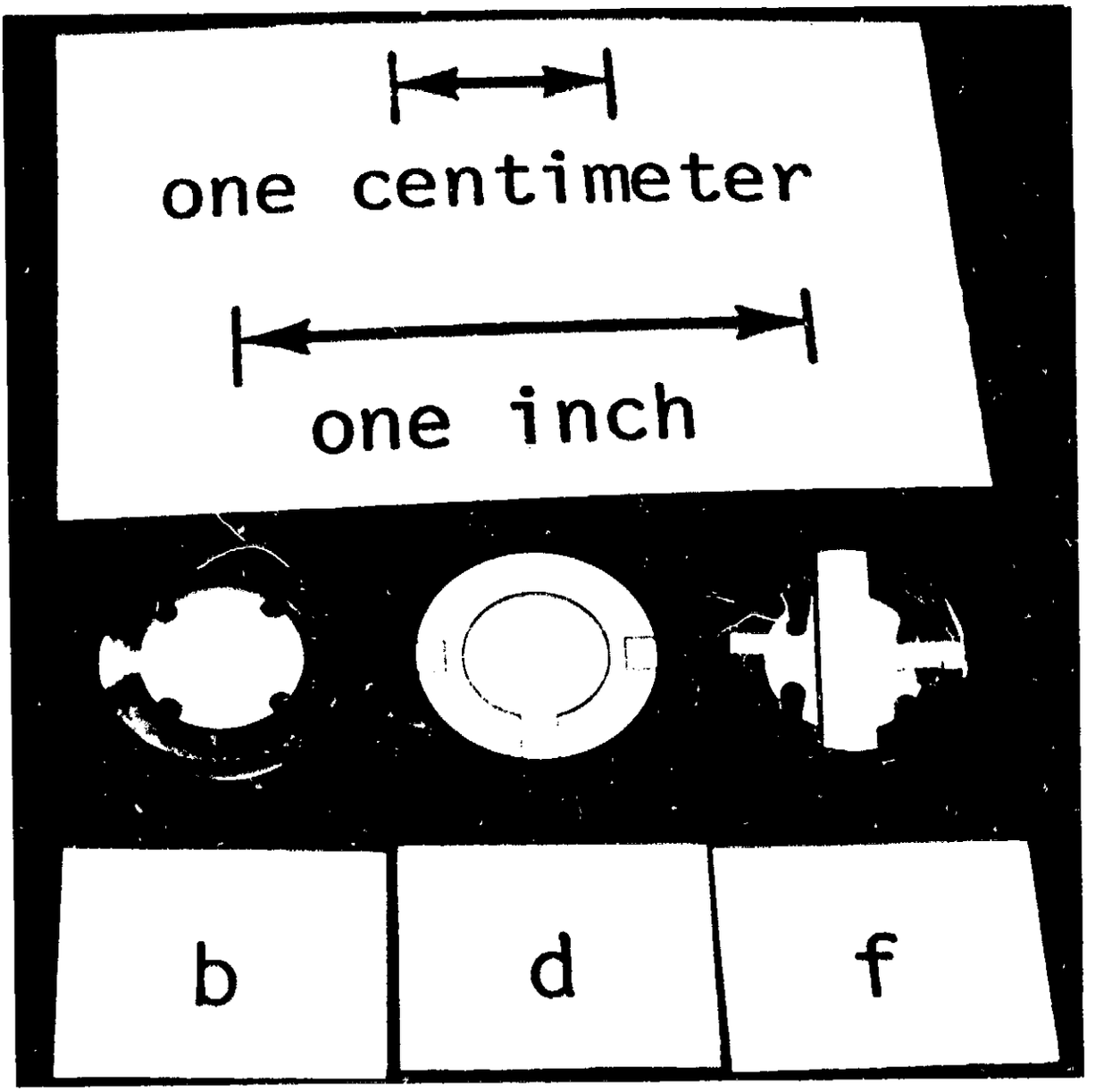

Figure 30. Sensor Components With Ground Planes

Figure 31. Sensor Assembly Lead Wire Attachment

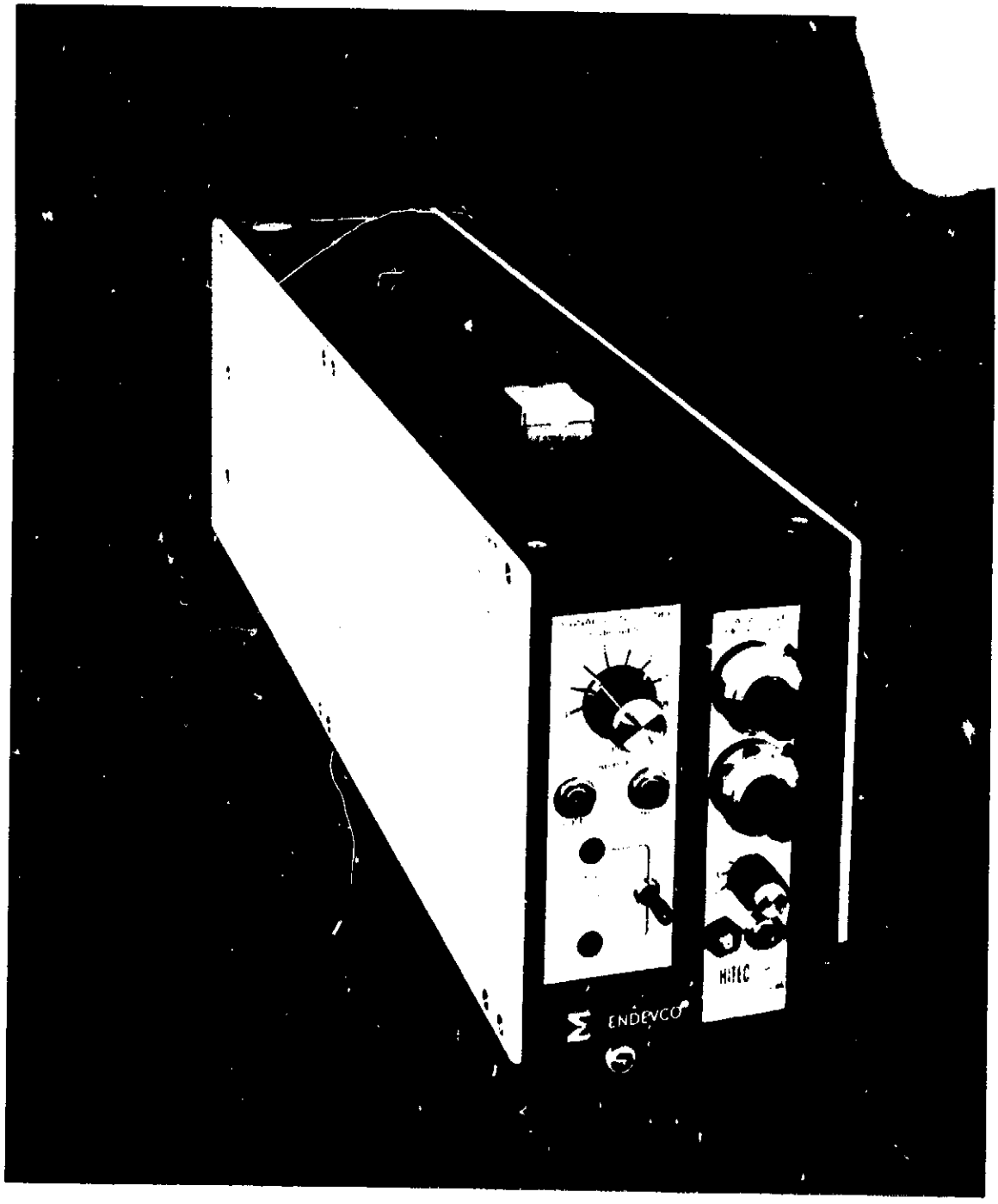

Figure 32. Signal Conditioning Carrying Case, Power Supply Module and Mode Card

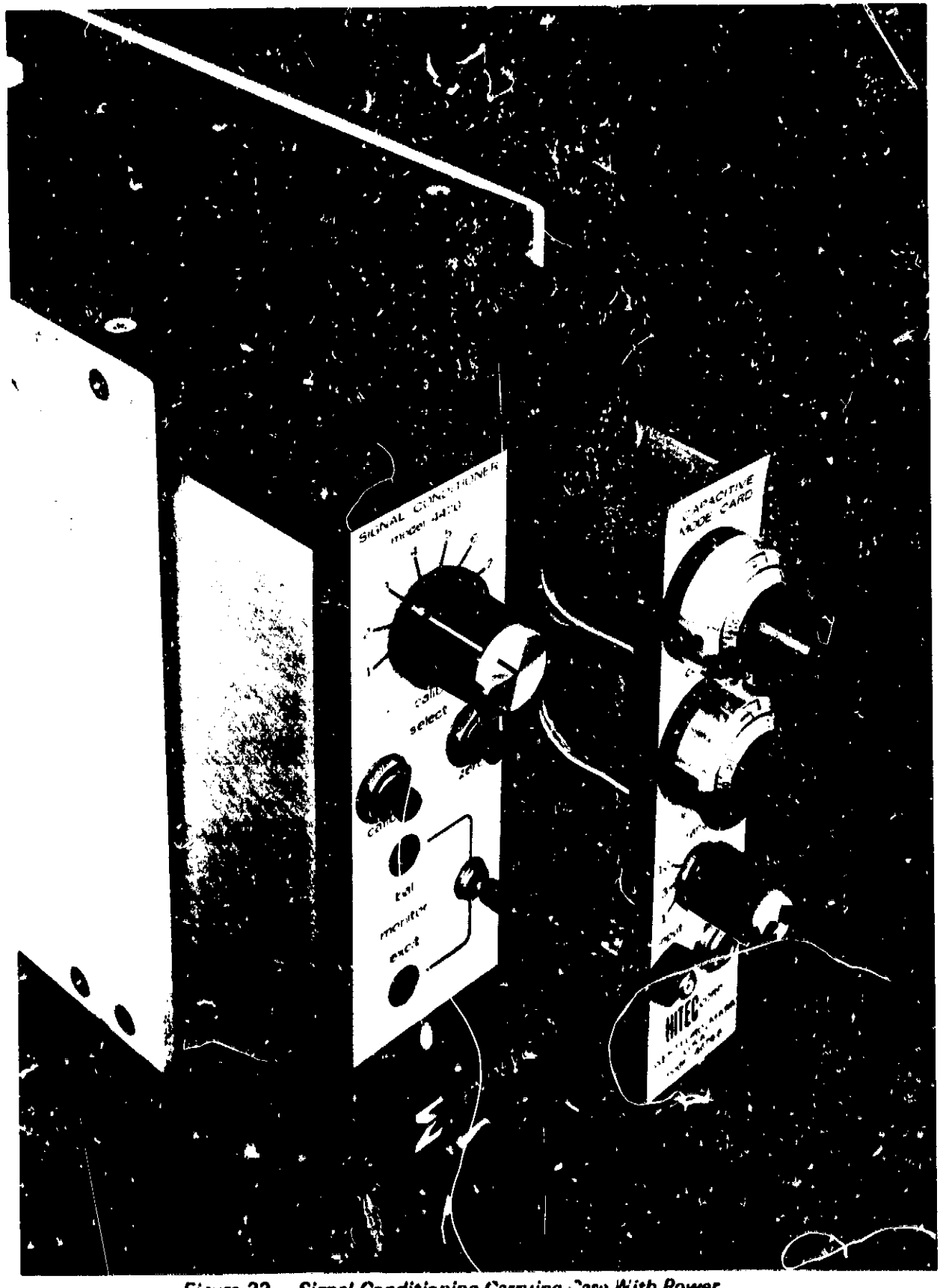

Figure 33. Signal Conditioning Carrying Case With Power Supply Module and Mode Card Extended

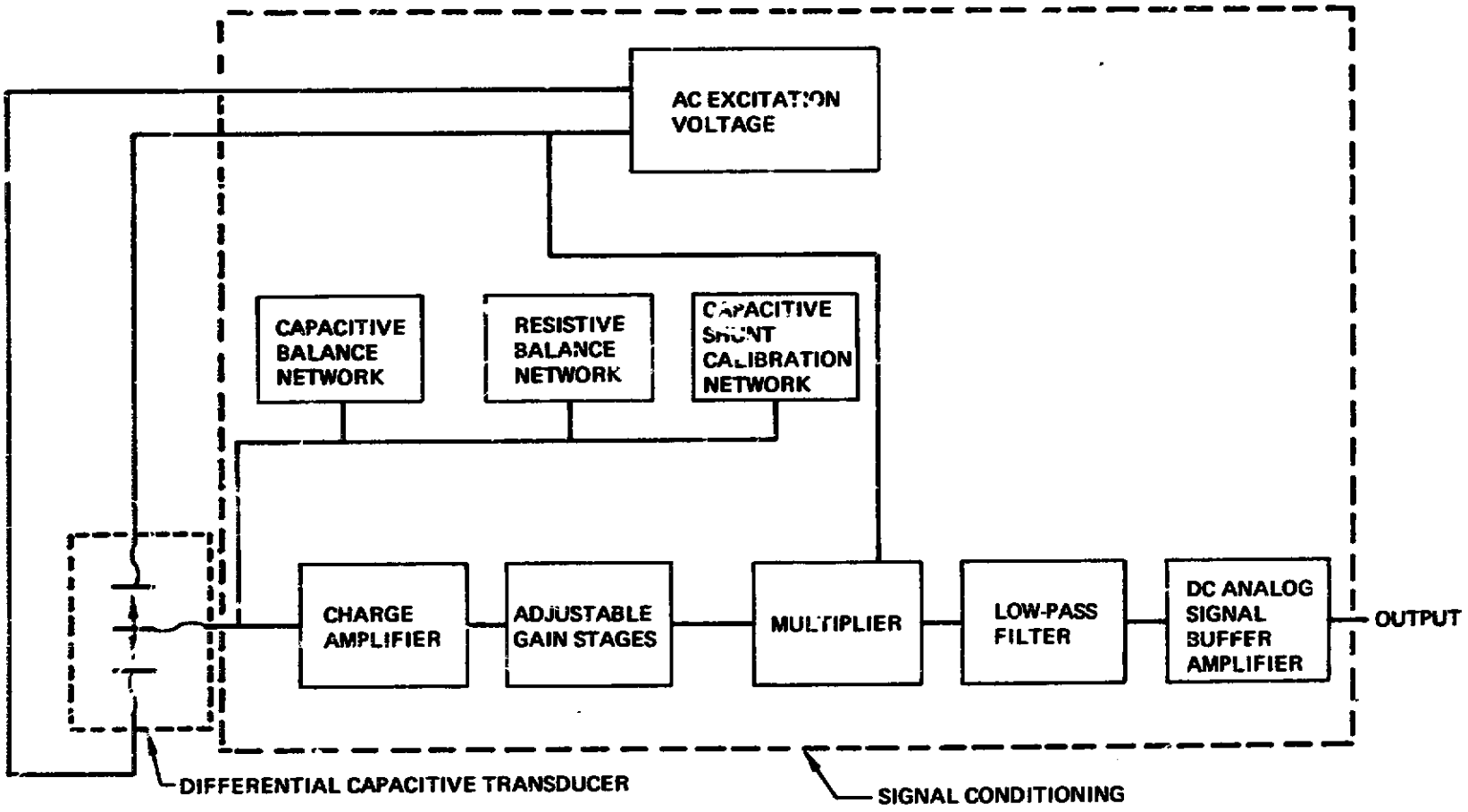

Figure 34. Signal Conditioning Block Diagram

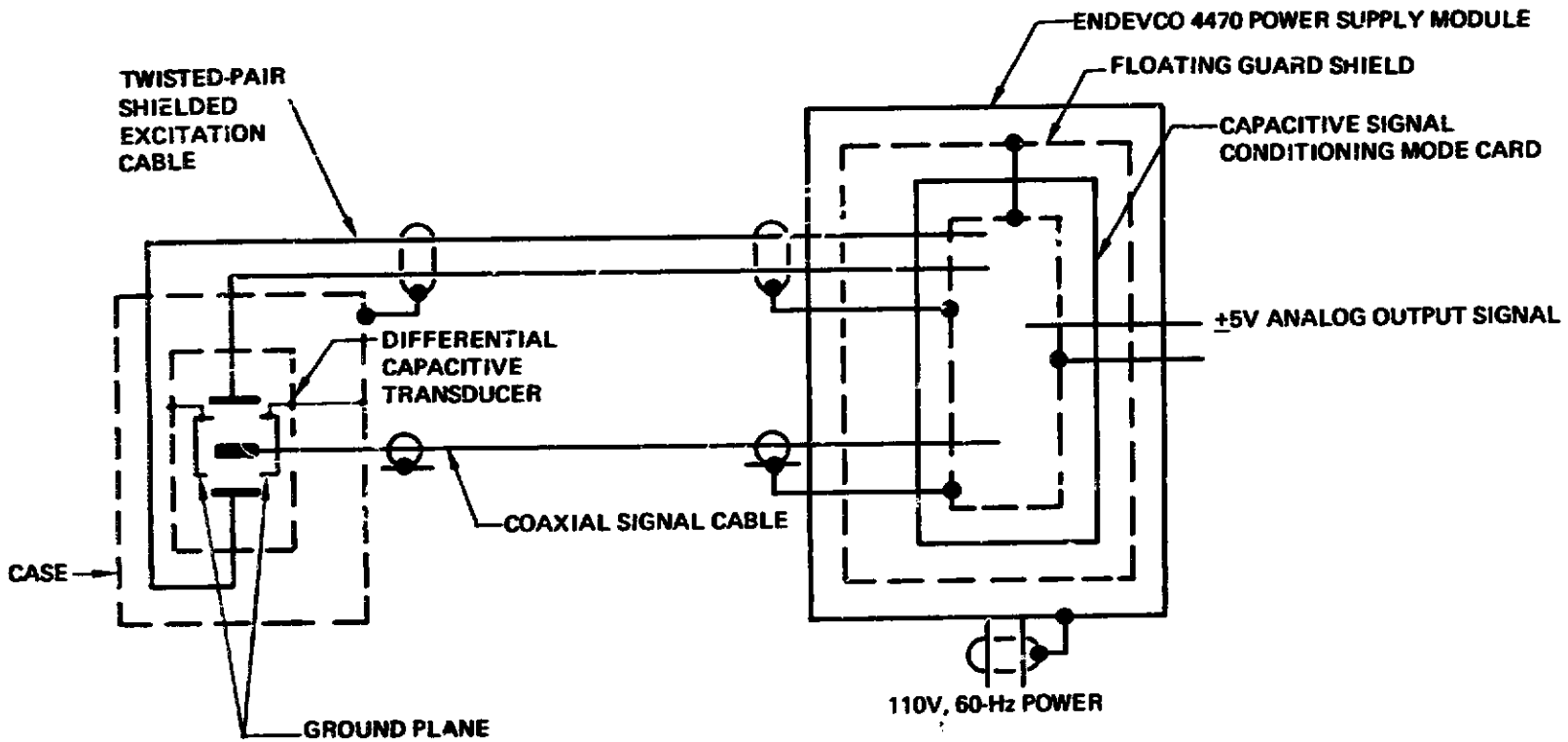

- One twisted-pair shielded cable for excitation
- One coaxial type cable for signal
- Floating internal guard shield for ground isolation
- Output signal referenced to isolated guard shield

Figure 35. Transducer and Signal Conditioning Electrical Connections

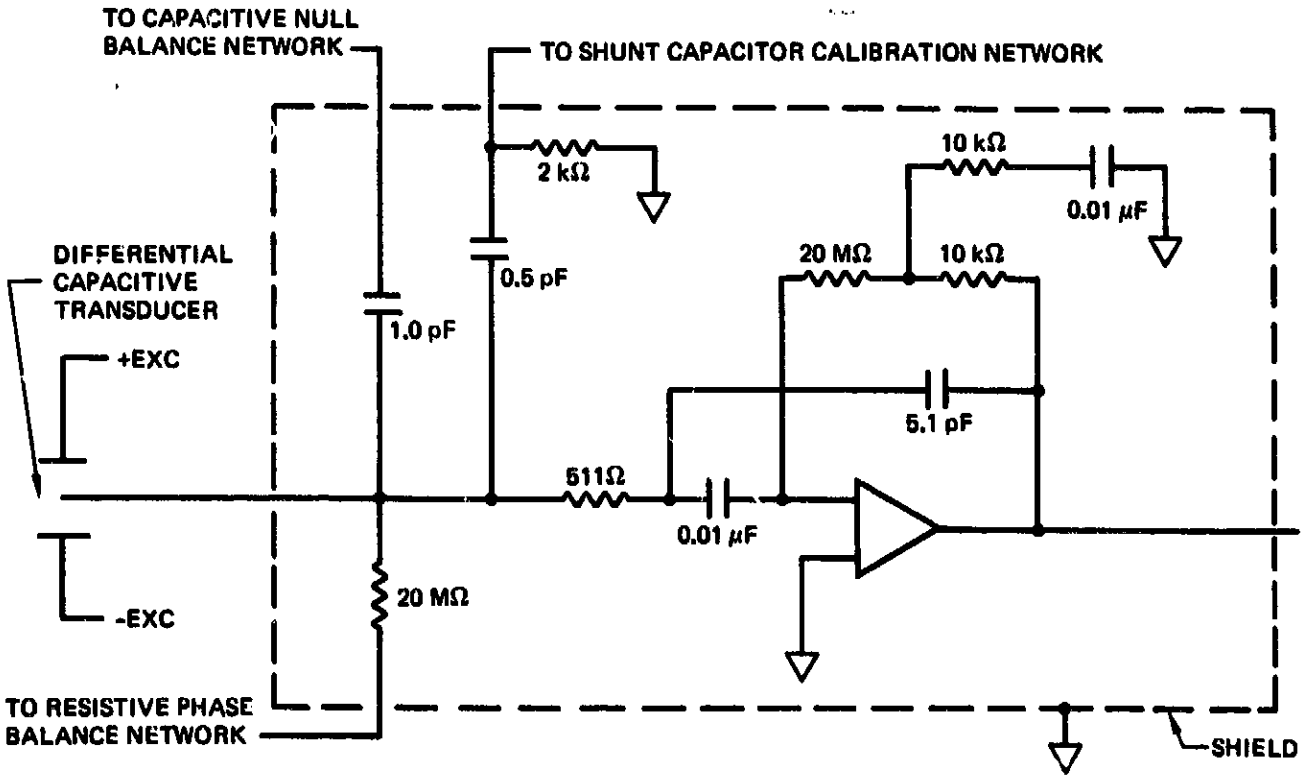

- Capacitively coupled signal input (blocks unwanted direct current signals)
- Charge-sensitive input (represses cable length effects)
- Input stage gain optimized for excitation frequency (less gain for lower frequencies)
- Resolution better than 0.00002 pF

Figure 36. Signal Input Circuit

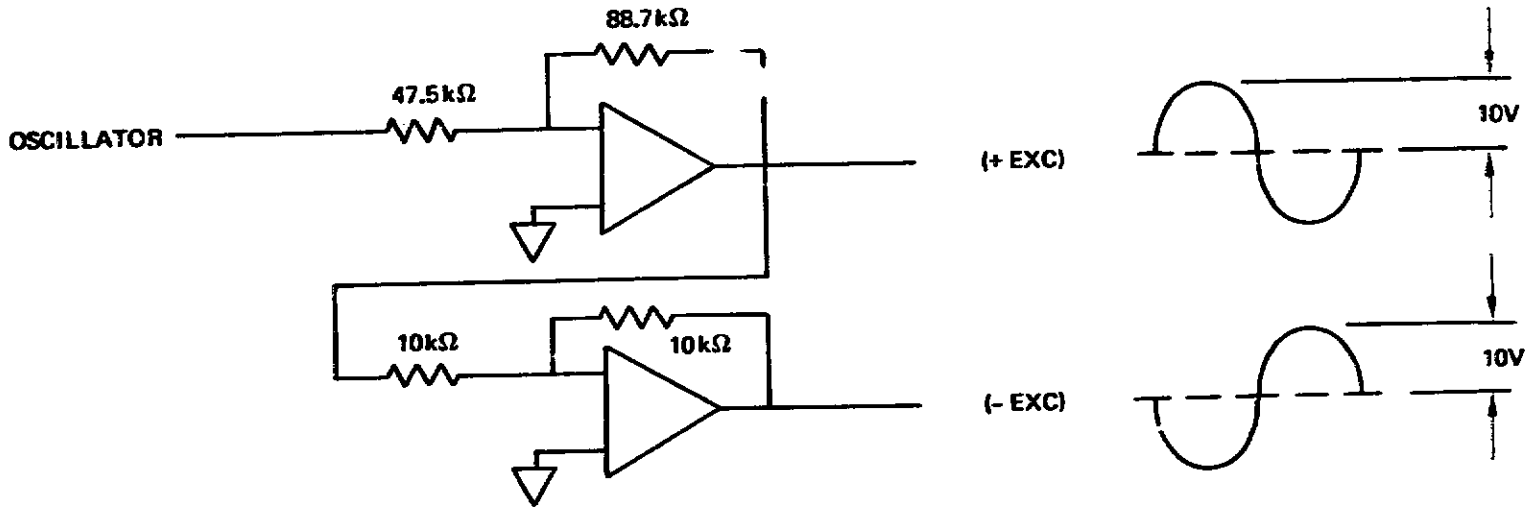

- 40V peak to peak
- Opposing phase outputs balanced to guard shield (i.e., ground)

Figure 37. AC Excitation Voltage Driver Circuit

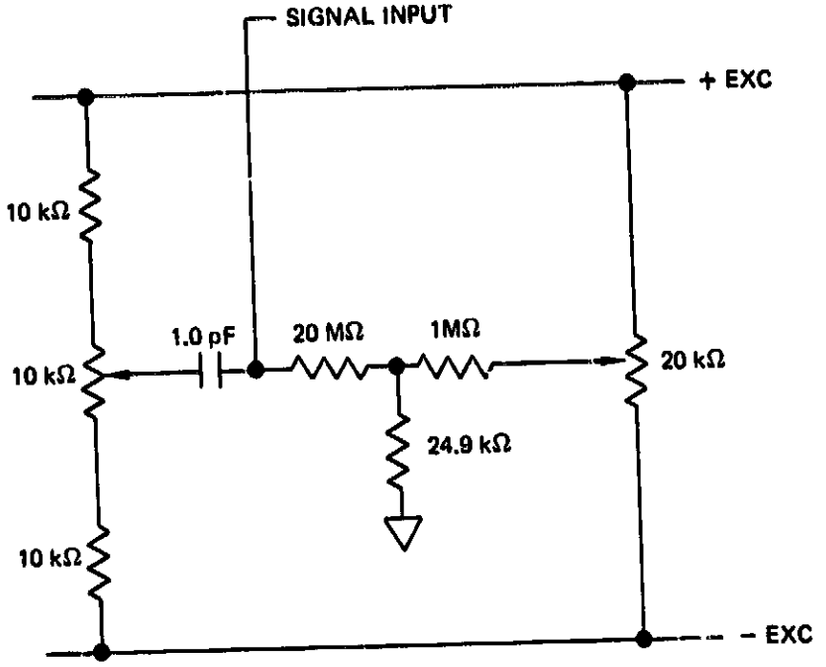

- Capacitive balance for nulling output (1.0 pF)
- Resistive phase balance adjustment

Figure 38. Capacitive and Resistive Balance Circuit

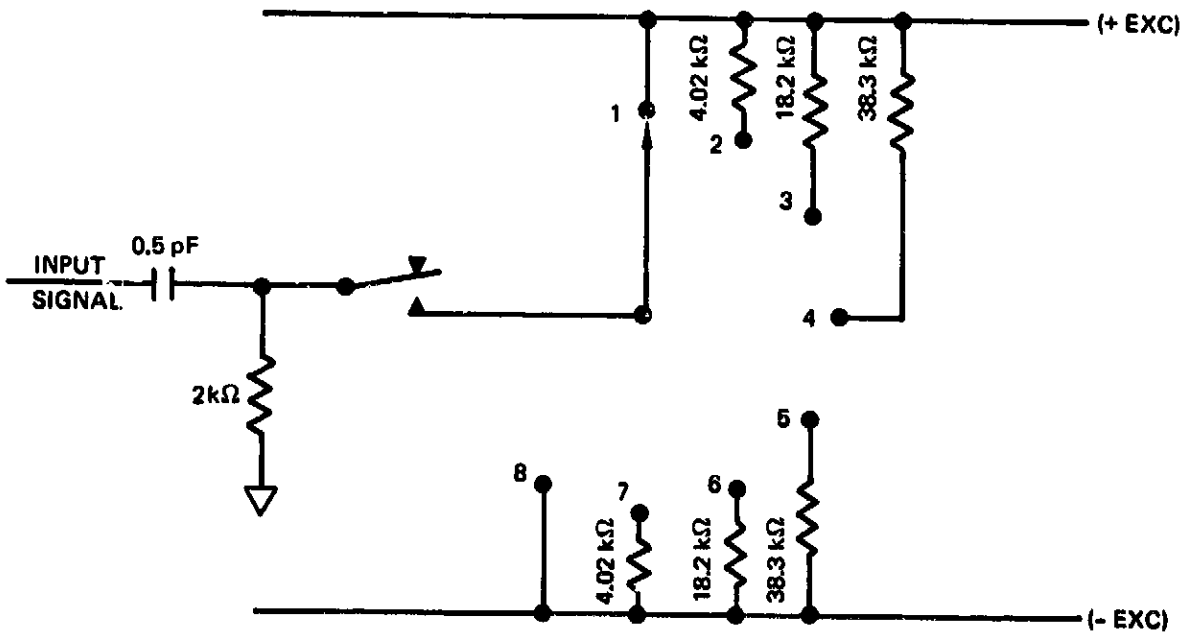

- Four positive and four negative positions
- Series 0.5-pF capacitor
- Certifiable calibration

Figure 39. Shunt Capacitor Calibration Circuit

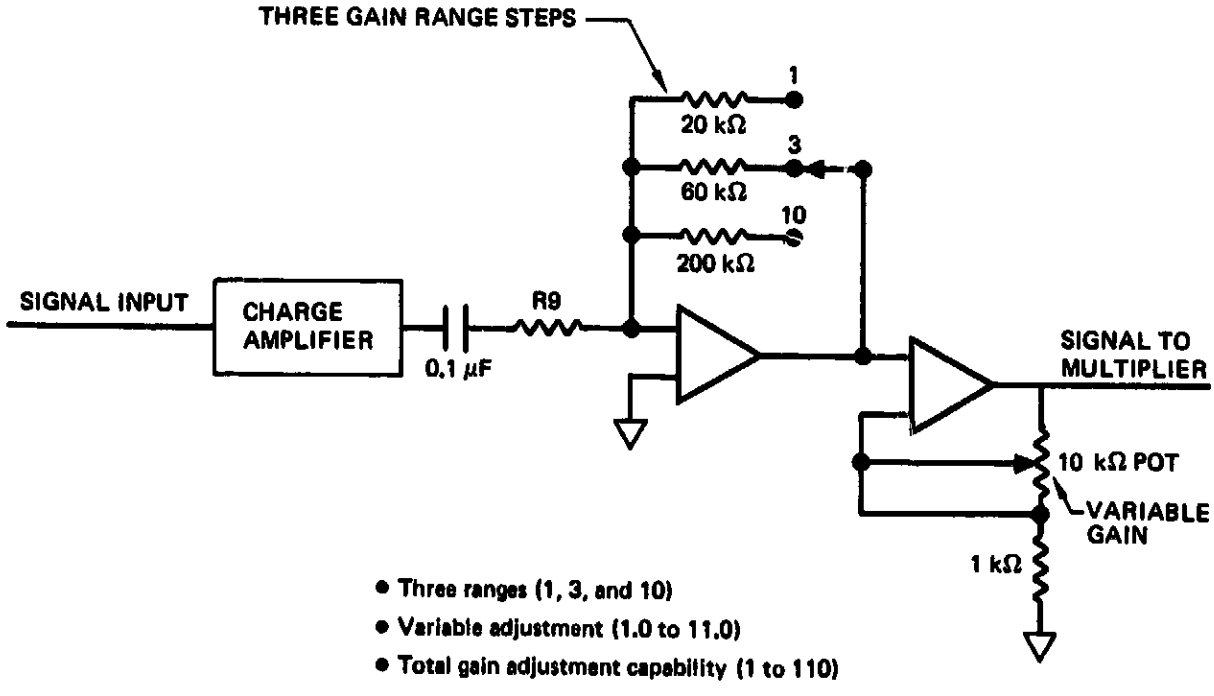

Figure 40. Adjustable Gain Circuit

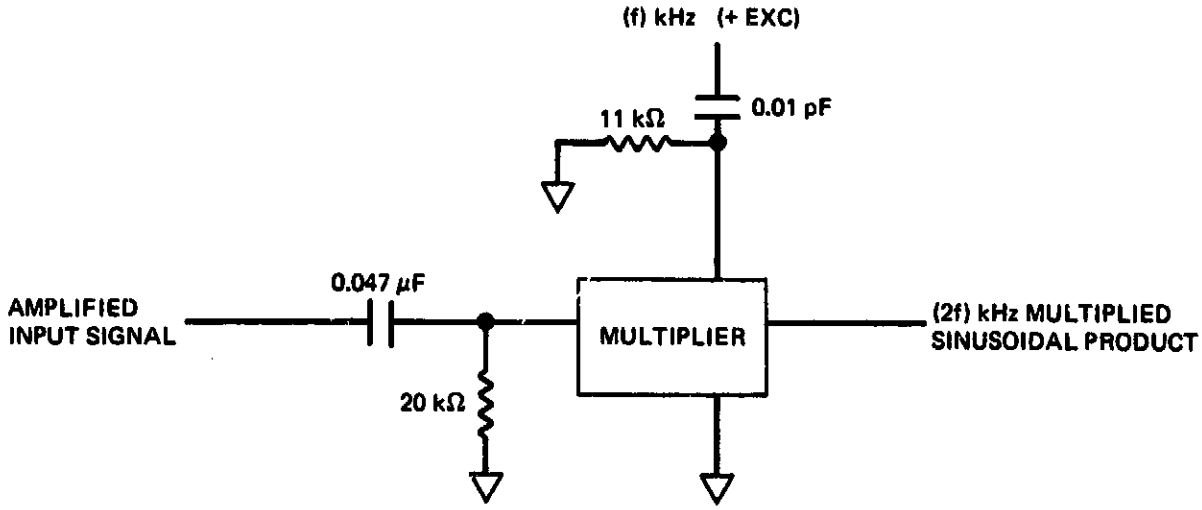

- Signal multiplied by carrier produces double frequency output with direct current component
- Represses out-of-phase signal effects

Figure 41. Multiplier Demodulator Circuit

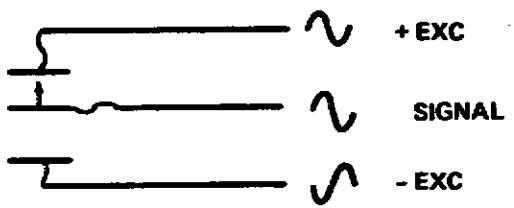

POSITIVE DIFFERENTIAL PRESSURE

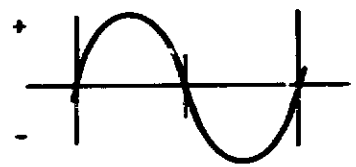

SIGNAL INPUT TO MULTIPLIER

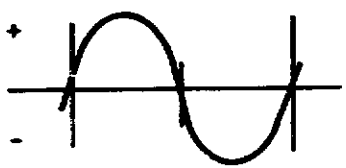

EXCITATION INPUT TO MULTIPLIER

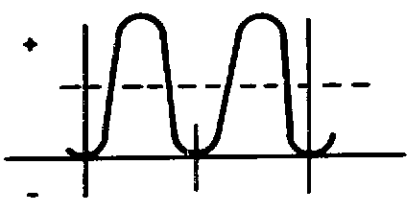

MULTIPLIER OUTPUT

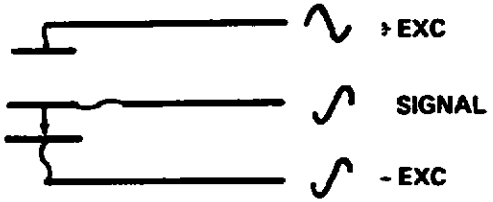

NEGATIVE DIFFERENTIAL PRESSURE

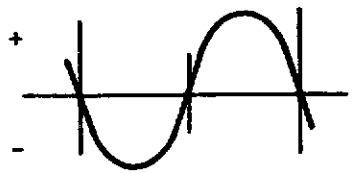

SIGNAL INPUT TO MULTIPLIER

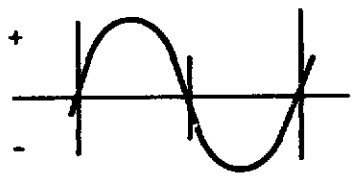

EXCITATION INPUT TO MULTIPLIER

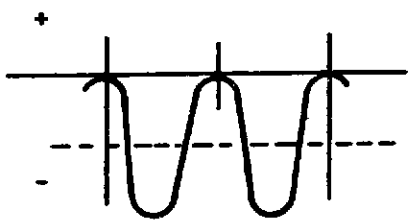

MULTIPLIER OUTPUT

Figure 42. Multiplier Operation

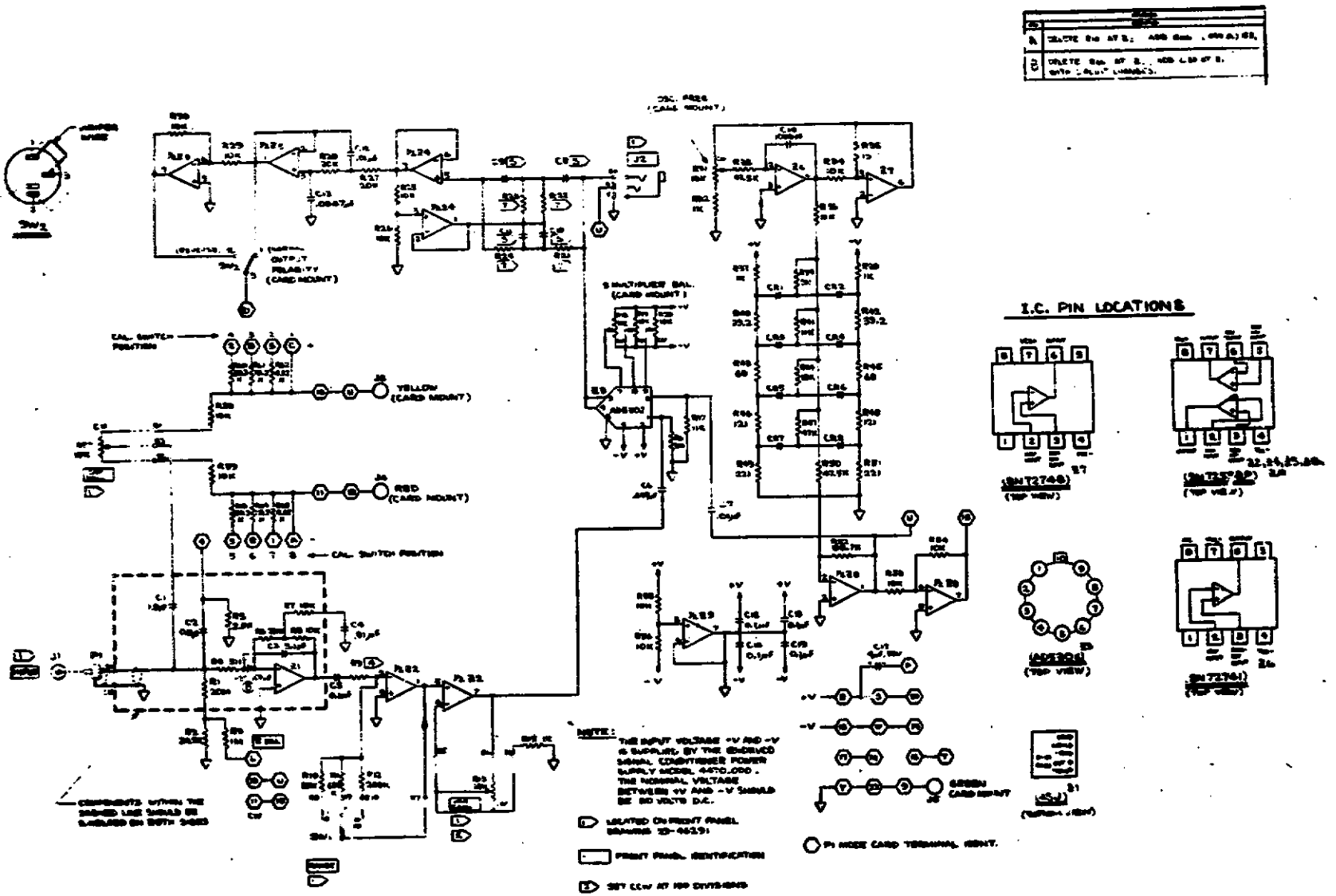

Note: Excitation frequency = 3.39 kHz

Figure 43. Mode Card Circuit Diagram

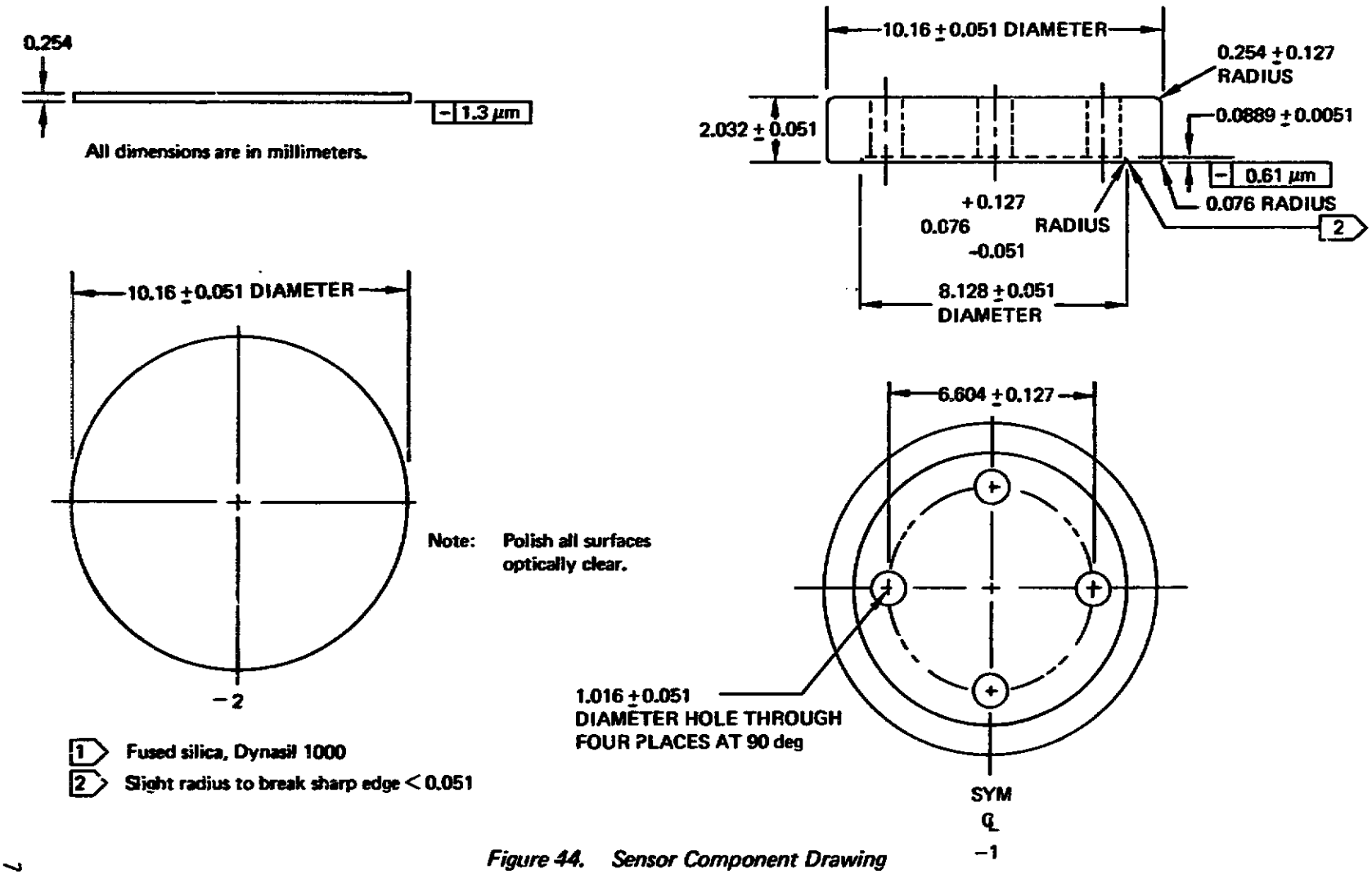

Figure 44. Sensor Component Drawing

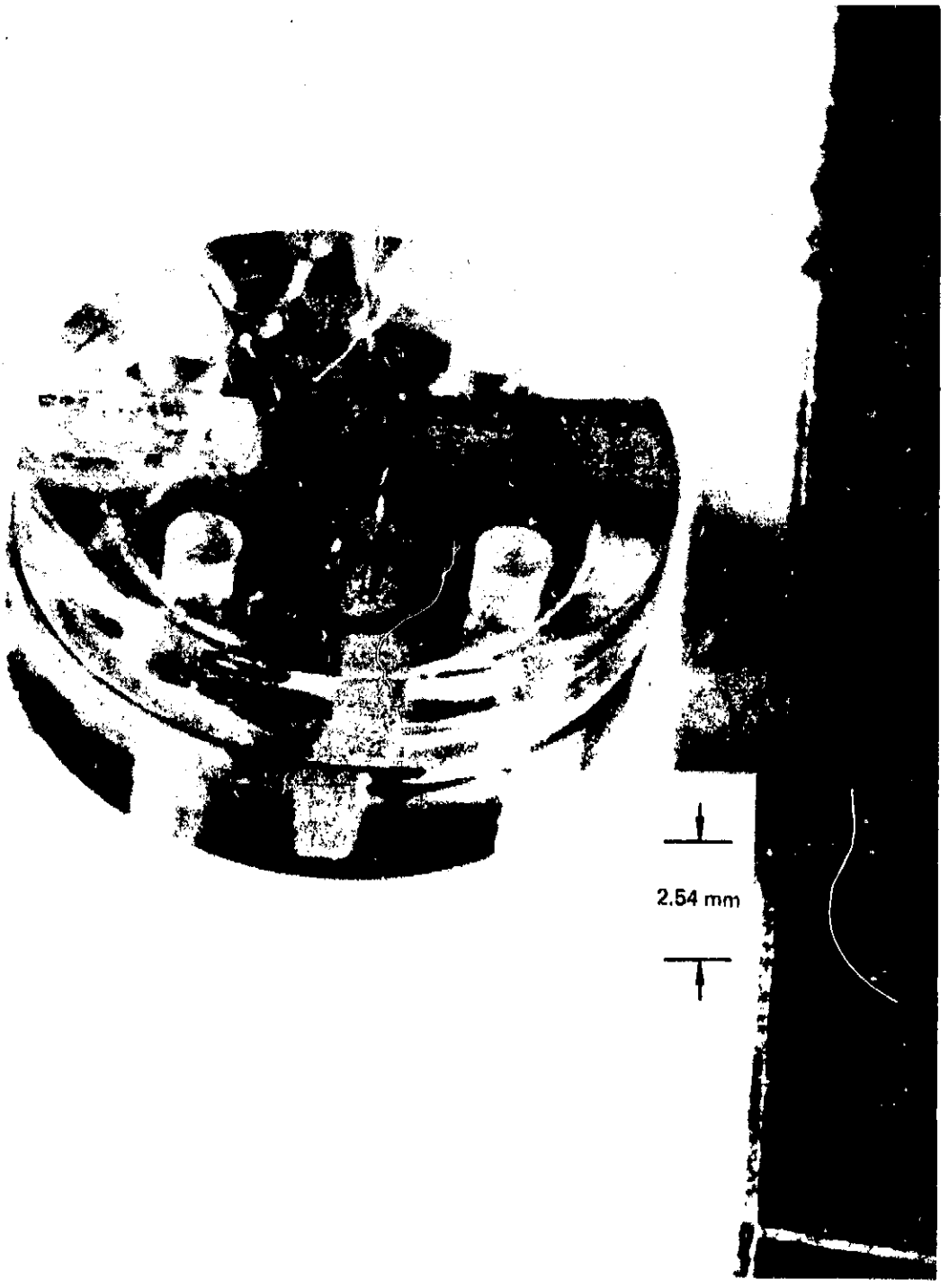

Figure 45. Sensor Assembly With Lead Wires

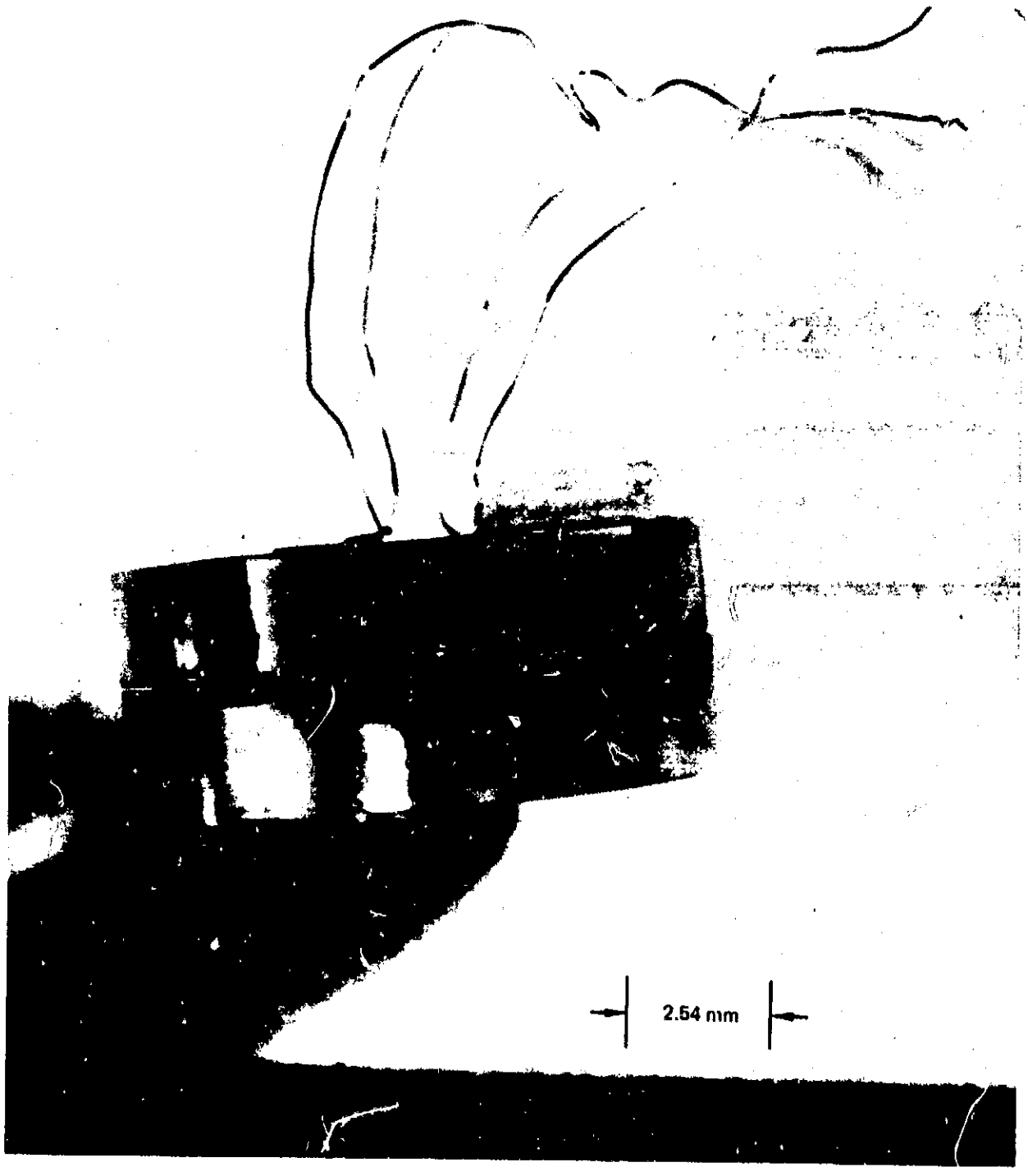

Figure 46. Sensor Assembly With Lead Wires

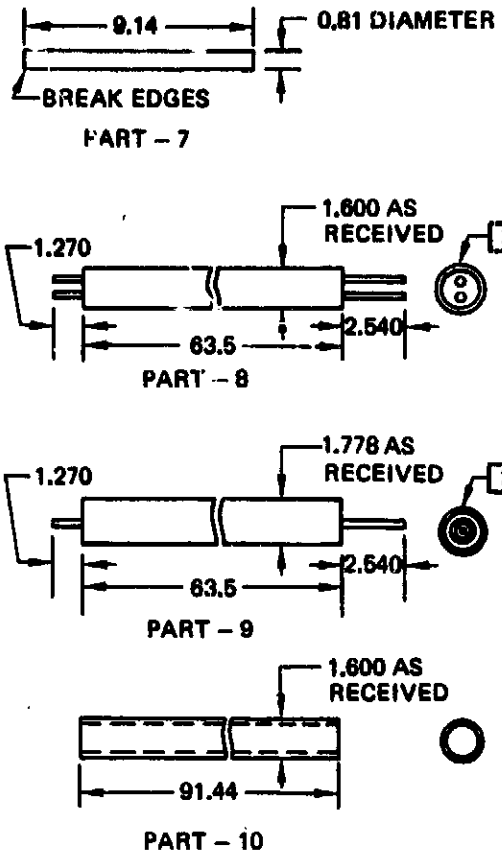

1. Part -3 diameter must be machined for slip-fit in -2, 0.0127- to 0.025- mm tolerance
2. Square corner; do not break edge
3. Clean cut; metal edges must not fold over on insulation
4. Heat treat BAC 5616 in vacuum,
   Solution treat IB.
   Age condition IIa:
   (1,080° ± 14°C, 10 to 15 min) air quench
   (900° ± 14°C, 50 to 60 min) air cool
   (760° ± 14°C, 10 to 11 hr) air cool
5. Grind A plane first; then grind B plane.
6. Harmon high-temperature 910 brazing powder, 325 mesh, AMS 4778A
7. Electron beam weld

Notes:

Linear dimensions in millimeters
Linear tolerance:
X.XXX ±0.127 mm
X.XX ± 0.25 mm
X.X ± 1.2 mm
except as noted
Finish: 1.6 μm except as noted

-12	-1	Part number	Part description	Material and heat treat	Stock size
	✓	-1	Case assembly		
	1	-2	Outer case	321 SS rod	19.05 dia x 2.54
1		-3	End plate	321 SS rod	19.05 dia x 2.54
1		-4	Center cylinder	321 SS tubing	6.350 dia x 0.711 x 10.16
	1	-5	Spacer ring	321 SS rod	12.70 dia x 7.62
	1	-6	Alumina washer	Alumina rod	19.05 dia x 20.32
	1	-7	Pin	321 SS wire	0.813 dia x 12.7
1		-8	Excitation lead	0.063 - MgO-K	76.2 long
1		-9	Signal lead	0.070 - 347 SS- MgO	76.2 long
1		-10	Vent tube	321 SS tubing	1.600 x 0.254 x 101.6
	1	-11	Spring	Rene '41 [4] wire	1.143 dia x 254.0
✓	1	-12	End cap assembly		

Figure 47a. Case Assembly Drawing, Sheet 1

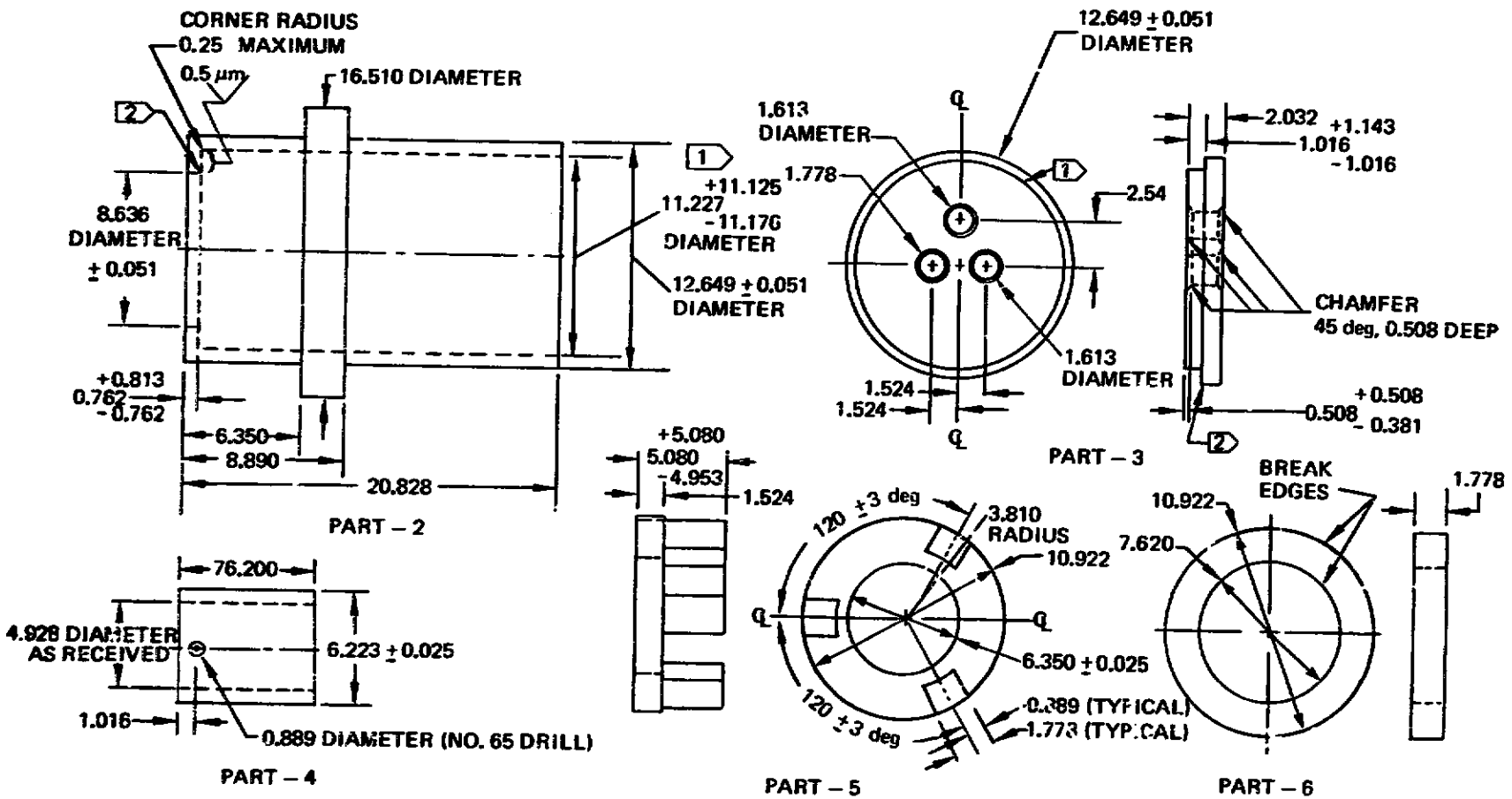

Refer to sheet 1 for flagnotes.

Figure 47b. Case Assembly Drawing, Sheet 2

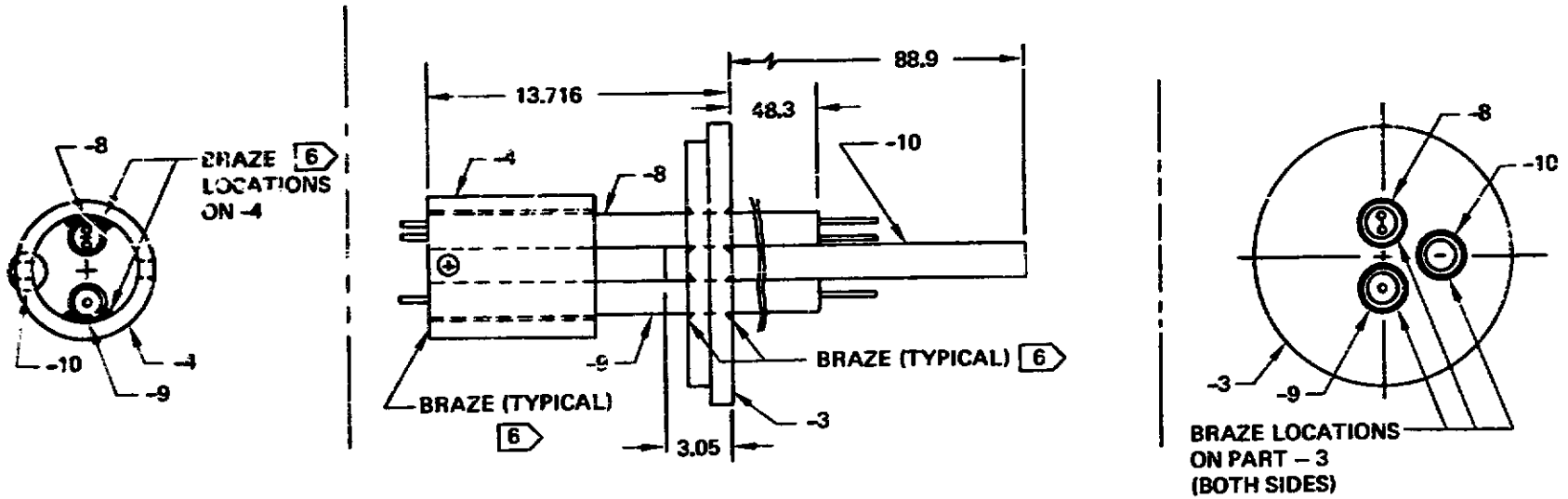

ASSEMBLY -12

Refer to sheet 1 for flagnotes.

Figure 47c. Case Assembly Drawing, Sheet 3

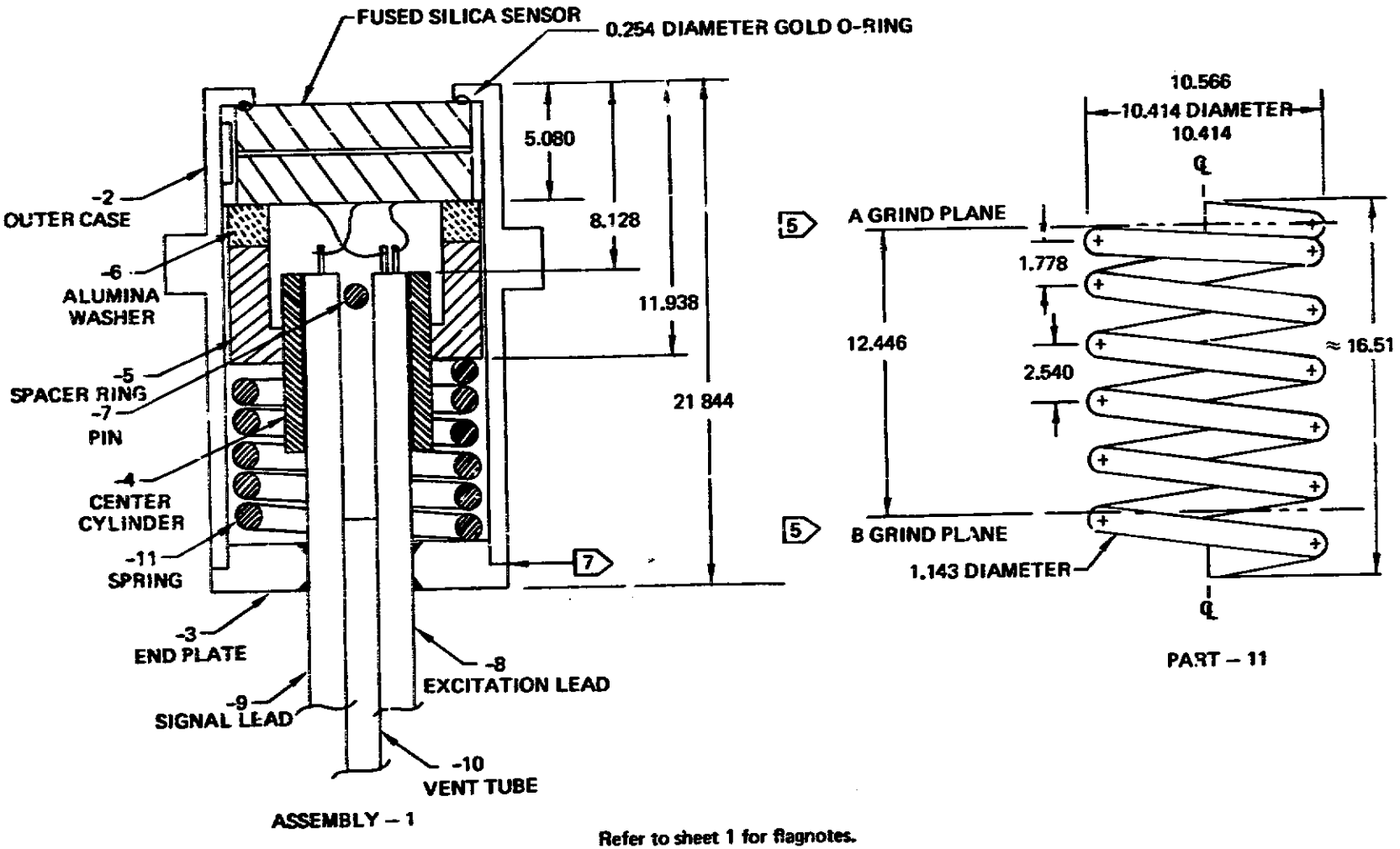

Refer to sheet 1 for flagnotes.

Figure 47d. Case Assembly Drawing, Sheet 4

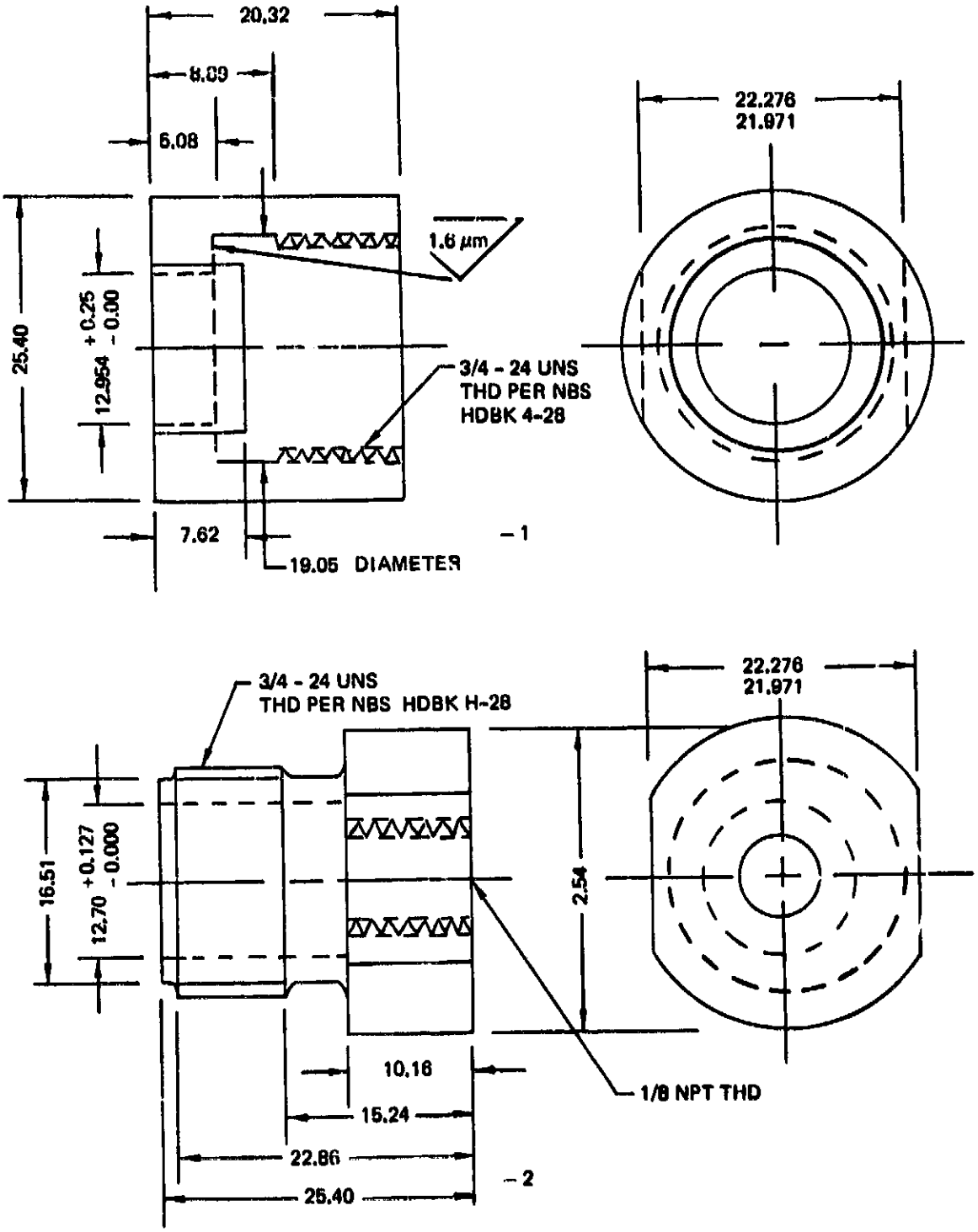

Note: Break sharp edges.

- Material: Inconel X-750
- Tolerance: ± 0.25 except as noted
- Finish: 3.2 µm except as noted
- All dimensions are in millimeters

Figure 48. Adapter Fittings Drawing

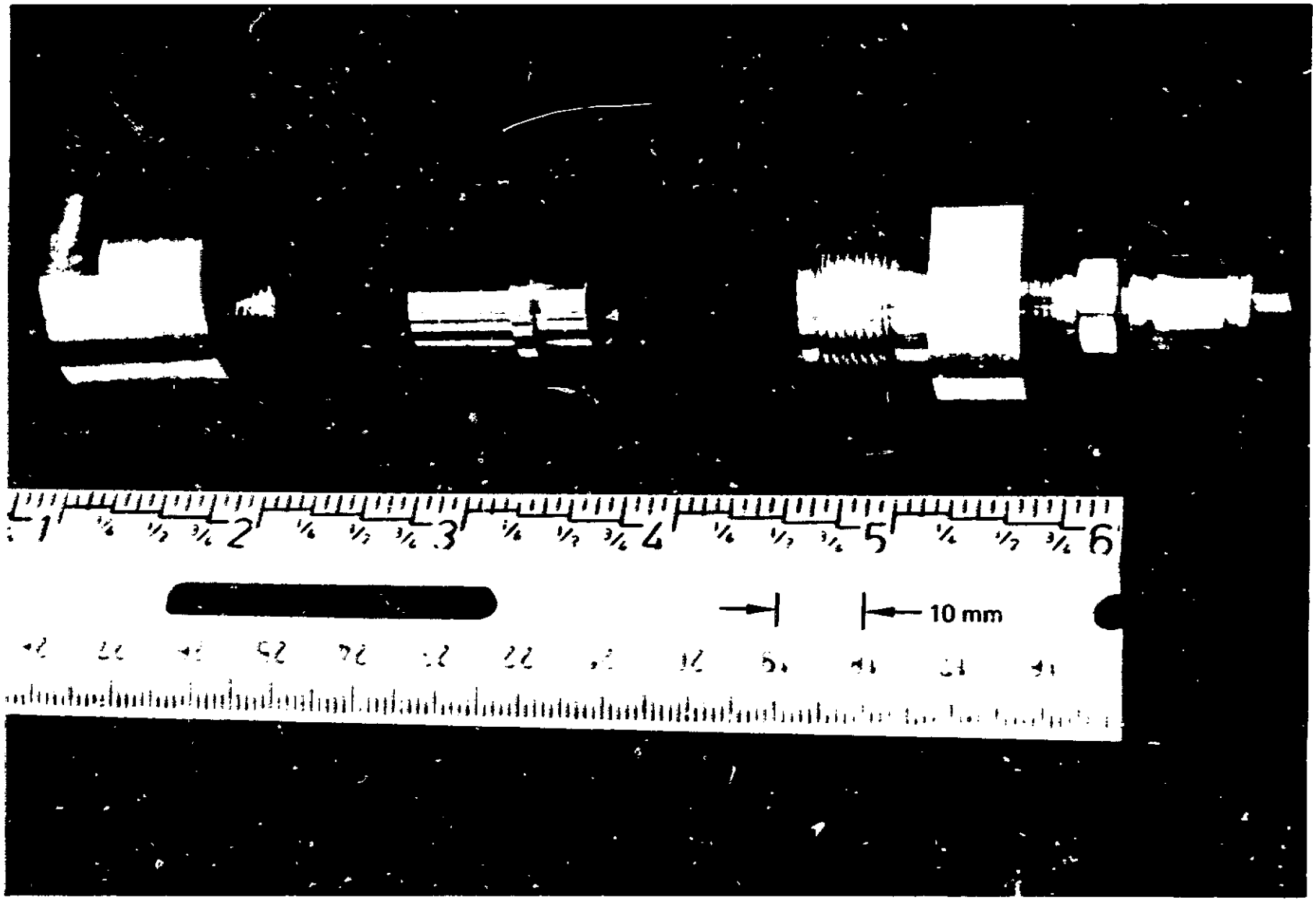

Figure 49. Adapter Fittings (With Outer Case)

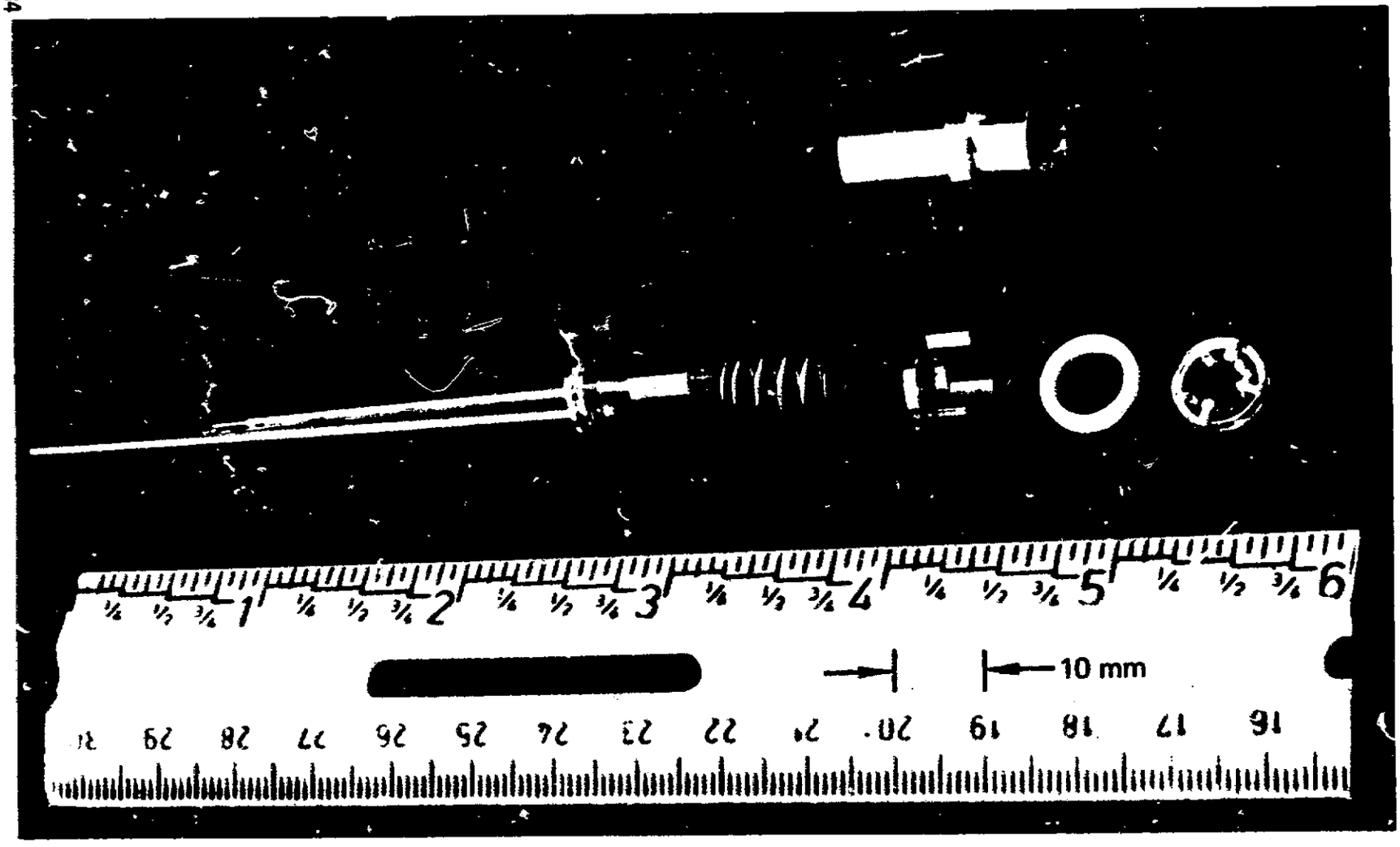

Figure 50. Transducer Components (Without Gold O-Ring)

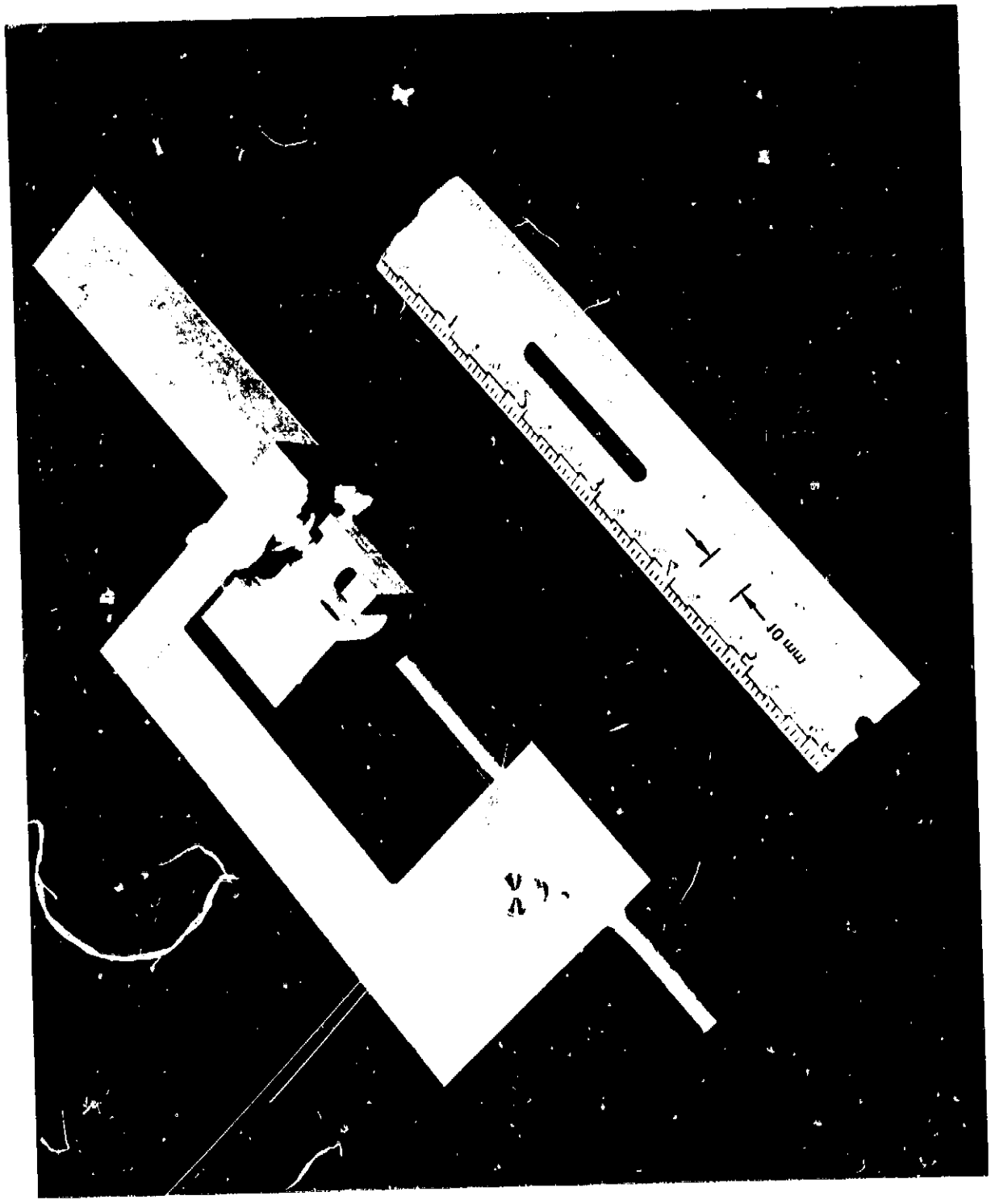

Figure 51. Transducer Assembling Fixture

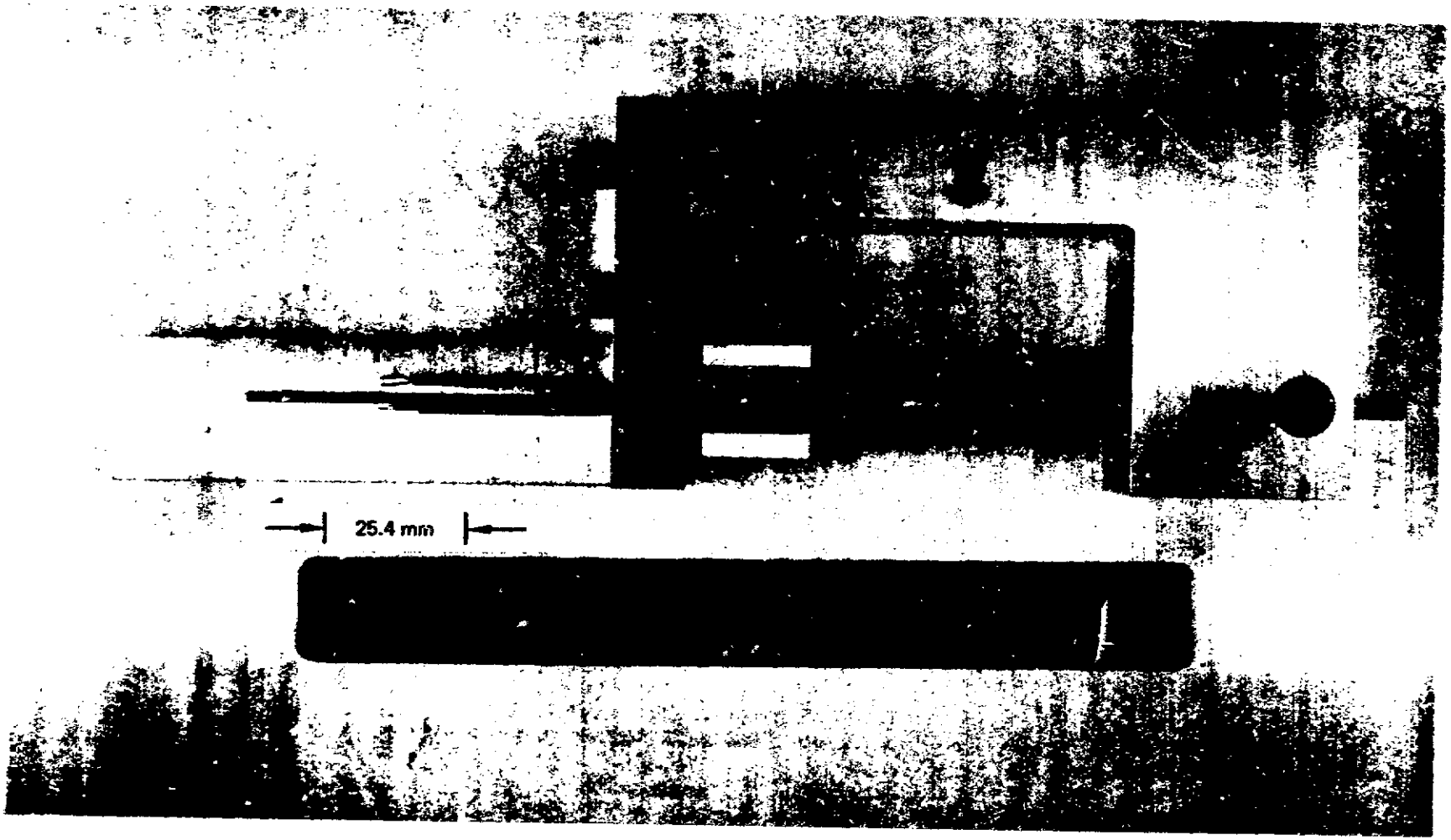

Figure 52. Transducer Components in Assembling Fixture

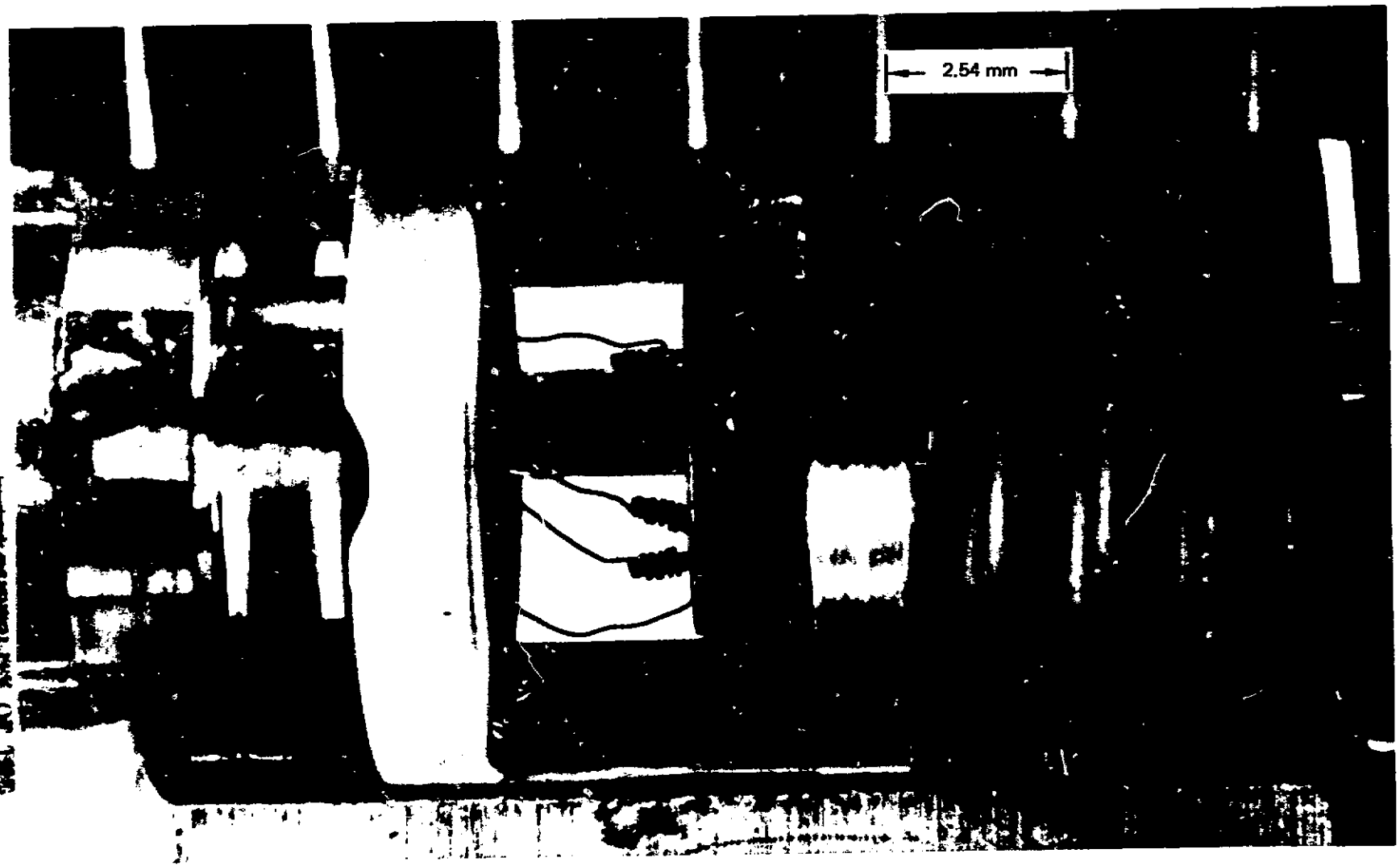

Figure 53. Transducer Components in Assembling Fixture

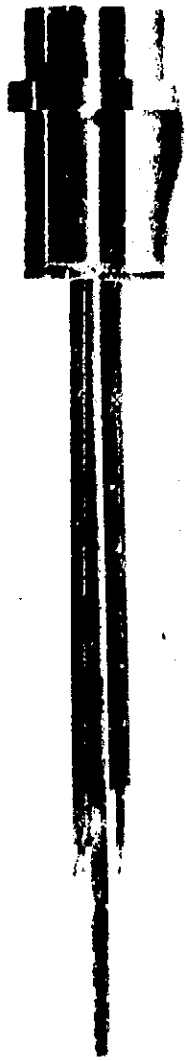

Figure 54. Transducer Assembly

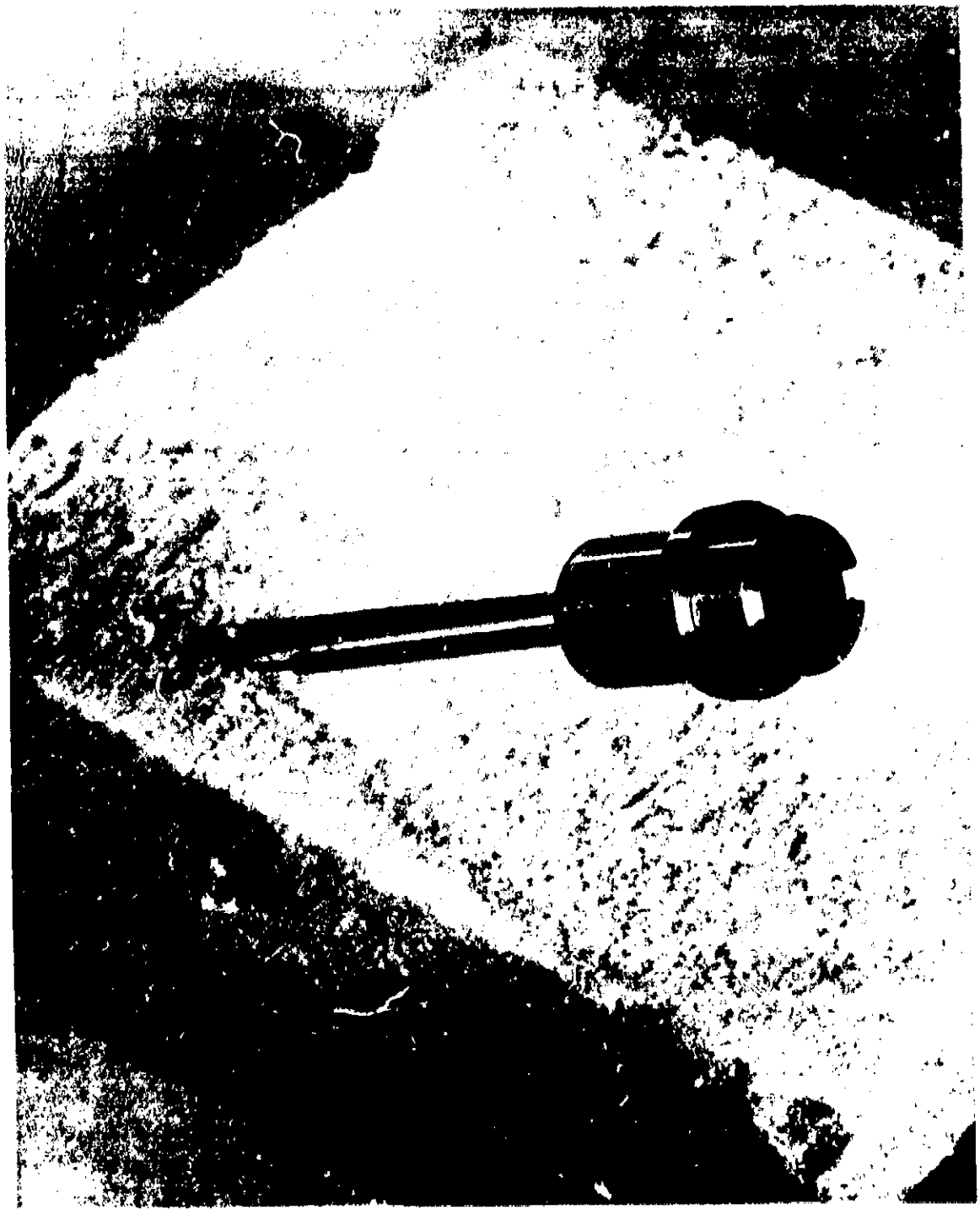

Figure 55. Transducer Assembly

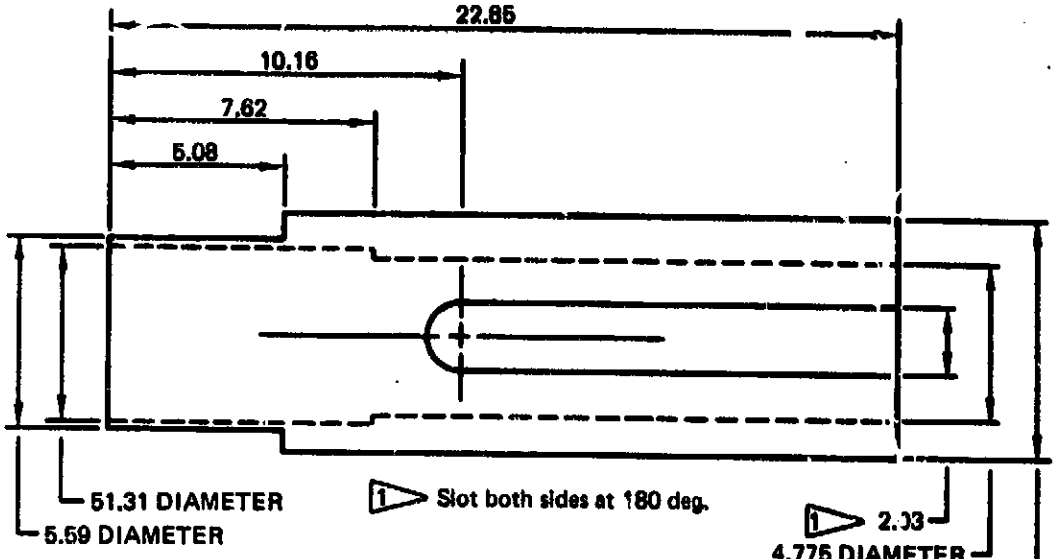

–1 CABLE FITTING (321 STAINLESS STEEL)

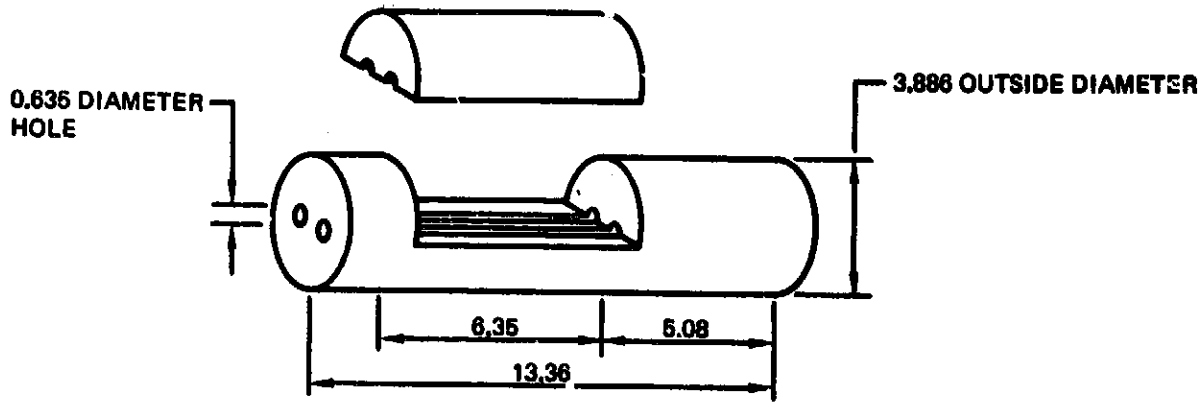

–2 INSULATOH (HIGH DENSITY ALUMINA)

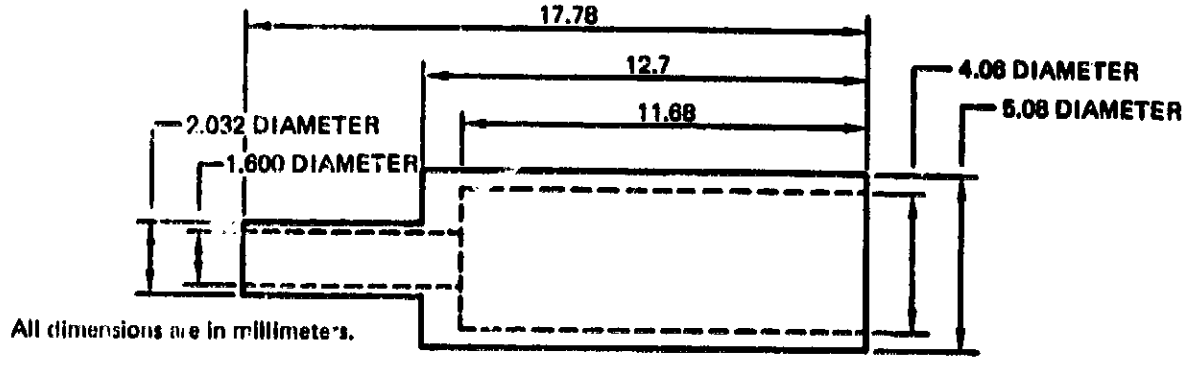

–3 TRANSDUCER FITTING (321 STAINLESS STEEL)

Figure 56. Excitation Cable Transition Couplings

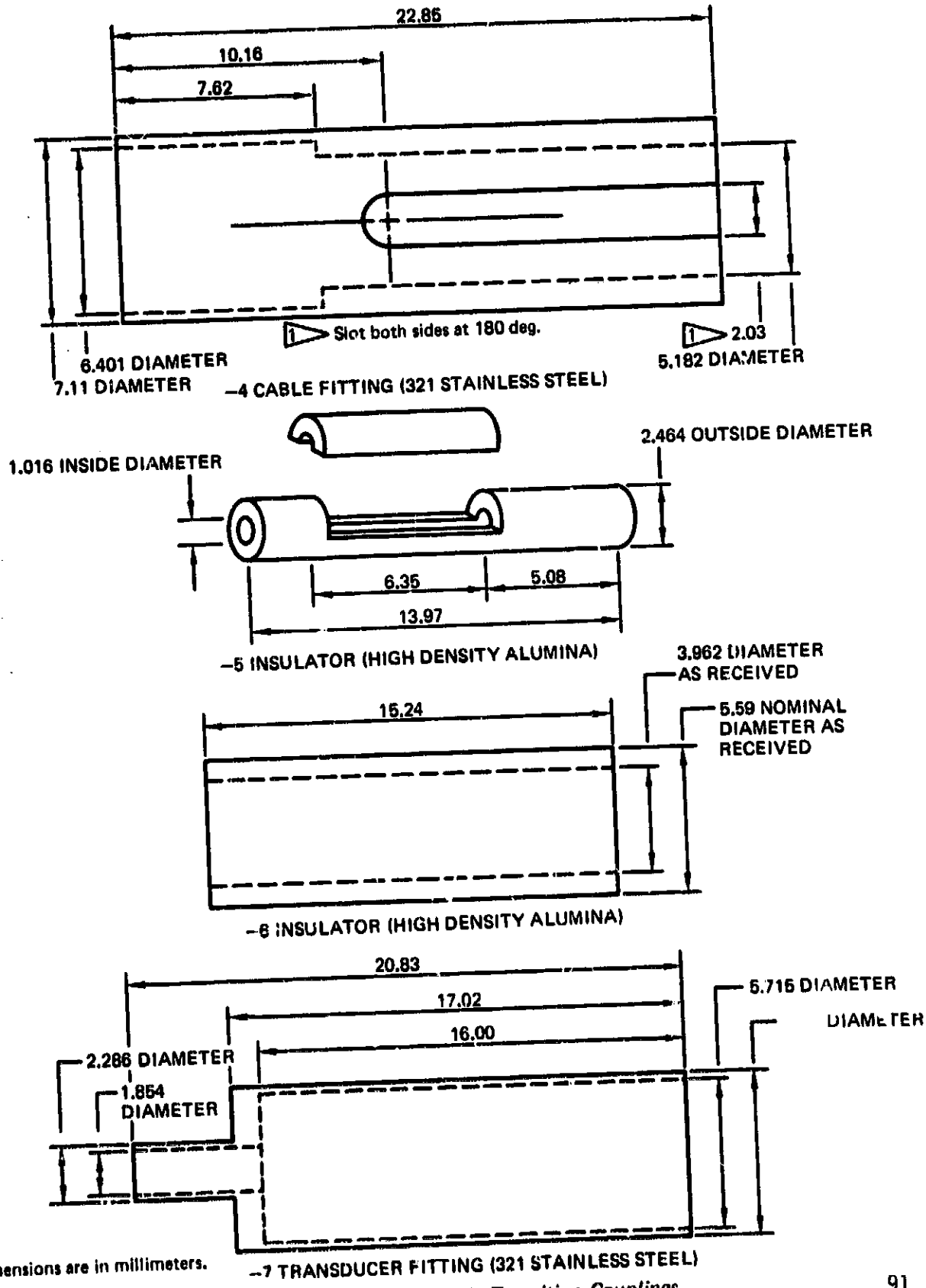

All dimensions are in millimeters.

Figure 57. Signal Cable Transition Couplings

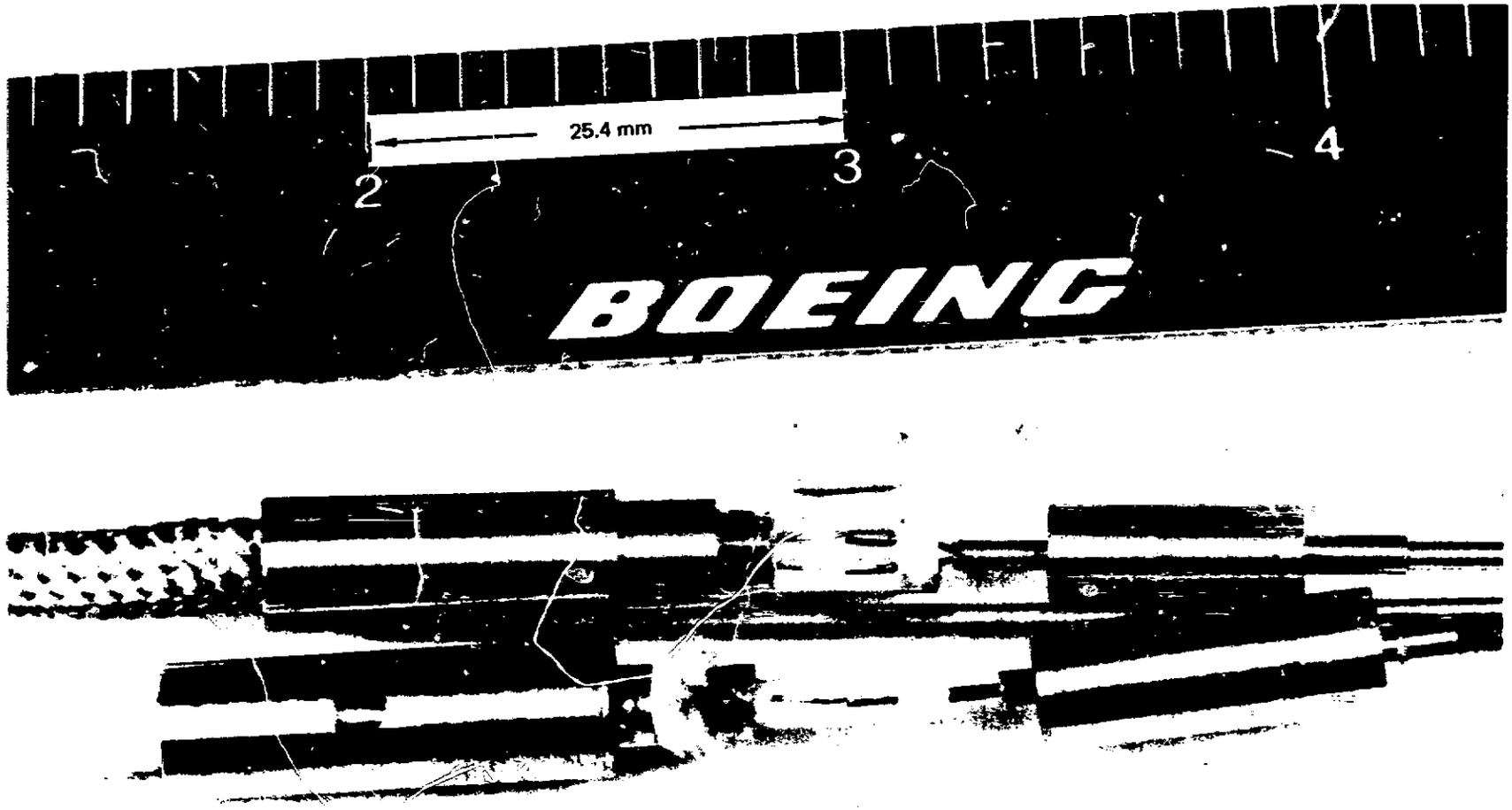

Figure 58. Cable Transition Couplings

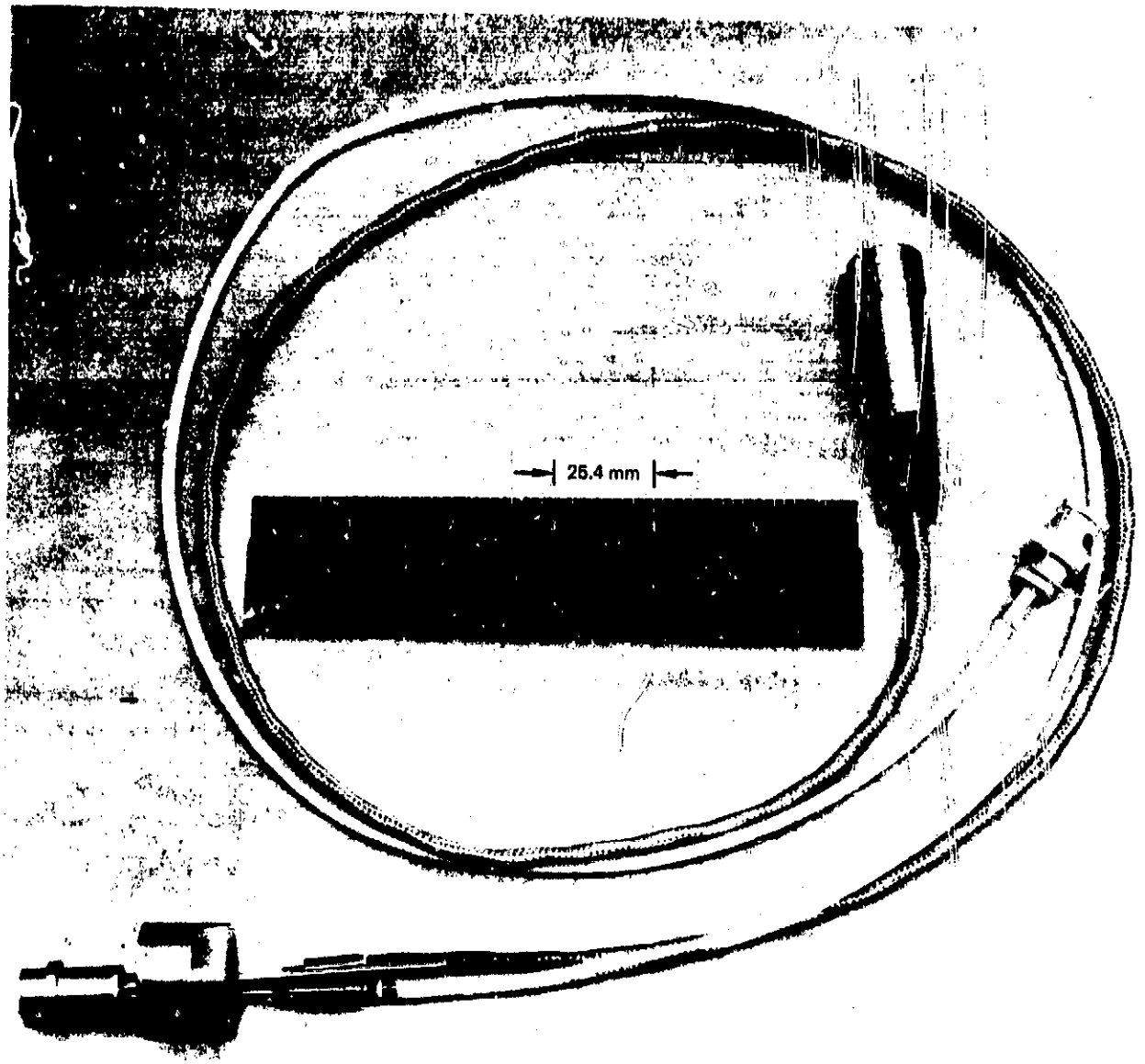

Figure 59. Pressure Transducer With Cables

Sensor serial number		2	5	7	7	7	8	19	19	21	21
Sensor mounting		Test fixture	Test fixture	Test fixture	Test fixture	Case	Test fixture	Case	Case	Case	Case
Excitation frequency (kHz)		3.37	3.39	3.39	10	10	10	10	10	10	10
Diaphragm thickness (μm)		305	305	203	203	203	254	248	248	243	243
Plate distance (μm)		150	180	180	180	180	100	110	110	130	130
Voltage output (at 69 kPa and 20°C)		3.15	2.87	3.60	3.00	3.65	3.71	5.00	2.00	5.00	2.00
Sensivitity at 20°C (pF/69 kPa)		0.0315	0.0287	0.072	0.072	0.073	0.111	0.072	0.072	0.069	0.069
Zero shift at 650°C (percent of 20°C full-scale output)		70	63	64	38	42	6.5	6.0 ▷	6.5	6.0 ▷	3.7
Sensitivity change (percent between 20° and 650°C)	+69 kPa	-52	-36	-21.6 ▷	-6.0	-7.4	-6.5	-20 ▷	-12.2	-9.0 ▷	-6.8
	-69 kPa	-30	-47	-7.1 ▷	-8.7	-14.0	-6.5	-20 ▷	-6.2	-50.0 ▷	-3.1

▷ Electronics saturated, output unstable, values not significant.

Figure 60. Comparison of Sensor Performances

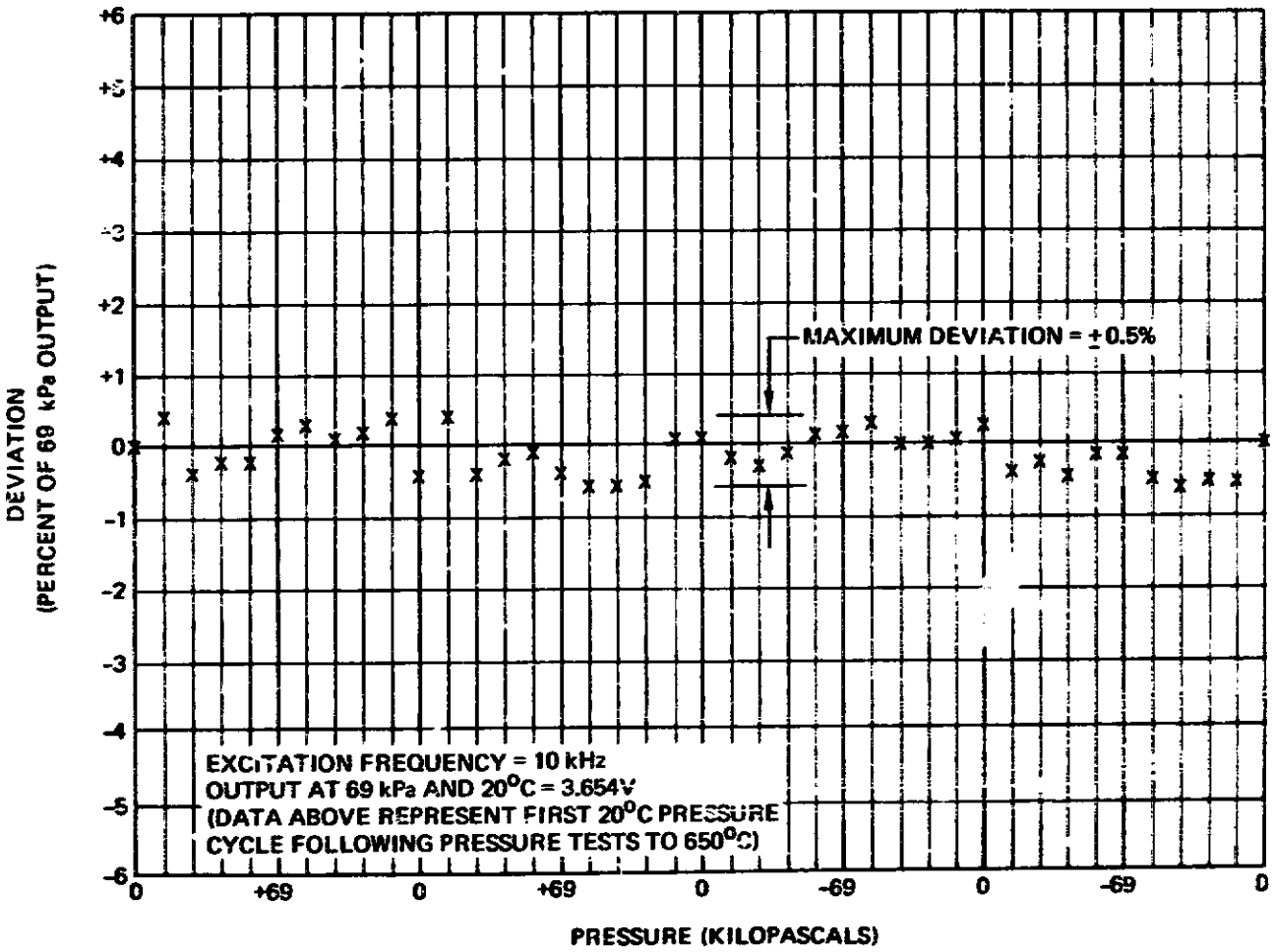

Figure 61. Sensor S/N 7 Deviation at 20°C

Temperature (°C)	Test cycle sequence number	Pressure cycle (kPa)	Hysteresis (%)
20	1	0 to -69 to 0	0.0
	2	0 to +69 to 0	0.0
	3	0 to -69 to 0	0.0
650	4	0 to +69 to 0	+0.5
	5	0 to -69 to 0	-0.9
	6	0 to +69 to 0	+0.6
	7	0 to +69 to 0	+0.3
	8	0 to -69 to 0	-0.6
	9	0 to -69 to 0	0.0
20	10	0 to +69 to 0	+0.1
	11	0 to -69 to 0	-0.1
	12	0 to +138 to 0	+0.6
	13	0 to -95 to 0	-0.2
	14	0 to +207 to 0	+1.9
	15	0 to -95 to 0	-0.8
650	16	0 to +69 to 0	0.0
	17	0 to -69 to 0	+1.2
	18	0 to +138 to 0	+1.7
20	19	0 to +69 to 0	+0.3
	20	0 to -69 to 0	0.0

Note: The hysteresis values represent the difference between the outputs at zero pressure preceding and following the cycle. The hysteresis values are expressed in percent of the 20°C full-scale (69 kPa) output, rounded off to the nearest 0.1%.

Figure 62. Sensor S/N 8 Response to Overpressure

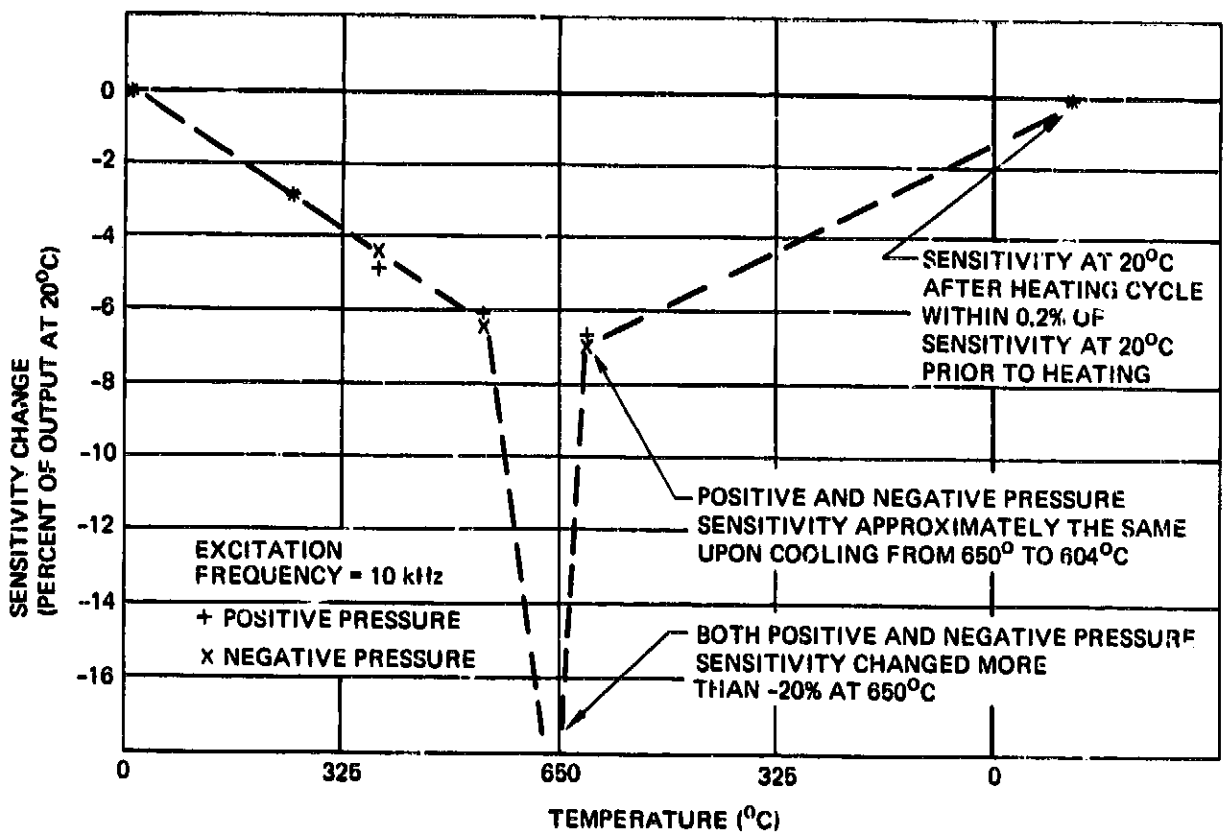

Figure 63. Sensor S/N 19 Sensitivity Change With Temperature--5V Full-Scale Output

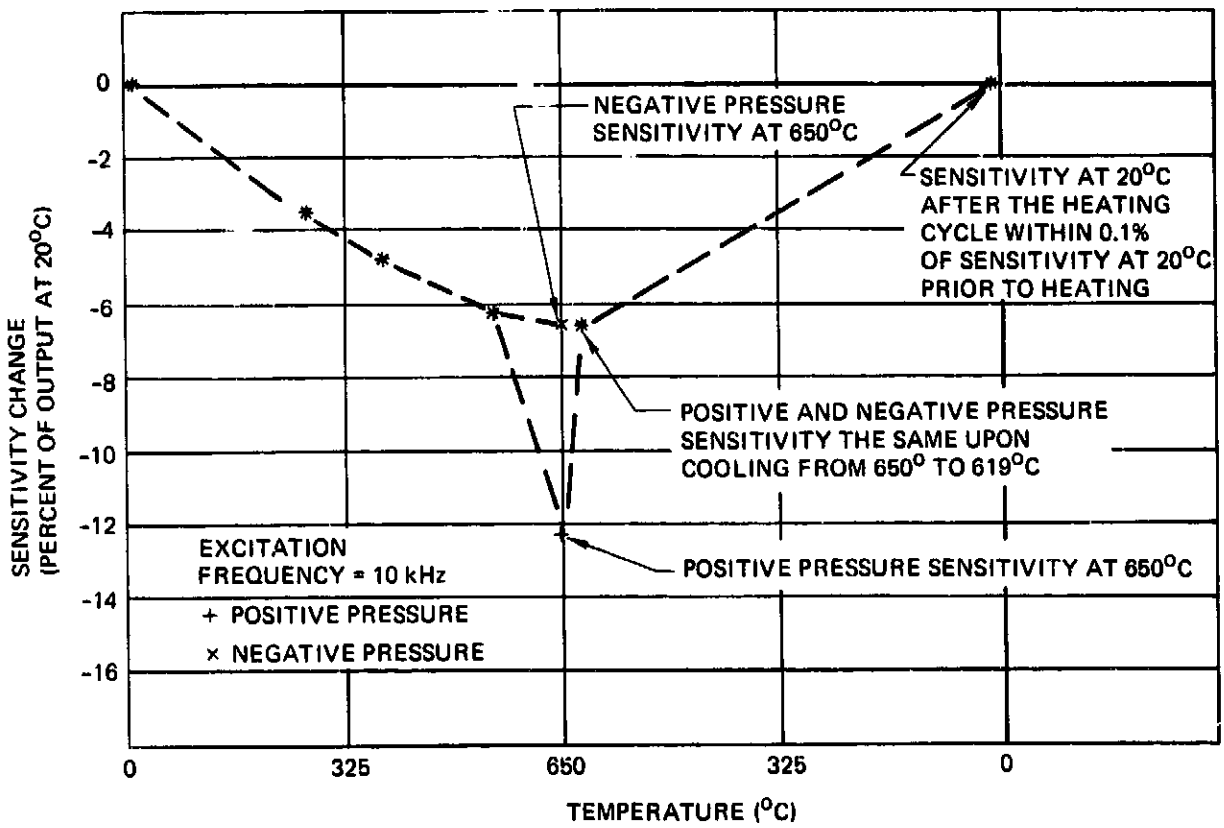

Figure 64. Sensor S/N 19 Sensitivity Change With Temperature— 2V Full-Scale Output

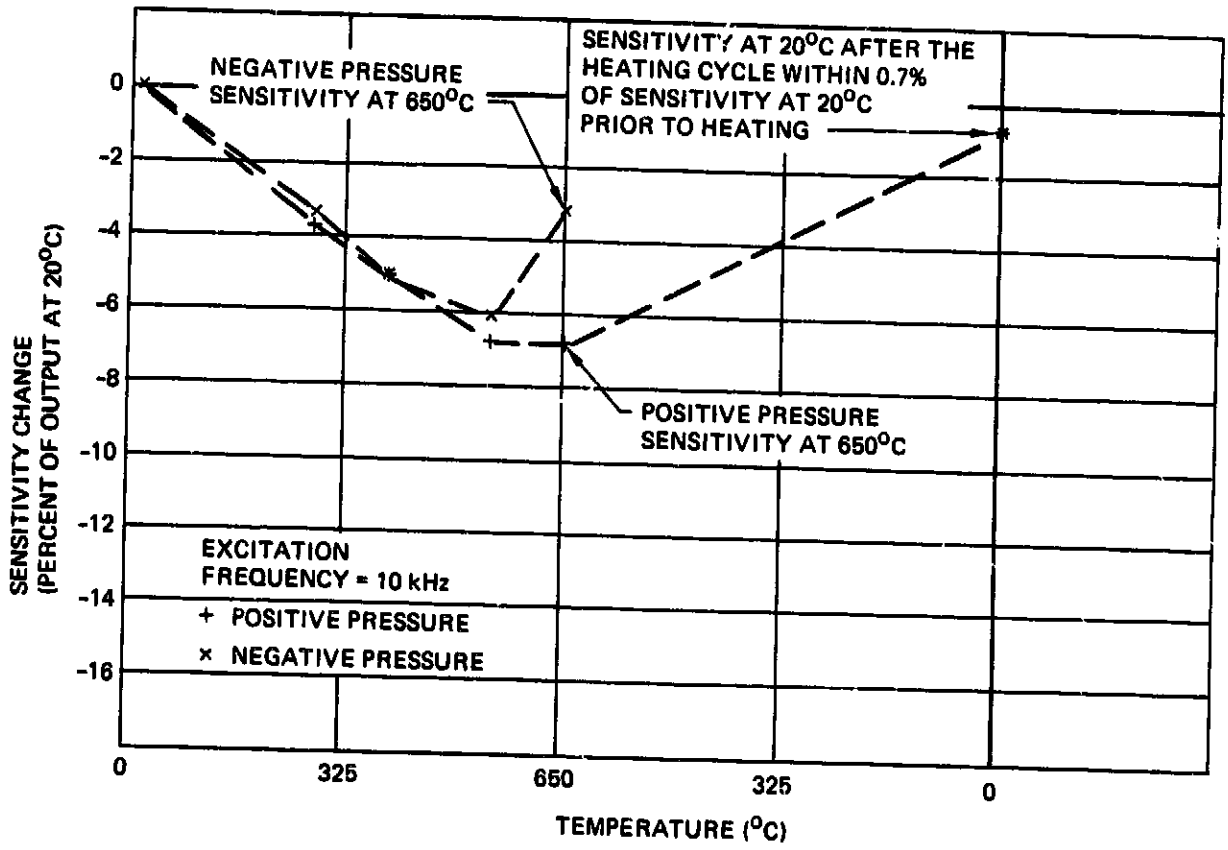

Figure 65. Sensor S/N 21 Sensitivity Change With Temperature— 2V Full-Scale Output

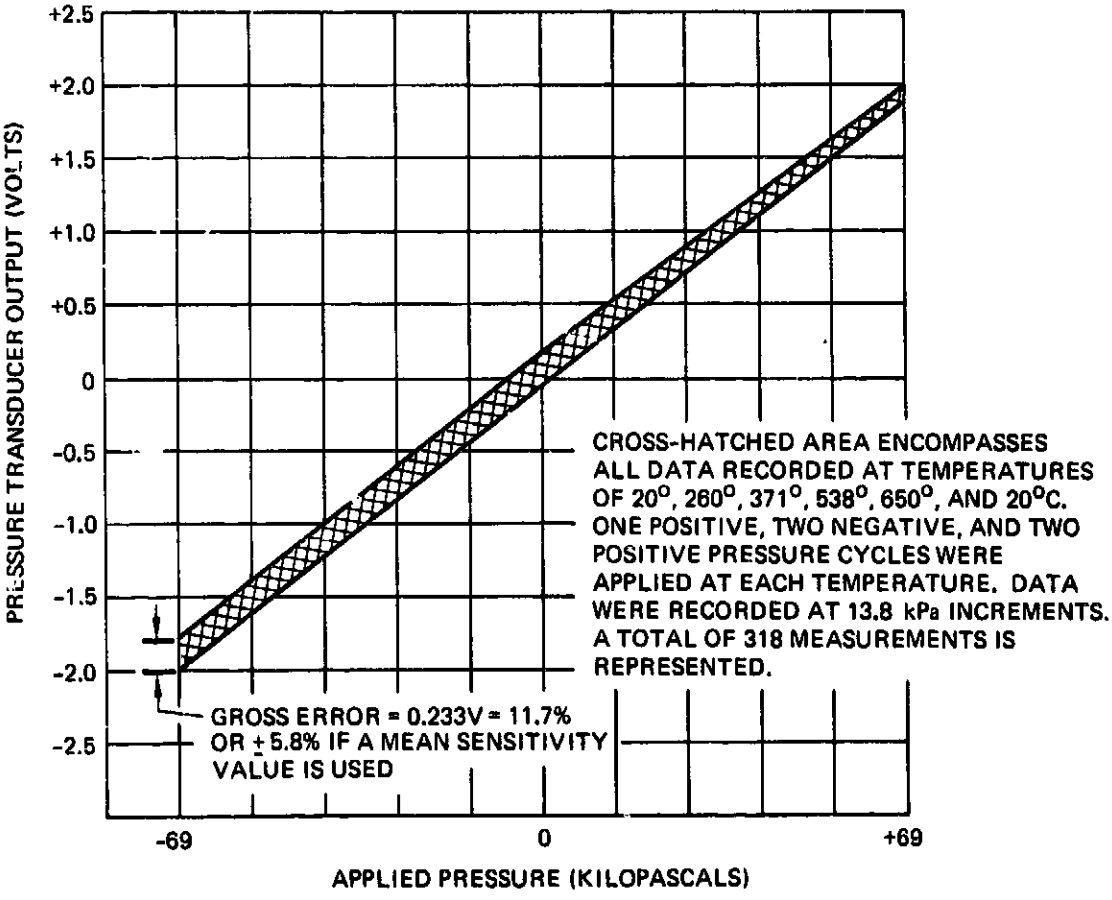

Figure 66. Sensor S/N 19 Overall Response, 20° to 650°C

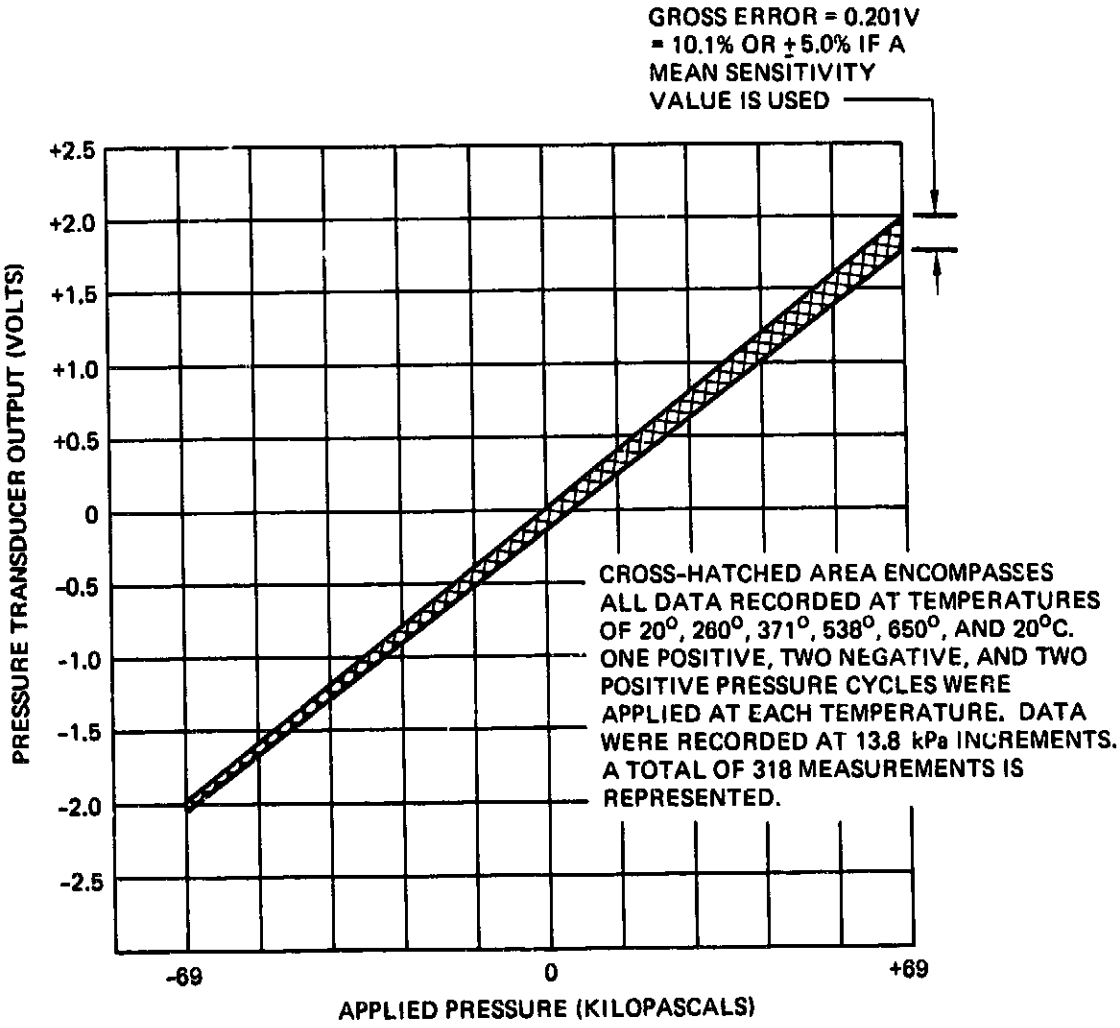

Figure 67. Sensor S/N 21 Overall Response, 20° to 650°C

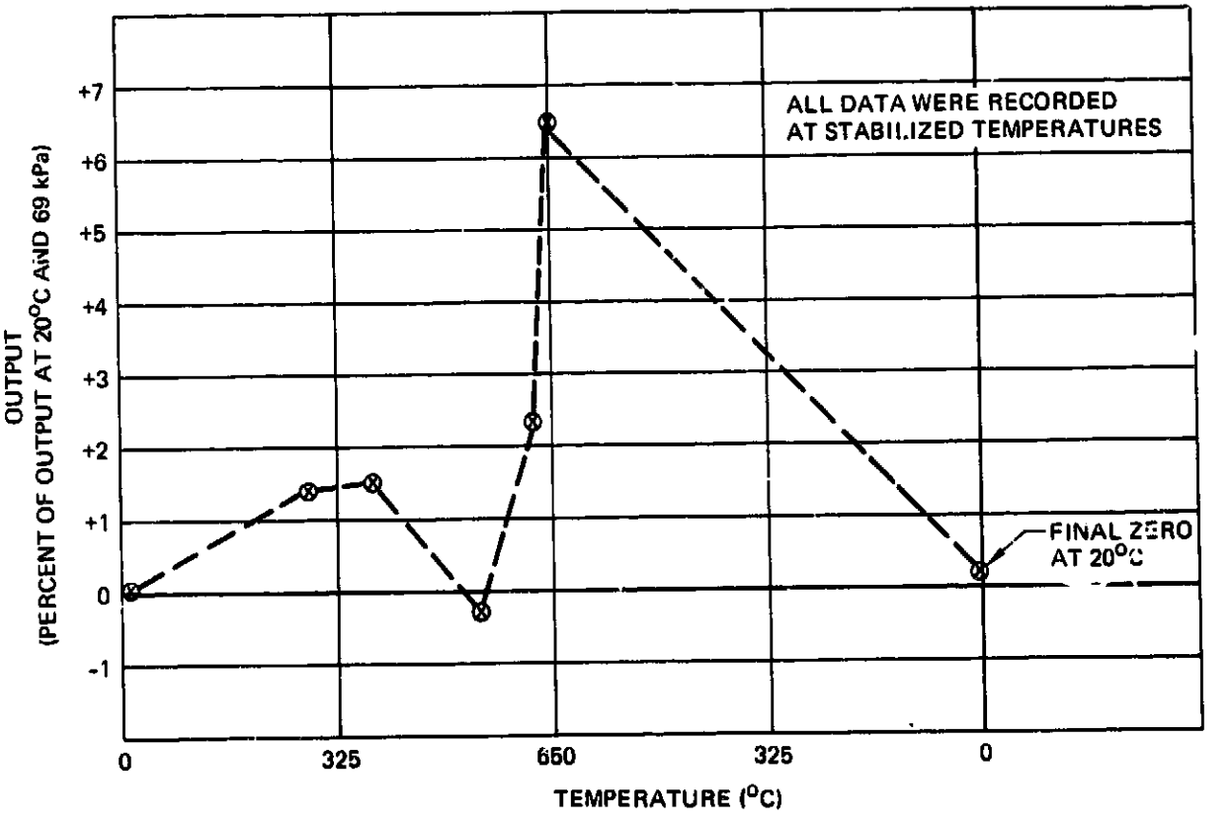

Figure 68. Sensor S/N 19 Zero Shift With Temperature

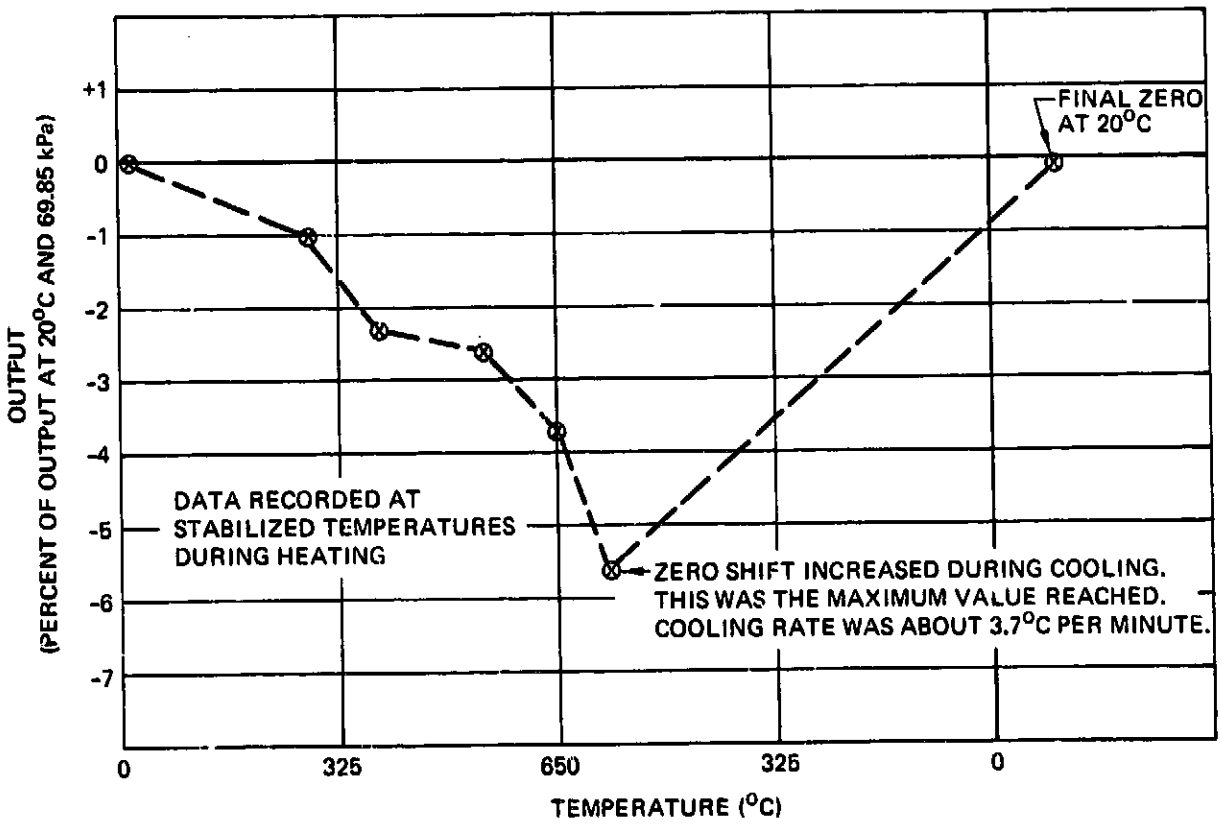

Figure 69. Sensor S/N 21 Zero Shift With Temperature

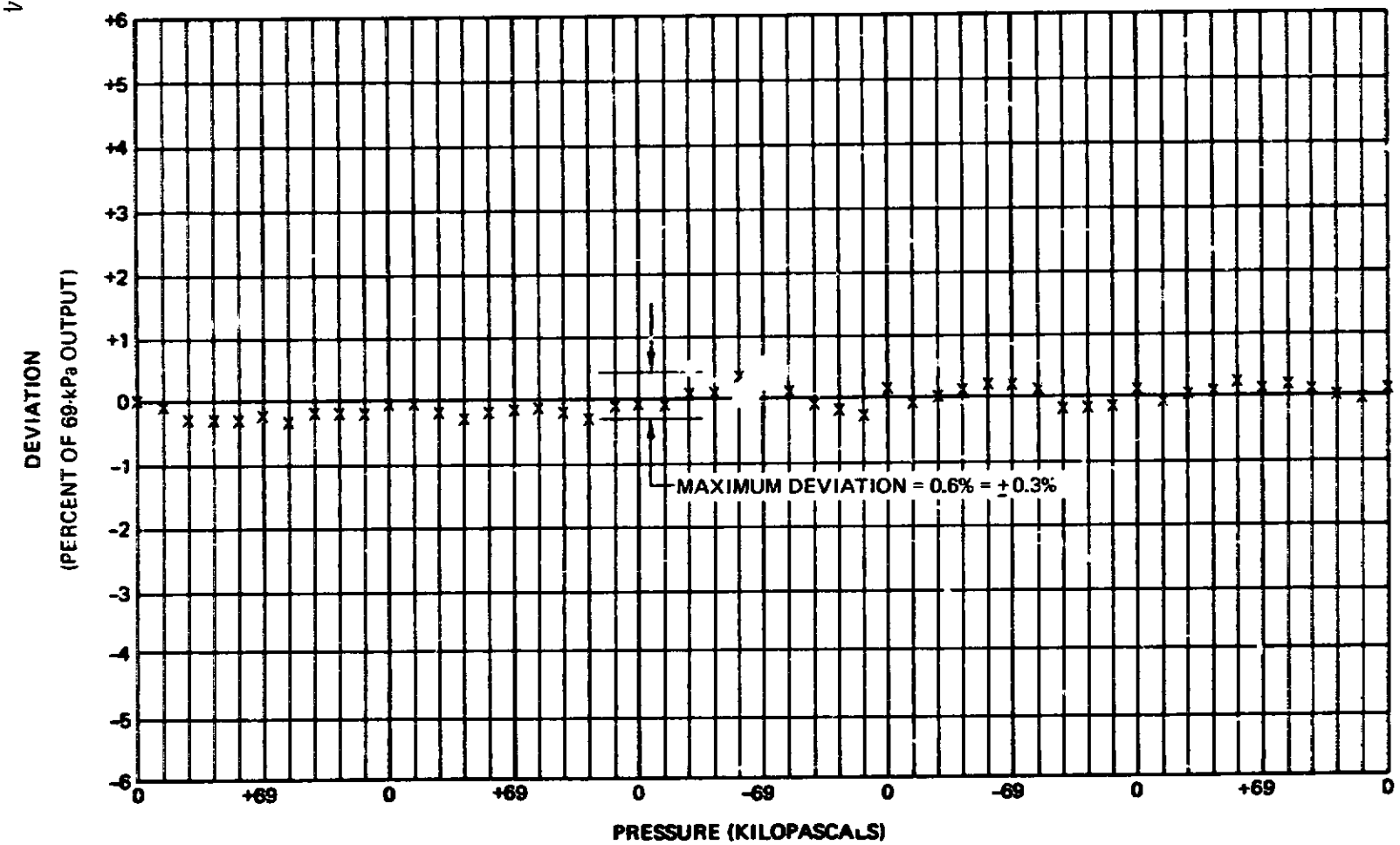

Note: Deviation is based on a linear output of 2.000V at 69 kPa and 20°C.

Figure 70. Sensor S/N 19 Deviation at 20°C—Before Heat Cycle

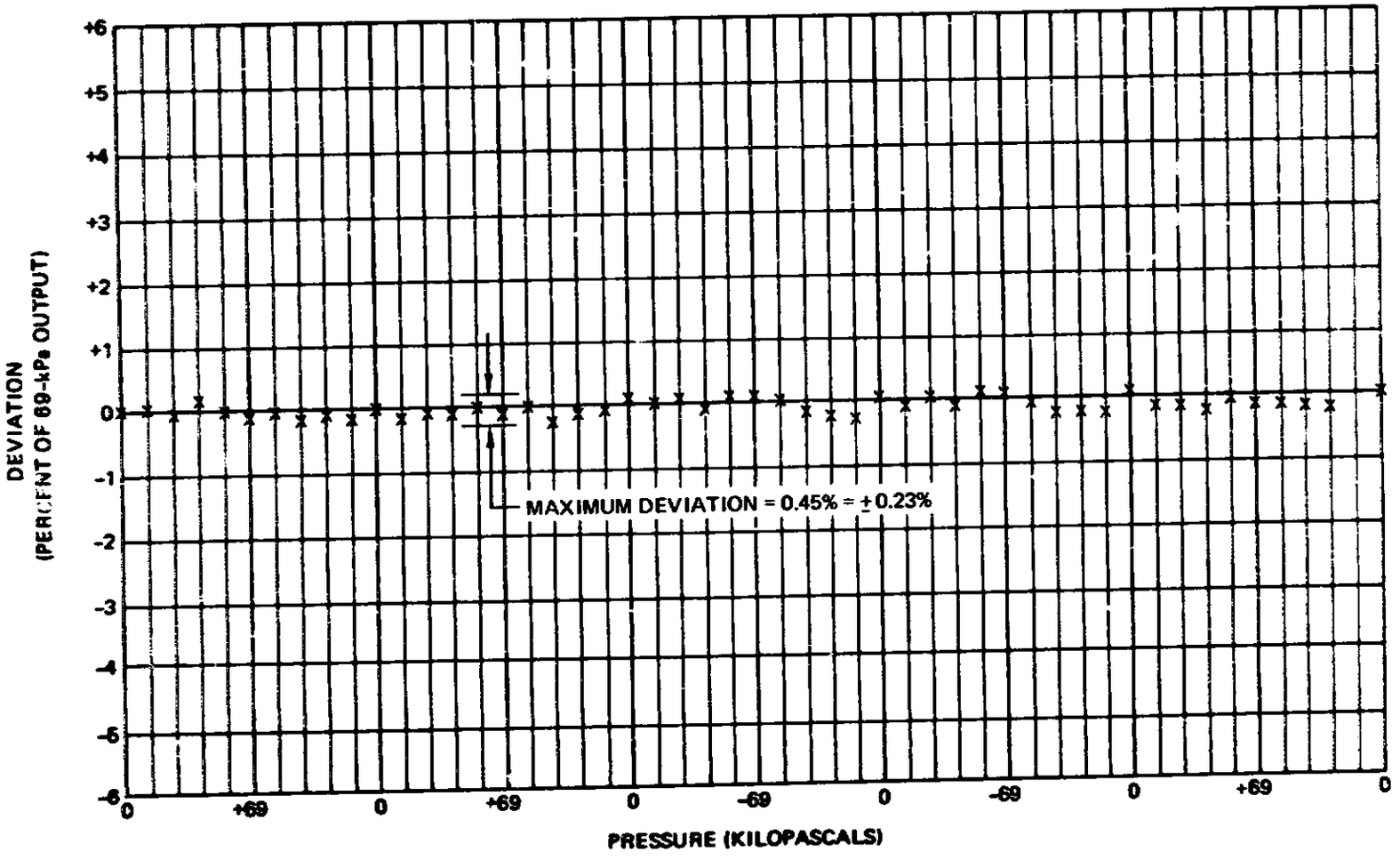

Note: Deviation is based on a linear output of 1.931V at 69 kPa and 260°C.

Figure 71. Sensor S/N 19 Deviation at 260°C

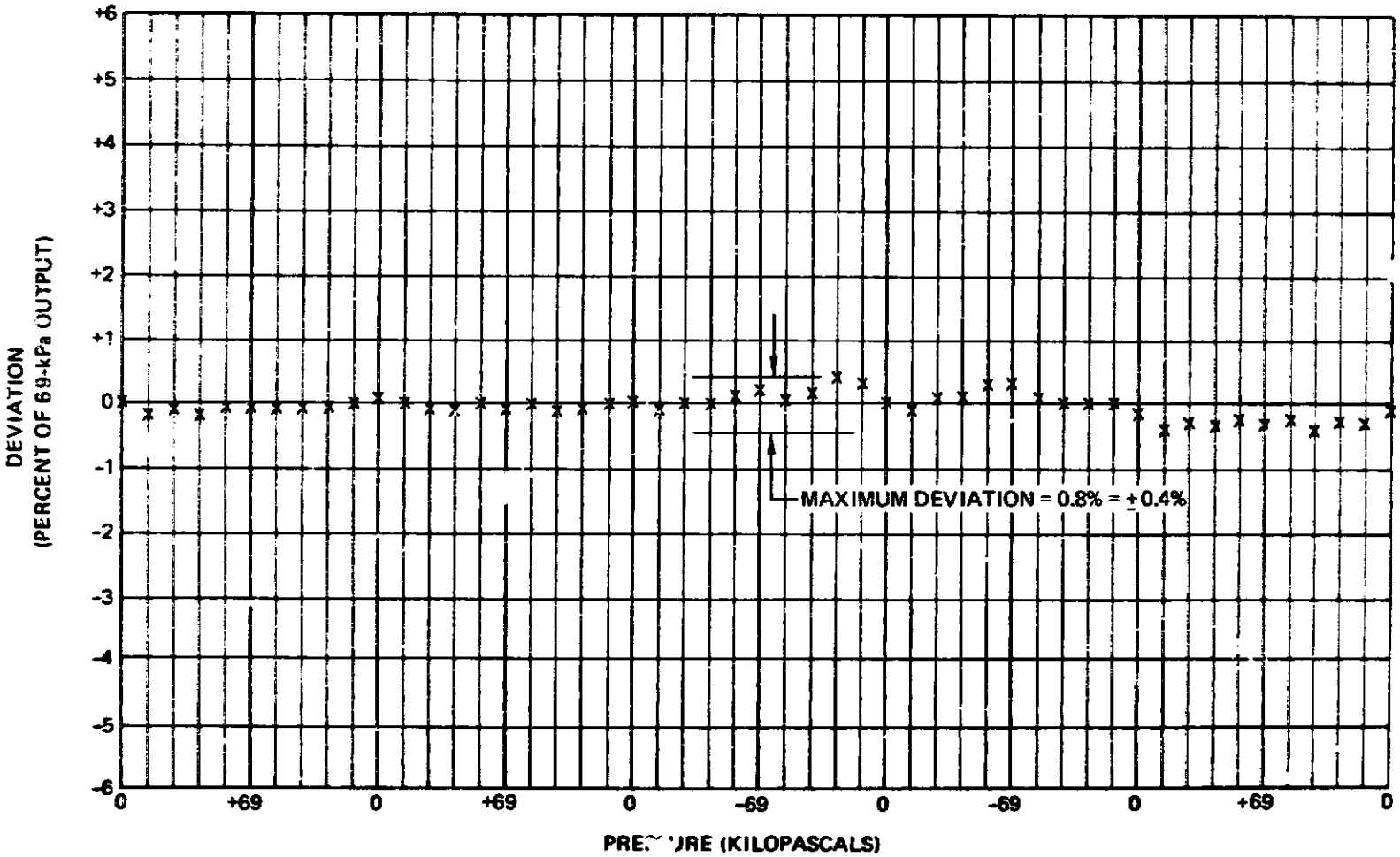

Note: Deviation is based on a linear output of 1.906V at 69 kPa and 371°C.

Figure 72. Sensor S/N 19 Deviation at 371°C

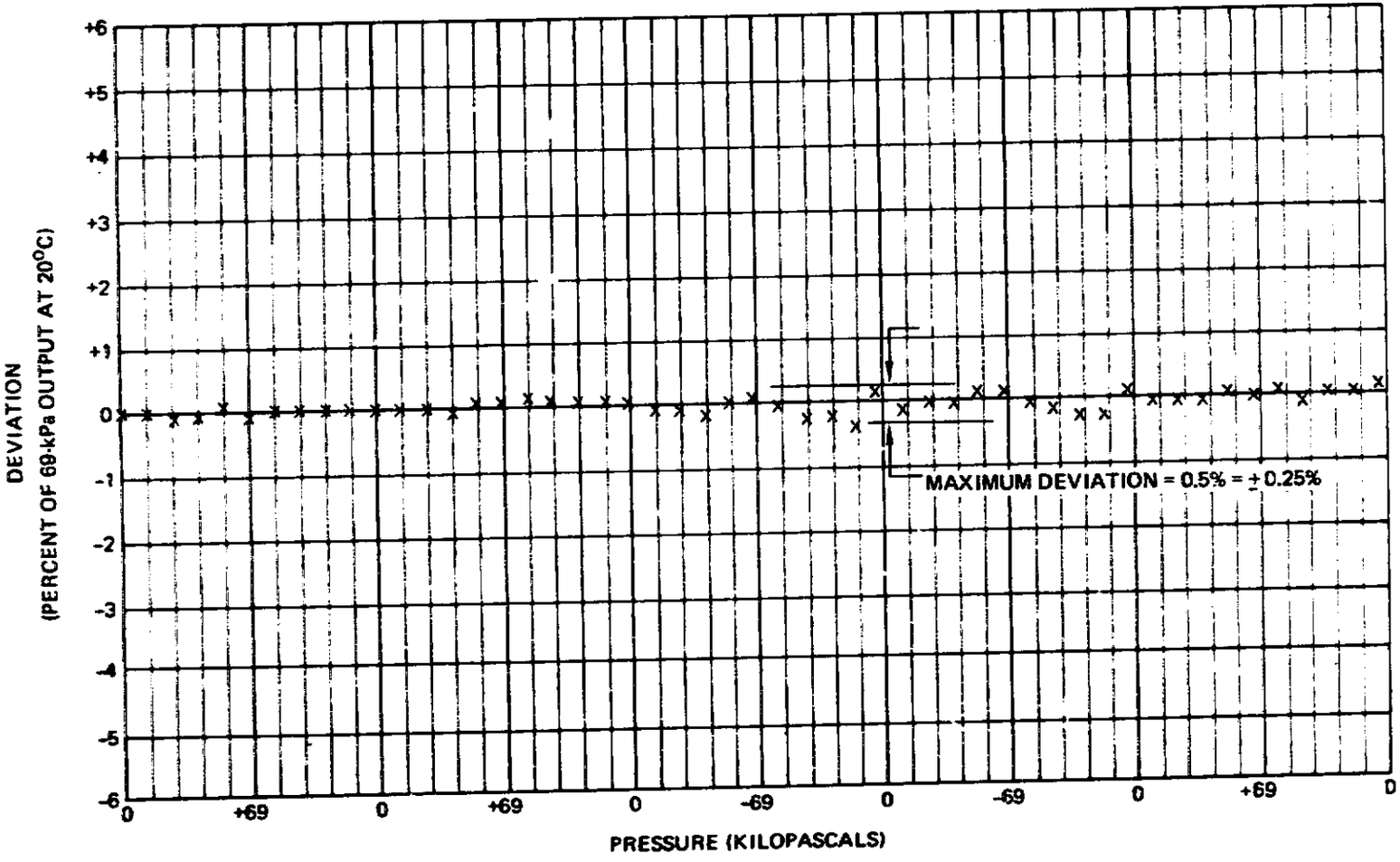

Note: Deviation is based on a linear output of 1.877V at 69 kPa and 538°C.

Figure 73. Sensor S/N 19 Deviation at 538°C

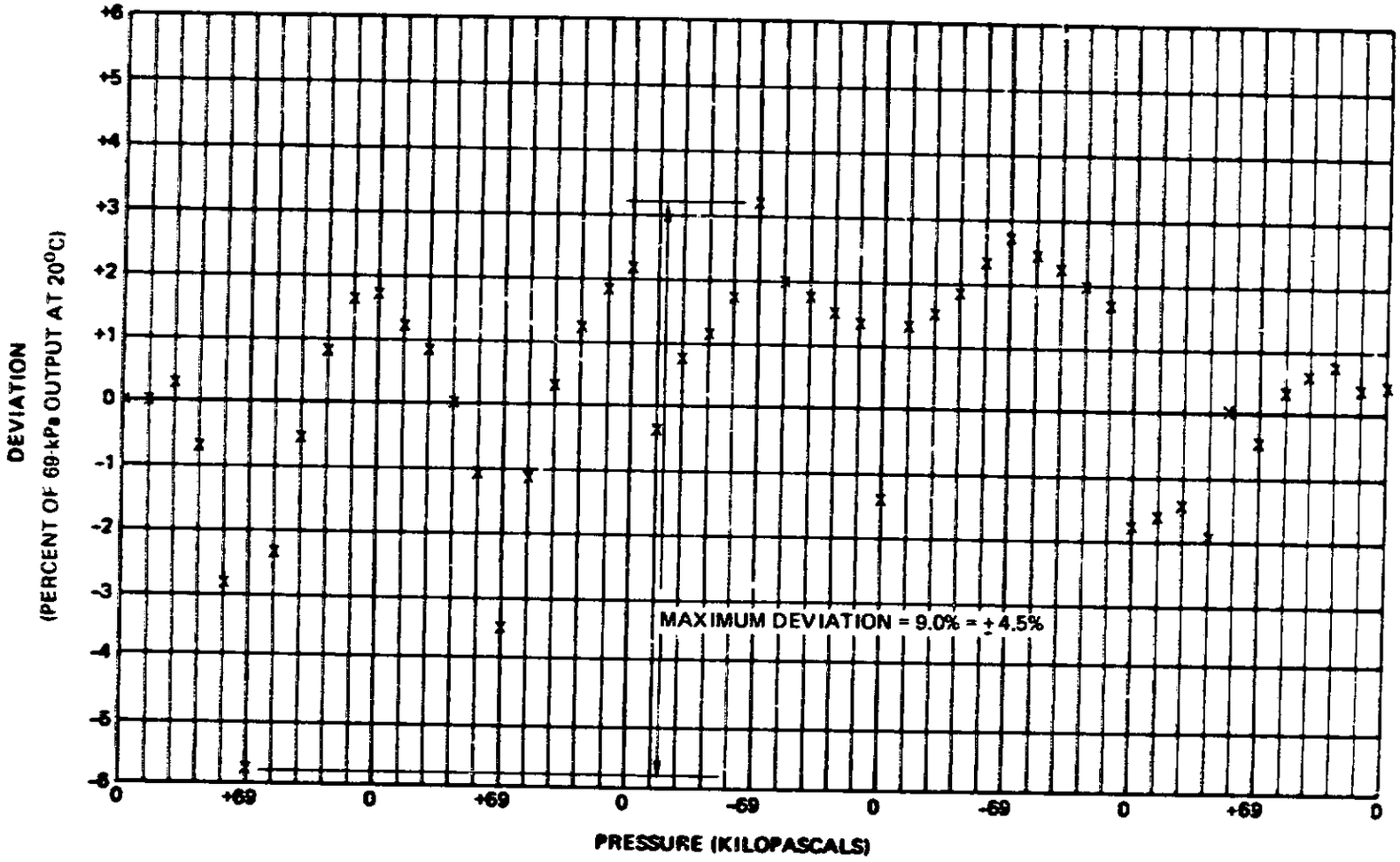

Note: Deviation is based on a linear output of 1.860V at 69 kPa and 650°C.

Figure 74. Sensor S/N 19 Deviation at 650°C

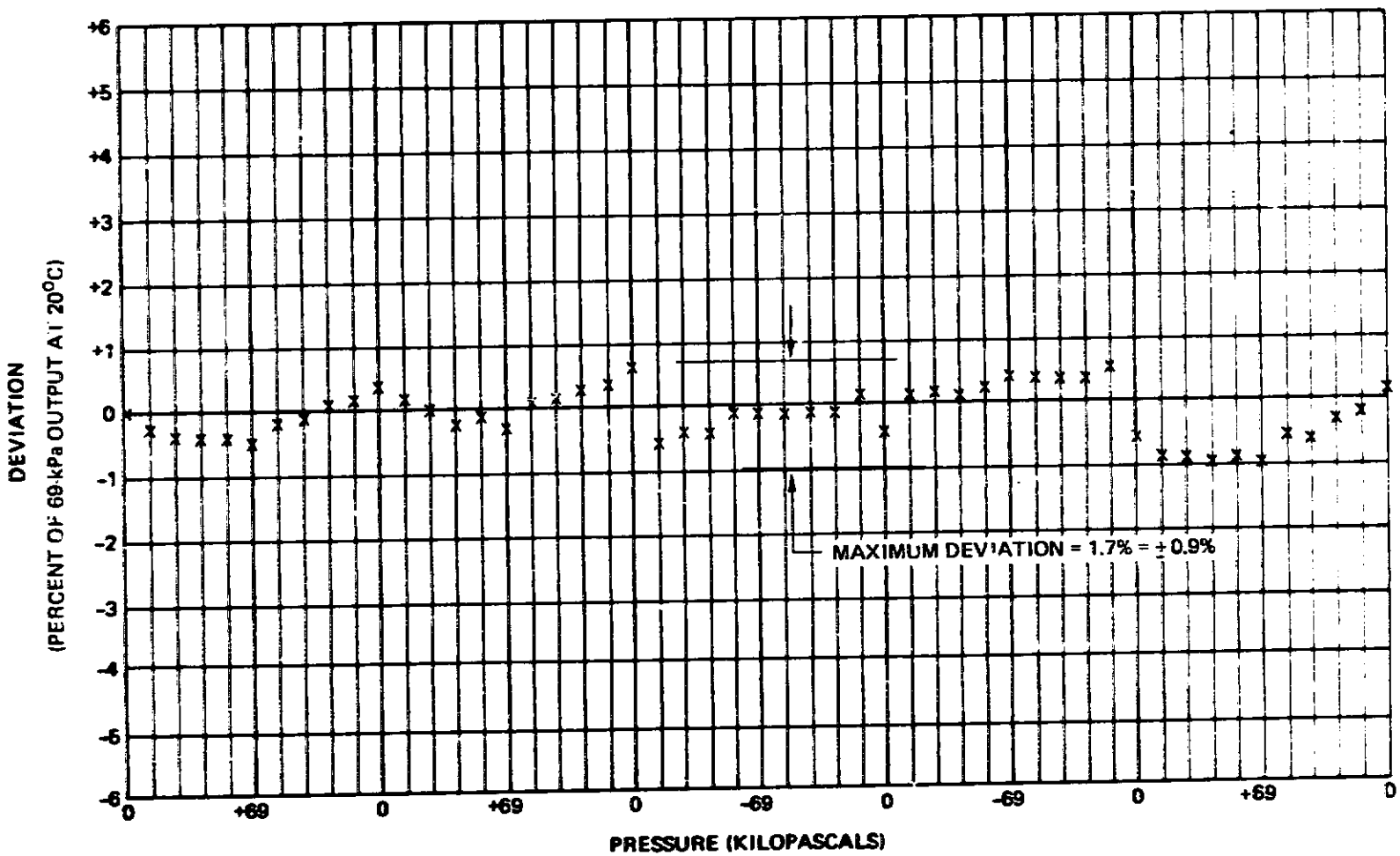

Note: Deviation is based on a linear output of 1.880V at 69 kPa and 619°C.

Figure 75. Sensor S/N 19 Deviation at 619°C

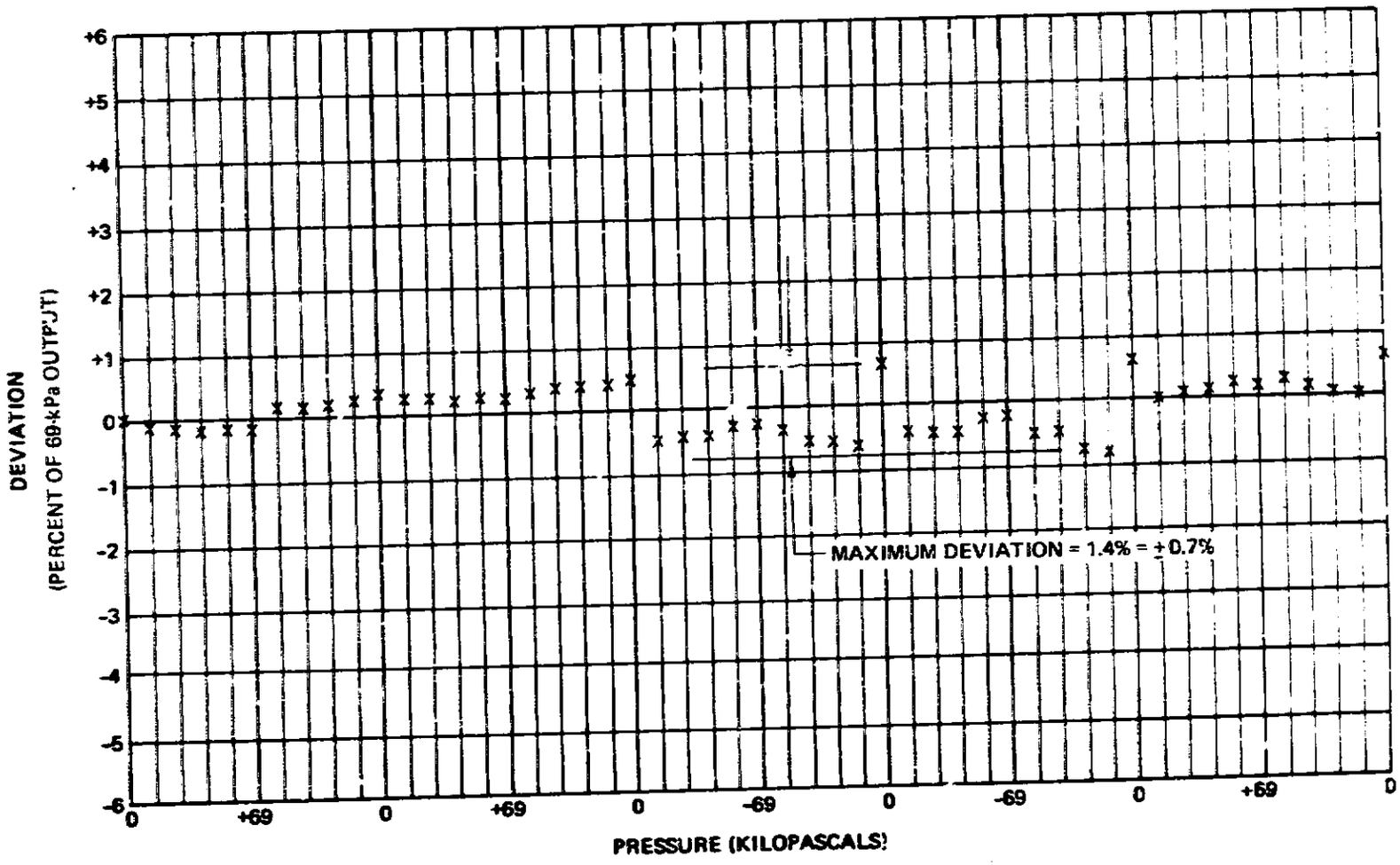

Note: Deviation is based on a linear output of 2.000V at 69 kPa.

Figure 76. Sensor S/N 19 Deviation at 20°C—After Heat Cycle

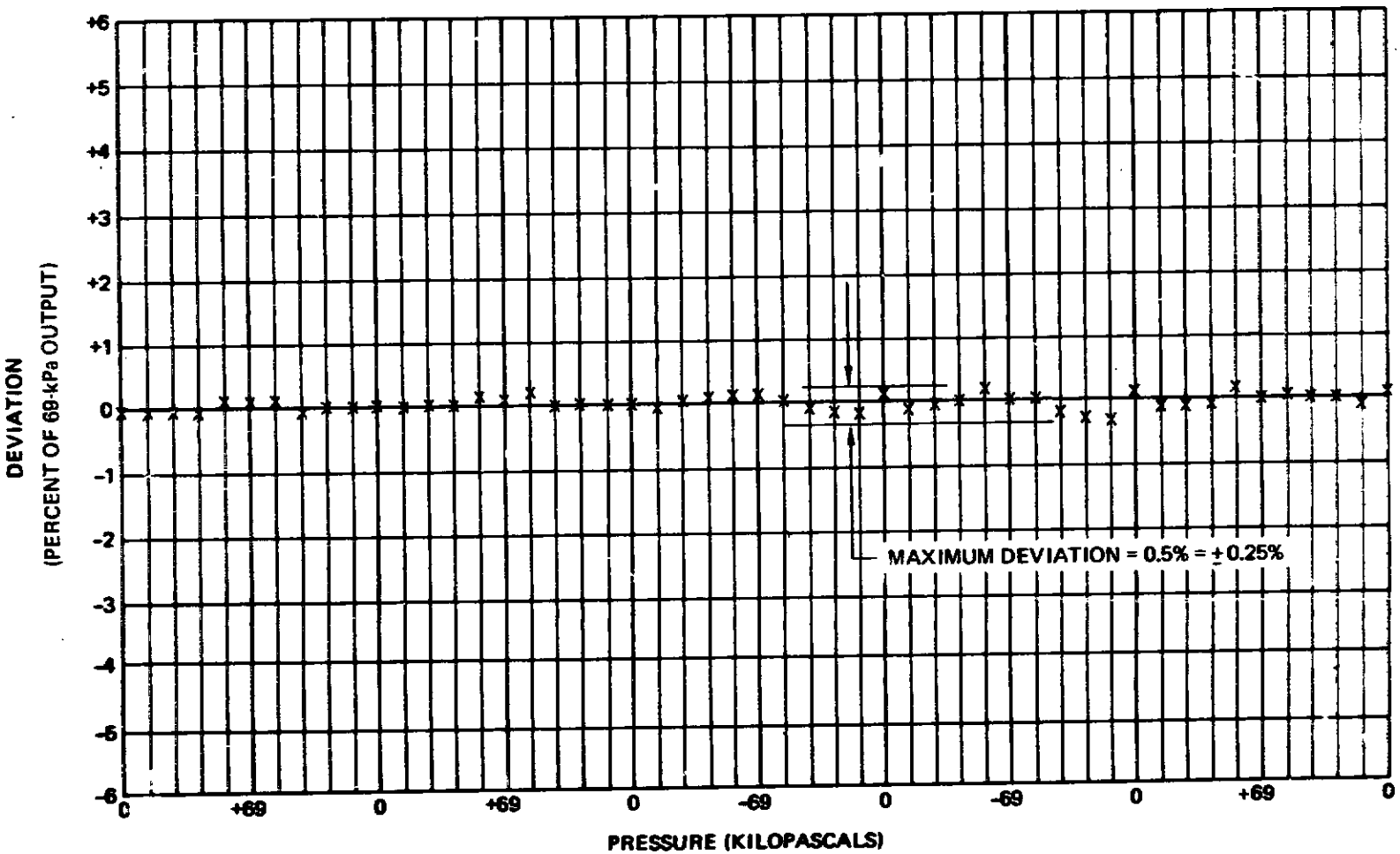

Note: Deviation is based on linear output of 2.000V at 69 kPa.

Figure 77. Sensor S/N 21 Deviation at 20°C—Before Heat Cycle

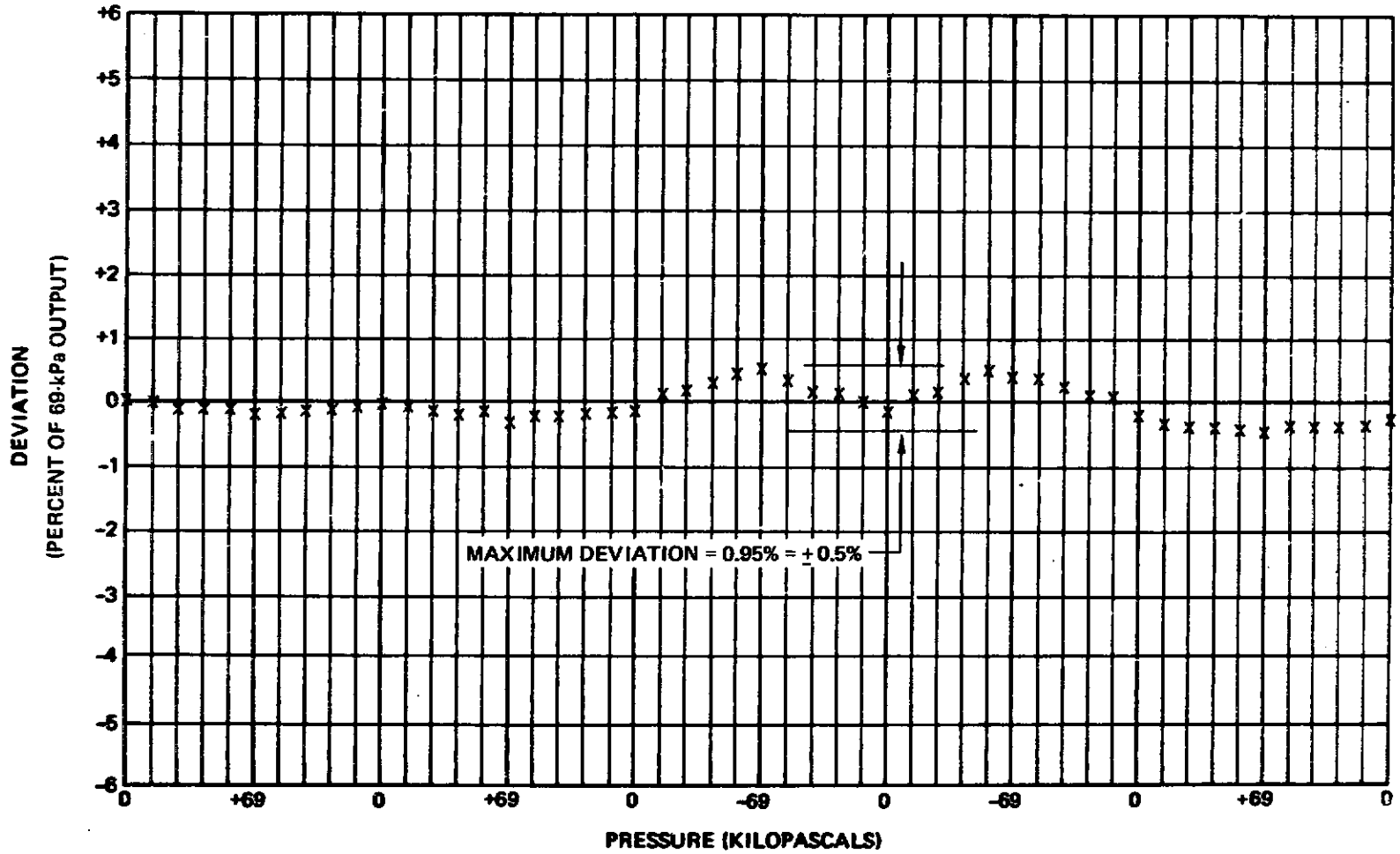

Note: Deviation is based on linear output of 1.872V at 69 kPa and 538°C.

Figure 78. Sensor S/N 21 Deviation at 538°C

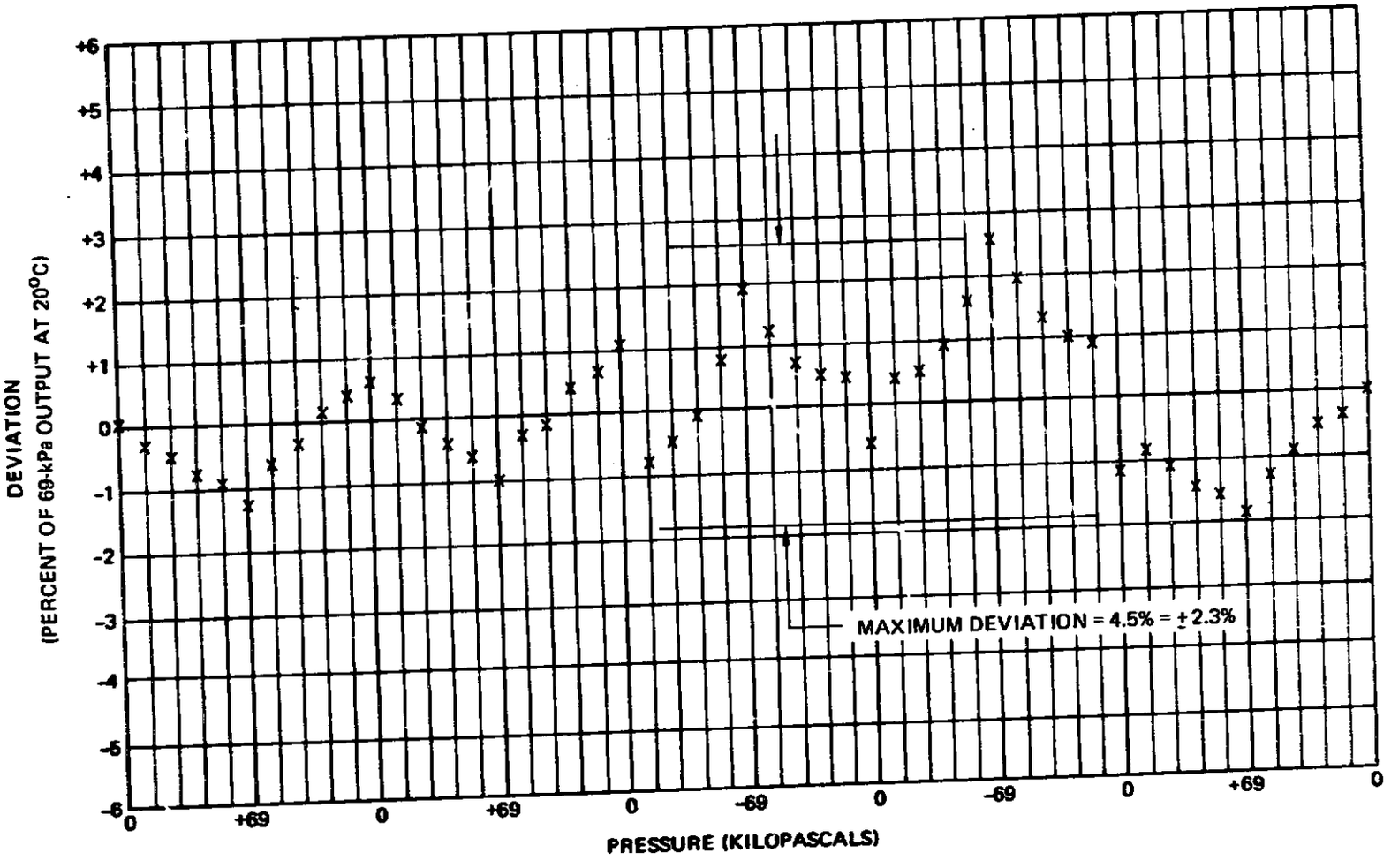

Note: Deviation is based on a linear output of 1.907V at 69 kPa and 650°C.

Figure 79. Sensor S/N 21 Deviation at 650°C

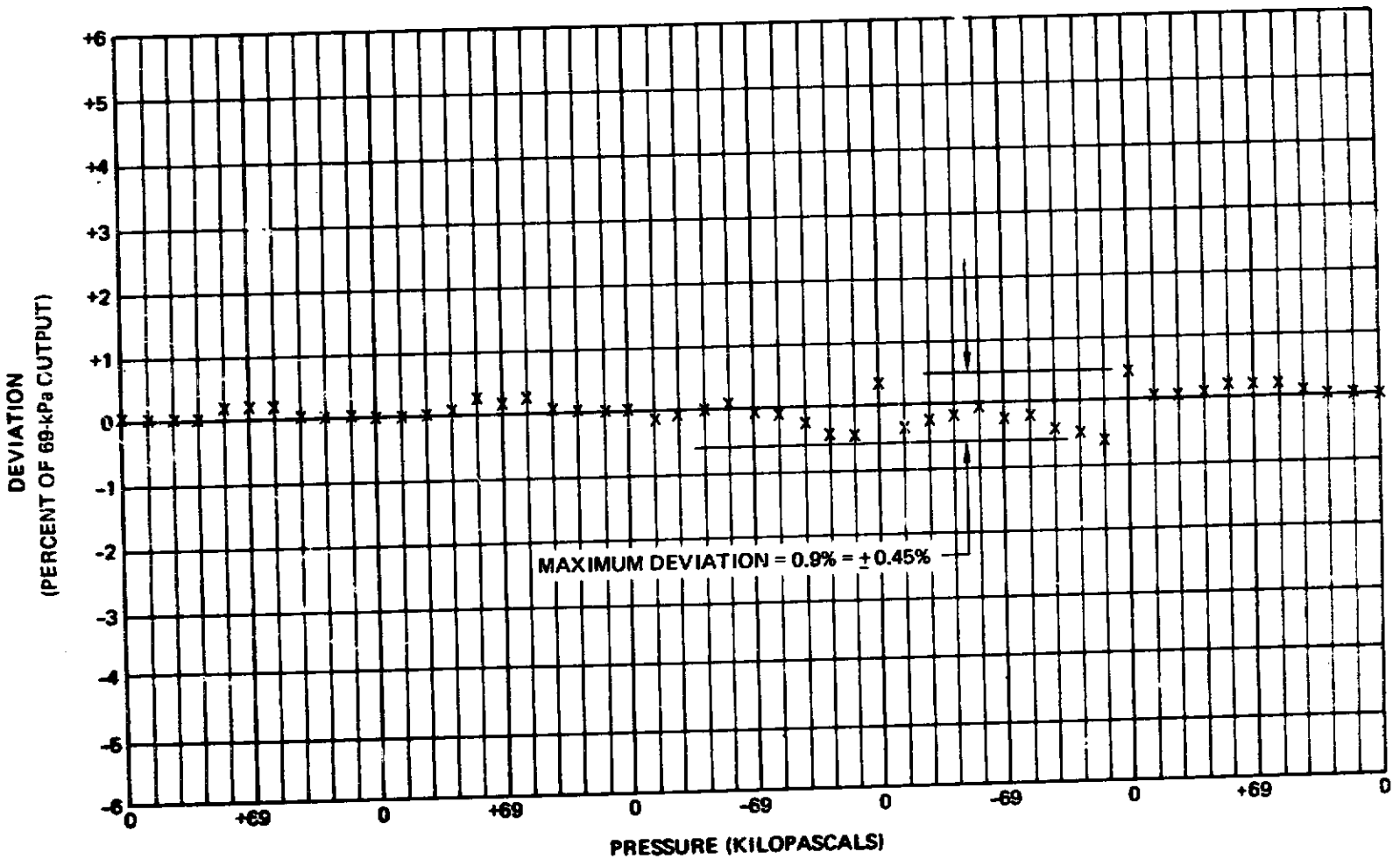

Note: Deviation is based on a linear output of 1.982V at 69 kPa.

Figure 80. Sensor S/N 21 Deviation at 20°C–After Heat Cycle